Extensional Thin Layer Flows

P.D. Howell
St. Catherine's College
Oxford

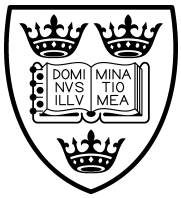

Thesis submitted for the degree of Doctor of Philosophy

Trinity Term 1994

Abstract

In this thesis we derive and solve equations governing the flow of slender threads and sheets of viscous fluid. Our method is to solve the Navier-Stokes equations and free surface conditions in the form of asymptotic expansions in powers of the inverse aspect ratio of the fluid, *i.e.* the ratio of a typical thickness to a typical length.

In the first chapter we describe some of the many industrial processes in which such flows are important, and summarise some of the related work which has been carried out by other authors. We introduce the basic asymptotic methods which are employed throughout this thesis in the second chapter, while deriving models for two–dimensional viscous sheets and axisymmetric viscous fibres. In chapter 3 we show that when these equations govern the straightening or buckling of a curved viscous sheet, simplification may be made via the use of a suitable short timescale. In the following four chapters, we derive models for nonaxisymmetric viscous fibres and fully three–dimensional viscous sheets; for each we consider separately the cases where the dimensionless curvature is small and where the dimensionless curvature is of order one. We find that the models which result bear a marked similarity to the theories of elastic rods, plates and shells. In chapter 8 we explain in some detail why the Trouton ratio — the ratio between the extensional viscosity and the shear viscosity — is 3 for a slender viscous fibre and 4 for a slender viscous sheet. We draw our conclusions and suggest further work in the final chapter.

Acknowledgements

I would like to thank my supervisors, Dr. J.R. Ockendon and Dr. P. Wilmott, for their guidance and encouragement over the past three years. I have had many helpful discussions with Dr. J.N. Dewynne, Dr. D.M. Burley and Mr. D. Gelder, by whom many of the problems tackled in this thesis were suggested. I also wish to thank the SERC (now EPSRC) for their financial support. I am very grateful to Dan Waterhouse, Linda Cummings and Dale Heron for help with proof–reading and to John Morgan for passing on his technical expertise.

Finally, I would like to thank my family, especially my parents, for all their support and the friends who have helped make the last three years so enjoyable.

Contents

1 Introduction **1**

1.1 Overview 1

1.2 Relevant industrial processes 5

1.2.1 Manufacture of Optical Fibres 5

1.2.2 Manufacture of Optical Fibre Couplers 7

1.2.3 The float glass process 8

1.2.4 Manufacture of Windscreens 9

1.2.5 Glass Blowing 10

1.2.6 Dimensionless parameters 11

1.3 Literature review 11

2 The "Trouton" model **14**

2.1 A two–dimensional sheet 15

2.1.1 Nondimensionalisation and scaling 16

2.1.2 Asymptotic expansions 16

2.1.3 Leading–order solution 17

2.2 An axisymmetric fibre 19

2.3 General comments 20

2.4 Solution of the Trouton Model 22

2.4.1 Can the fibre break ? 24

2.5 Extensions to the Trouton model 25
2.5.1 A two–dimensional sheet with inertia, surface tension and gravity 25
2.5.2 An axisymmetric viscous fibre with inertia, surface tension and gravity 28
2.5.3 The break–up of a two–dimensional sheet with surface tension 32
2.5.4 The twisting of an axisymmetric fibre 34
2.6 Conclusions 35

3 Short timescale analyses **37**

3.1 Two–dimensional Stokes flow 38
3.1.1 Timescale L/U 38
3.1.2 Timescale $\epsilon^2 L/U$ 38
3.1.3 Large displacements 40
3.1.4 Summary 43
3.2 Inertia effects 44
3.2.1 $Re = O(1)$ 44
3.2.2 $Re = O(\epsilon^2)$ 45
3.2.3 $Re = O(\epsilon^4)$ 47
3.2.4 Summary 48
3.3 Short lengthscales and timescales 48
3.4 Conclusions 51

4 Nonaxisymmetric viscous fibres **52**

4.1 Equations of motion and boundary conditions 53
4.2 Fibres with low surface tension 56
4.2.1 Leading–order equations 56
4.2.2 Motion of the centre–line 59

4.2.3 Rotation of the fibre 60
4.2.4 Lagrangian description 60
4.2.5 Example — fibres with elliptical cross–section 63
4.3 Fibres with higher surface tension 65
4.3.1 A fibre with circular cross–section 69
4.4 The quasi–two–dimensional sintering problem 71
4.4.1 The coupling of two equal cylinders 76
4.4.2 The twisting problem 77
4.5 Conclusions 78

5 Highly curved viscous fibres **79**
5.1 Geometrical Preamble 80
5.1.1 Modified Serret–Frenet coordinates 80
5.1.2 Velocity of the centre–line 82
5.2 The Stokes equations and boundary conditions 82
5.3 Nondimensionalisation and scaling 84
5.4 Leading–order equations 84
5.5 Integrated equations 87
5.6 Rotated coordinates 88
5.7 The "viscida" equation 90
5.8 Higher order body forces 90
5.9 Conclusions 92
5.9.1 Relation with nearly straight fibres 93

6 The dynamics of nearly planar viscous sheets **94**
6.1 The viscous sheet equations 95
6.2 A model for the float glass process 97
6.2.1 The float glass equations 98

6.2.2 Edge conditions 99
6.3 One–dimensional approximation 103
6.3.1 Steady state solution 104
6.3.2 Neglecting gravity 105
6.4 Transverse motion of a viscous sheet 105
6.4.1 The Stokes equations and boundary conditions 106
6.4.2 Uniform thickness 108
6.5 Surface tension and inertia 109
6.6 Conclusions 110

7 The dynamics of curved viscous sheets 111

7.1 Geometrical preamble 112
7.1.1 Setting up the coordinate system 112
7.1.2 Velocity of the centre–surface 113
7.2 The Stokes equations and boundary conditions 114
7.3 Nondimensionalisation and scaling 116
7.4 Leading–order equations 116
7.5 The "viscous shell" equations 119
7.6 The axisymmetric "bottle" 121
7.6.1 The two–dimensional circular bottle 122
7.6.2 The spherical bottle 123
7.7 The dynamics of a two–dimensional curved sheet 124
7.7.1 The two–dimensional "bottle" 125
7.7.2 Asymptotic behaviour of a two–dimensional bottle 127
7.8 Surface tension effects 129
7.8.1 A two–dimensional bottle with surface tension 129
7.9 Inertia effects 130

7.10 Conclusions 133

8 The Trouton ratio: 3 or 4 ? 136

8.1 A hollow axisymmetric fibre 137

8.2 A flat sheet with variable tension at its edge 139

8.3 The Trouton ratio 141

9 Conclusions 142

9.1 Summary of results 142

9.2 Future Work 145

9.3 Discussion 146

References 148

List of Figures

1.1 A draw–down fibre manufacturing process 6

1.2 A tapering optical fibre 6

1.3 An optical fibre coupler manufacturing process 7

1.4 The float glass process, viewed from above 8

1.5 A windscreen manufacturing process 9

1.6 A bottle blowing process 10

2.1 A two-dimensional sheet of fluid 15

2.2 An axisymmetric fibre 19

2.3 The radius of a stretching fibre with surface tension 30

2.4 The formation of a cusp in an axisymmetric fibre 31

4.1 Definition sketch for a slender fibre 55

4.2 The twisting of a uniform elliptic fibre 65

6.1 Plan view of the edge of a glass ribbon 100

6.2 Normal forces at the edge of a glass ribbon 101

7.1 Configuration for a two–dimensional bottle 125

7.2 The sheet radius as a function of its length 126

7.3 Phase plane for a circular sheet with inertia 132

7.4 An inflating balloon 135

8.1 Definition sketch for a hollow axisymmetric fibre 137
8.2 Definition sketch for a slender sheet 140

Chapter 1

Introduction

1.1 Overview

This thesis is concerned with the dynamics of slender sheets and threads of viscous fluid. It is motivated by such industrial processes as the manufacture of optical fibres , the "Float Glass" process for the production of plate glass and the working of thin layers of glass, for example when making bottles or windscreens. Such technologies are widely used and increasingly important, and a full understanding of the fluid mechanics of the underlying physical processes is required in order to devise more efficient production methods and reduce wastage and redundancy.

The processes listed above have two broad properties in common. Firstly, the fluid geometry is slender, enabling the use of asymptotic perturbation schemes based on the inverse aspect ratio, a technique similar to that used in lubrication theory. Secondly, in these flows most of the surface of the fluid is free; the fluid is often free to move as a whole, restricted only by boundary conditions applied at its edges. This means that the fluid geometry is not known in advance, and these problems are potentially far more complex than those encountered in lubrication theory.

We model the fluid as Newtonian and incompressible, though many of the equations we derive may easily be extended to allow for more complicated rheology. We consider the effects of viscosity, inertia, gravity and surface tension; the relative magnitude of these effects dictates the character of the resultant flow. Our aim in

each case is, by a systematic perturbation scheme, to simplify the Navier-Stokes equations with appropriate free-surface conditions, thereby deriving a considerably reduced system of equations. In many of the flows we examine, it is necessary to consider different length– and timescales over which different physical effects are important.

In the remainder of this chapter we first give short descriptions of some of the industrial processes by which this work is motivated, then we review briefly some of the related work which has been carried out by other authors.

In chapter 2 we introduce the basic asymptotic methods which will be applied throughout this thesis, while considering two very simple examples: a slender two–dimensional sheet and a slender axisymmetric fibre. We show that in each case the leading–order flow is governed by the so–called "Trouton model", and describe how this model may be solved using Lagrangian variables. We also show how the model may be generalised in these two very simple geometries to include such effects as inertia, surface tension, gravity and twisting.

One of the interesting findings of chapter 2 is that a slender inertia–free two–dimensional sheet which is put under tension by pulling its ends apart is forced to be straight to leading order. In chapter 3 we show that, by consideration of a suitable short timescale, we can obtain equations describing the evolution of an initially curved sheet as it straightens under tension or buckles under compression. We find that inertia effects cannot be ignored, even when the Reynolds number is relatively small, and that in the buckling case they result in the introduction of a new dominant lengthscale which depends on the size of the Reynolds number.

In chapter 4 we show how the models derived in chapter 2 for axisymmetric fibres may be generalised to describe nonaxisymmetric fibres. This work constitutes an extension of the work of Dewynne, Ockendon & Wilmott (1992), who performed a similar analysis while neglecting inertia, surface tension and gravity. We discuss two important regimes: one in which surface tension effects can be ignored entirely to leading order and another in which surface tension plays an important part in the evolution of the shape of the cross–section of the fibre. In the former case, we

find that the ideas introduced in Dewynne, Ockendon & Wilmott (1992) can be followed fairly closely, while in the latter analytical progress is much more difficult. In particular, in the latter case we show how the cross–section may be described by means of a conformal map which depends on time and distance along the fibre, an idea similar to that used by Hopper (1990) and Richardson (1992) when considering two–dimensional sintering.

The analysis of chapter 4 is all based on the assumption that the fibre is nearly straight, that is, that its dimensionless curvature is of the same order as its inverse aspect ratio. This means that a fixed Cartesian coordinate system can be used. In chapter 5, we derive models for fibres whose dimensionless curvature is of order one, by using curvilinear coordinates fixed in the fibre. We consider two regimes: one in which body forces are small or nonexistent, and one in which they are much larger. In the former case we find that the leading–order equations of motion are similar to the equations governing the equilibrium of a slender linearly elastic rod, while in the latter case, they are more akin to the equations for a catenary.

In chapter 6 we show how the equations for a two–dimensional sheet derived in chapter 2 can be generalised to describe a sheet which varies in two directions. We apply the equations so obtained in deriving a fully two–dimensional model, and then a simplified one–dimensional model, for the float glass process. We also show how transverse motion of a viscous sheet may be described by a model which is analogous to the von Kármán equations of linear elasticity.

As in the theory of fibres, rather different models result depending on whether the sheet is assumed nearly flat (so that its dimensionless curvatures are of the same order as its inverse aspect ratio) or not. In chapter 7 we derive models for sheets whose dimensionless curvatures are of order one, by employing curvilinear coordinates fixed in the sheet. The model which results bears a strong similarity to the shell equations of linear elasticity. In general these equations are very hard to solve, particularly as, in contrast with the corresponding theory in elasticity, the geometry of the sheet is not known in advance. However, we consider exact solutions which can be found in certain simplified geometries in order to make conjectures about the likely behaviour of more general solutions.

In chapter 2 we will see that, though a two–dimensional sheet and an axisymmetric fibre both satisfy the Trouton model, there is one important difference between the two. If the viscosity of the fluid is μ, then the ratio between the tension in a two–dimensional sheet and its rate of extension is 4μ times its thickness, while the same ratio for an axisymmetric fibre is 3μ times its cross–sectional area. This difference is quantified by the so–called "Trouton ratio", which is 4 for a two–dimensional sheet and 3 for an axisymmetric fibre. In chapter 8 we employ models derived from those in the previous chapters in order to explain in some detail this change from 4 to 3.

Finally, in chapter 9 we draw conclusions and discuss the implications of the work in this thesis, as well as noting future related work which should be carried out.

Though models for axisymmetric viscous fibres have been studied extensively, many of the models for more complicated geometries are derived in this thesis for the first time. These include the "twisting" equations at the end of chapter 2, the quantification of inertia effects on centre–line stability in chapter 3, the effect of surface tension on the evolution of the cross–sectional shape of a fibre in chapter 4, the "viscous rod" equations of chapter 5 and the "viscous shell" equations of chapter 7. New solutions of these models have deliberately been confined to a few simple special cases; our principal aim in this thesis is to establish a consistent and unified theory for slender viscous flows in many different geometries, similar to the well–established theory of rods, plates and shells in linear elasticity. With this aim in mind, it is important that our models are all derived systematically from the underlying Navier–Stokes equations[1].

Other novel, but more technical work in this thesis includes our extension of the work of Richardson (1992) on two–dimensional sintering to allow for slowly–varying three–dimensional effects and the solution via a Lagrangian description of the Trouton model in chapter 2. This Lagrangian description is found to simplify many more complicated models also, enabling us to obtain new asymptotic results concerning the break–up of viscous fibres due to surface tension and the dependence

[1]Unfortunately, such a systematic approach is rarely adopted in solid mechanics !

of the blow–up of a viscous sheet under an applied pressure drop upon nonuniformities in its thickness.

1.2 Relevant industrial processes

In this section we will describe briefly some industrial processes to which the theory of the following chapters may be applicable. Our examples are drawn exclusively from the glass industry. Glass processes are particularly amenable to our methods as glass is modelled very well as an incompressible Newtonian fluid, albeit with a viscosity that depends dramatically on its temperature. However, it is likely that the models that we shall derive will have applications in many other industries also.

The material properties of glass, as noted above particularly its viscosity, depend principally upon its composition and its temperature. The viscosity may typically vary anywhere from 10^2 to 10^8 N s m^{-2}, while the density and surface tension are typically of the order of 10^3 kg m^{-3} and 10^{-1} N m^{-1} respectively.

1.2.1 Manufacture of Optical Fibres

Optical fibres are manufactured by a variety of means, including the collapse of doped cylinders of heated glass under the action of surface tension, and the draw-down of doped glass cylinders under the action of gravity. While a draw-down technique may effectively be modelled as a steady state process, with fluid continuously fed in at one end and drawn off at the other (see figure 1.1), other processes are inherently unsteady. For example fibre tapering is a process typically performed by heating a length of optical fibre and simply pulling its ends apart (see figure 1.2).

The dimensions of the fibres and details of the dynamics of these processes can vary considerably. However, a reasonable lengthscale to consider is of the order of tens of millimetres, while a typical diameter for an optical fibre is of the order of a hundred microns, so that a typical inverse aspect ratio is around 10^{-3}. The

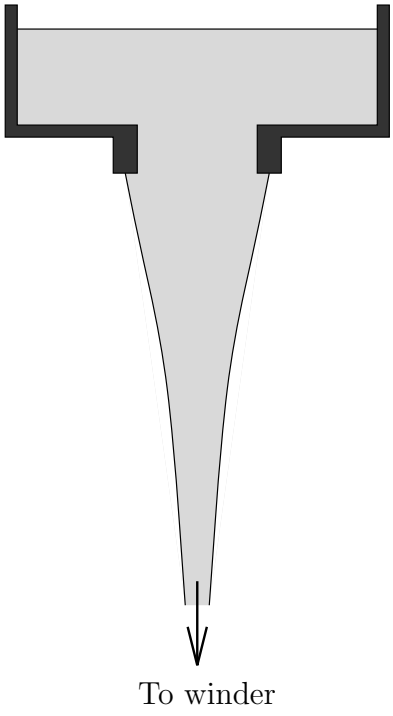

Figure 1.1: A draw–down fibre manufacturing process

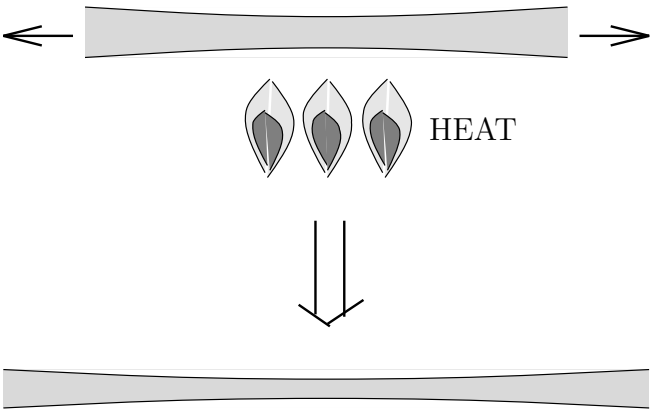

Figure 1.2: A tapering optical fibre

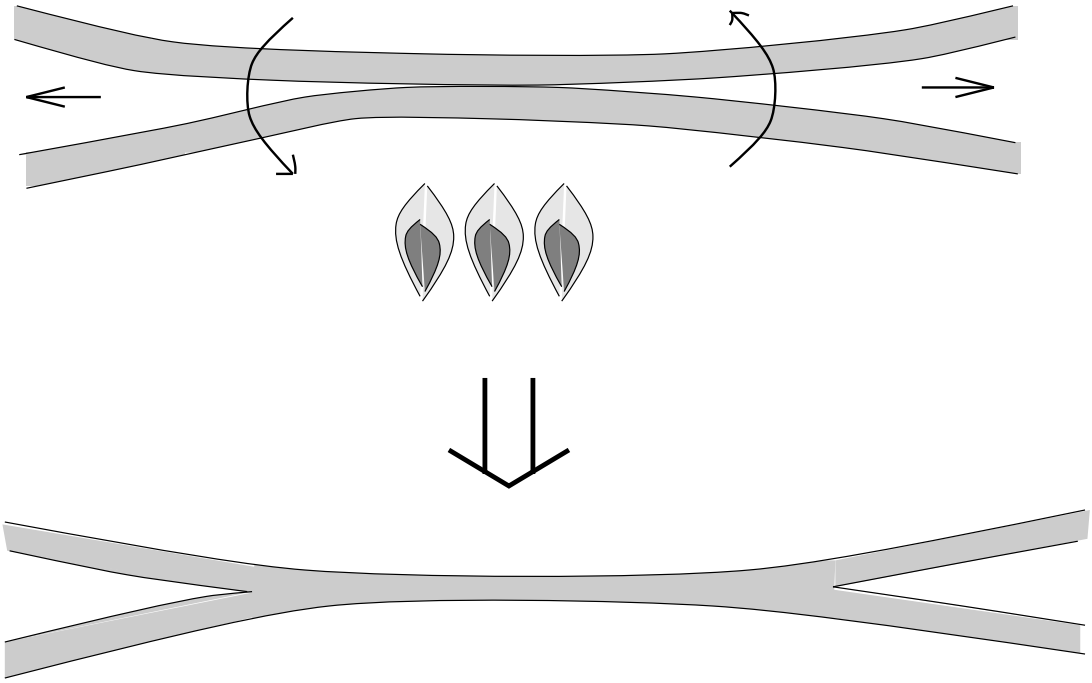

Figure 1.3: An optical fibre coupler manufacturing process

drawing speed may vary from millimetres per second for a tapering process to tens of metres per second for a draw–down process. See Rawson (1974) for more details.

1.2.2 Manufacture of Optical Fibre Couplers

Optical fibre couplers allow signals carried by several different optical fibres to interact. Typically, they are produced by joining two or more optical fibres which are then heated, twisted and/or stretched; this causes them to sinter together under the action of surface tension. A sketch of such a process involving two fibres is given in figure 1.3. The basic dimensions and other scalings are similar to those outlined above for fibre tapering, but in this coupling process the effects on the dynamics of the shape of the cross–section as it evolves become an important issue; such effects are currently little understood.

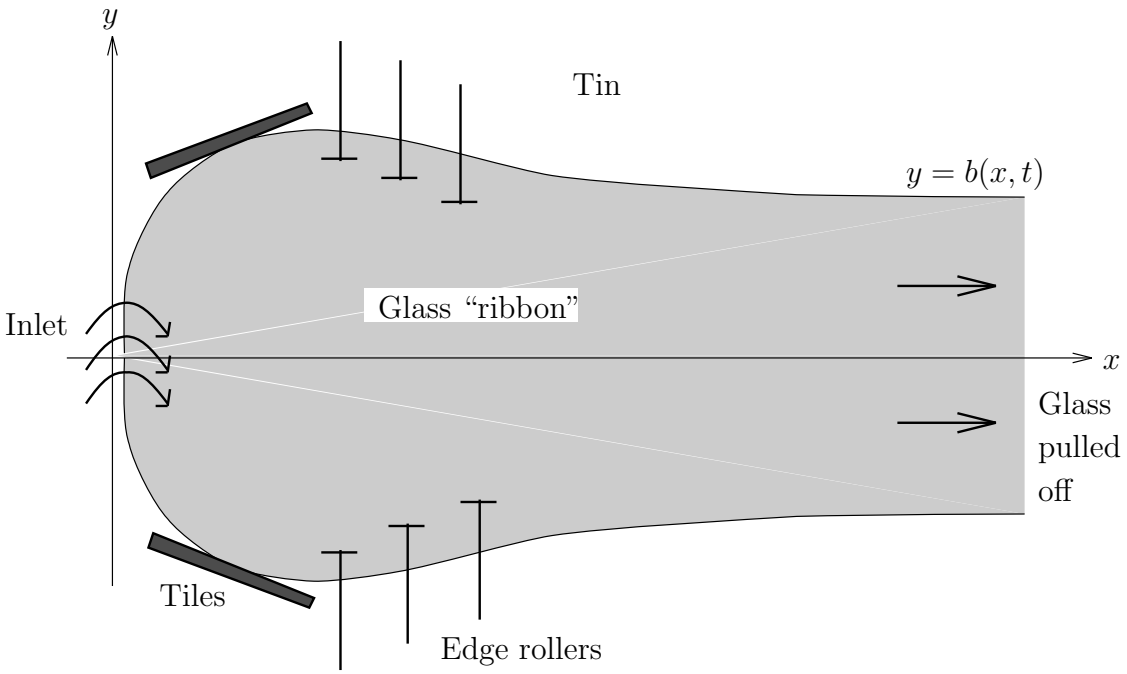

Figure 1.4: The float glass process, viewed from above

1.2.3 The float glass process

The float glass process is currently the most commonly used method for the manufacture of plate glass. The process consists of floating a thin sheet of molten glass on a bath of denser molten tin. This has been found to result in smooth, flat sheets which are desirable in many glass applications. However such a glass sheet will spread under the action of gravity only until it reaches an equilibrium thickness of approximately five millimetres at which the spreading effect of gravity is exactly balanced by surface tension forces acting inwards at the edge of the sheet. In order to make thinner sheets, the glass is *stretched* by the combined action of rollers at the edge of the glass "ribbon" and the pulling of the glass as it comes off as a solid sheet (see figure 1.4, or for a side view, figure 6.2).

The temperature (and hence the viscosity) of the glass is determined by controlling the temperature of the tin along the length of the bath. Typically, when the glass is poured on its viscosity is around 10^5 N s m^{-2} so that it is able to spread out uniformly. The viscosity is then varied along the bath in order to facilitate the most efficient stretching, reaching around 10^{11} N s m^{-2} as the glass sheet is removed from

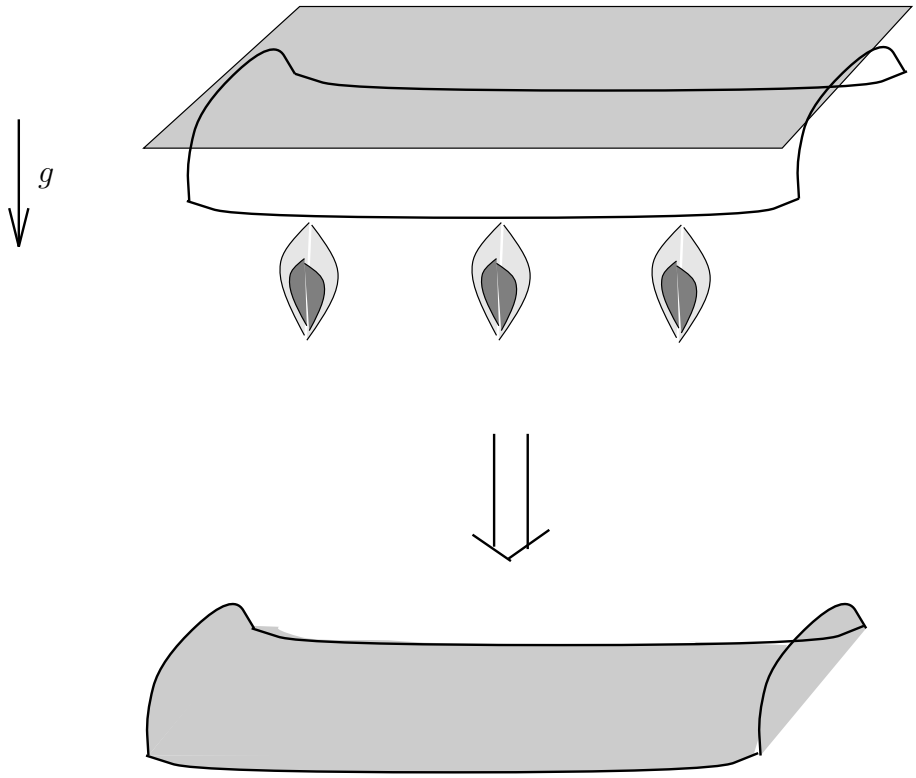

Figure 1.5: A windscreen manufacturing process

the bath.

A typical float bath is of the order of ten metres wide and hundreds of metres long. As mentioned above, a typical thickness of the glass ribbon is around 5 mm, so that the inverse aspect ratio may be taken to be of the order of 10^{-3} or smaller. A typical drawing–off speed is of the order of tens of metres per second. See Narayanaswamy (1977) or Edge (1992) for more details.

1.2.4 Manufacture of Windscreens

When forming windscreens it is sometimes necessary to do so without making contact with the glass, in order not to spoil its optical properties. A common technique consists of placing a glass sheet over a frame, then heating it and letting it "sag" under gravity until it reaches the desired shape (see figure 1.5). The problem of predicting how the glass should be heated in order to achieve a particular shape is extremely difficult, and a systematic simplified mathematical theory for this kind

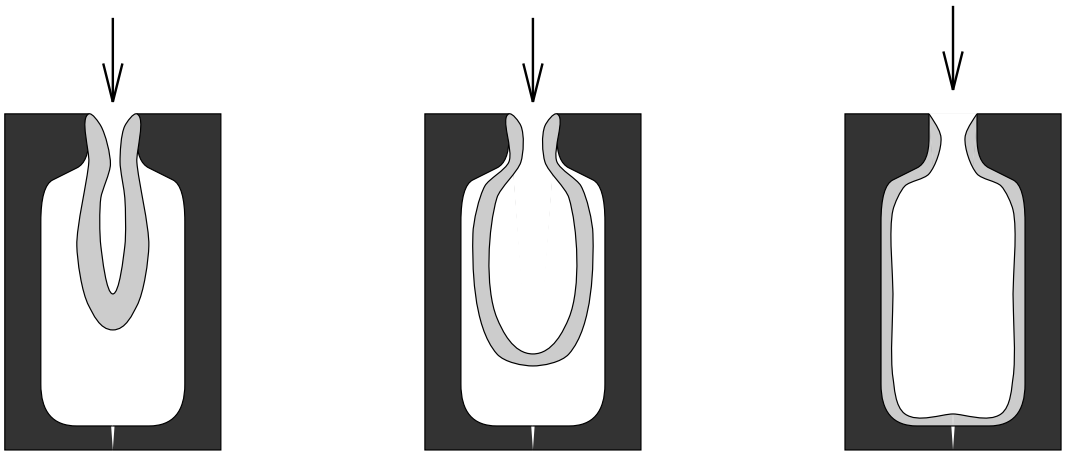

Figure 1.6: A bottle blowing process

of flow is still not available.

1.2.5 Glass Blowing

Bottles and other containers are often made by blowing hot glass into a mould, as depicted schematically in figure 1.6. In fact, many bottles go through two independent blowing stages during the course of their manufacture, the first resulting in a rough "parison" which is then blown to form the final bottle. As in windscreen manufacture, the temperature distribution in the glass is crucial to the quality of the product. Traditionally, this has been determined by trial and error; more recently finite–element codes have been used. However, little progress has been made analytically.

A typical lengthscale for one of these processes is of the order of tens of millimetres, while the thickness of the glass is of the order of millimetres, so the inverse aspect ratio may be taken to be around 10^{-1}. The viscosity of the glass may vary from around 10^2 to 10^8 N s m^{-2} during the process. As it is blown, the glass is subjected to a pressure drop of the order of 10^5 Pascals, and this induces it to move at a speed of the order of hundreds of millimetres per second. See Graham (1987) for more details.

Process	ϵ	Re	Ca	St
Fibre tapering	$\sim 10^{-3}$	$\sim 10^{-7}$	$\sim 10^{3}$	$\sim 10^{-2}$
Fibre draw–down	$\sim 10^{-3}$	$\sim 10^{-3}$	$\sim 10^{7}$	$\sim 10^{-6}$
Float glass	$\leq 10^{-3}$	$\sim 10^{-8}$ – 10^{-2}	$\sim 10^{3}$ – 10^{10}	$\sim 10^{-2}$ – 10^{2}
Windscreen sagging	$\sim 10^{-3}$	$\sim 10^{-4}$ – 10^{-2}	$\sim 10^{8}$	$\sim 10^{-3}$
Bottle blowing	$\sim 10^{-1}$	$\sim 10^{-9}$ – 1	$\sim 10^{3}$	$\sim 10^{-1}$

Table 1.1: Typical dimensionless parameter values for some glass processes

1.2.6 Dimensionless parameters

In the processes described above, the dimensionless parameters that determine the importance of inertia, surface tension and gravity effects relative to viscous stresses in the glass are the Reynolds number, capillary number and Stokes number. We shall denote by L a typical lengthscale for the process, by ϵ a typical inverse aspect ratio, by U a typical stretching speed, and by μ, ρ and γ the viscosity, density and surface tension of the glass respectively. Then the above parameters are given by

$$Re = \frac{\rho U L}{\mu} \quad , \quad Ca = \frac{\mu U}{\gamma} \quad , \quad St = \frac{\rho L^2 g}{\mu U} \quad ,$$

where g is the acceleration due to gravity. We summarise some approximate values of ϵ, Re, Ca and St for these various processes in table 1.1.

1.3 Literature review

There is a large body of literature on the flow of slender viscous jets, mostly devoted to the modelling of optical or synthetic fibre draw–down. The most common approach is to assume the jet is straight and possesses axisymmetry; equations for the cross–sectional area and axial velocity may then be derived with relative ease via either heuristic mass– and force–balances coupled with physically plausible assumptions or systematic asymptotic reduction of the underlying equations of motion and free surface conditions.

Trouton (1906) derived by heuristic means equations for the steady–state extrusion of a purely viscous fibre under gravity. His name is given to the simplest and most well–known model for fibre tapering, a time–dependent model in which only

viscous stresses are considered. This model was derived, for example, by Geyling (1976), who also included inertia and surface tension effects as perturbations to a simple steady state. This approach is common in the literature: draw–down is essentially a steady–state process and time–dependence need only be considered when determining the stability of a particular steady state. For example, Matovich & Pearson (1969) extended the steady–state Trouton model to include surface tension and non–Newtonian effects, and Pearson & Matovich (1969) investigated the linear stability of the resulting systems. The latter demonstrated the possibility of instability in the free surface, leading to the phenomenon of "draw resonance", while Shah & Pearson (1972) amd Geyling & Homsy (1980) incorporated the effects of heat transfer. Schultz & Davis (1982) also considered steady draw–down.

Dewynne, Ockendon & Wilmott (1989) obtained the general solution of the Trouton model for time–dependent purely viscous flow, and Dewynne, Ockendon & Wilmott (1992) derived the equations for the extension and twist of a purely viscous nonaxisymmetric fibre. Dewynne, Howell & Wilmott (1994) generalised this to include the effects of inertia and gravity. Non–Newtonian jets with elliptical cross–sections have been considered by Bechtel, Forest, Holm & Lin (1988) and Bechtel & Lin (1988), while Bechtel, Bolinger, Cao & Forest (1994) derived models for the stretching and twisting of non–Newtonian axisymmetric fibres.

Taylor (1969) described an experiment wherein a thread of viscous fluid was floated on mercury and caused to buckle by pushing its ends together. Buckmaster, Nachman & Ting (1975) explained this behaviour via a model for purely two–dimensional Stokes flow, and found that the initial stages of buckling occur over a timescale much shorter than the "stretching" timescale used in the tapering and draw–down models outlined above. Wilmott (1989) applied analogous equations to the stretching of a two–dimensional viscous sheet. Benjamin & Mullin (1988) discussed another experiment reported in Taylor (1969) in which a thin layer of viscous fluid was subjected to shear and hence made to buckle.

A simple, one–dimensional model of the float glass process was presented by Narayanaswamy (1977). A fully two–dimensional model including inertia effects was analysed using finite–element methods by Motoichi & Hiroshi (1991). An

overview of the history of the process and the principal problems involved may be found in Edge (1992).

Finite–element methods were applied to the blowing of thin viscous layers into bottle moulds by Graham (1987), Burley & Graham (1991) and Graham, Burley & Carling (1992). Other references may be found in these papers. A related problem, namely that of a lamella driven by a pressure drop through a capillary tube, has been modelled by Ida & Miksis (1994).

Chapter 2

The "Trouton" model

In this chapter we discuss the simplest model for extensional viscous flows. In doing so we aim both to illustrate the asymptotic techniques which will be employed throughout this thesis and to indicate the important features of this very simple model which will recur in many of the more complicated models to follow.

In section 2.1 we consider the stretching of a two–dimensional viscous sheet, neglecting inertia and all forces except the viscous stresses in the fluid. We perform asymptotic analysis of the Stokes equations and thereby derive a pair of coupled partial differential equations governing the sheet thickness and the fluid velocity, often referred to as the *Trouton model*, along with a decoupled equation for the centre–line of the sheet.

In section 2.2 we show how the Trouton model also applies to the stretching of an axisymmetric viscous fibre, with a change in the so–called "Trouton ratio" from 4 in the two–dimensional case to 3 in the axisymmetric case.

We discuss the solution of the Trouton model in section 2.4 and describe some ways in which the model may be extended in section 2.5. Finally, we draw conclusions from the whole chapter in section 2.6.

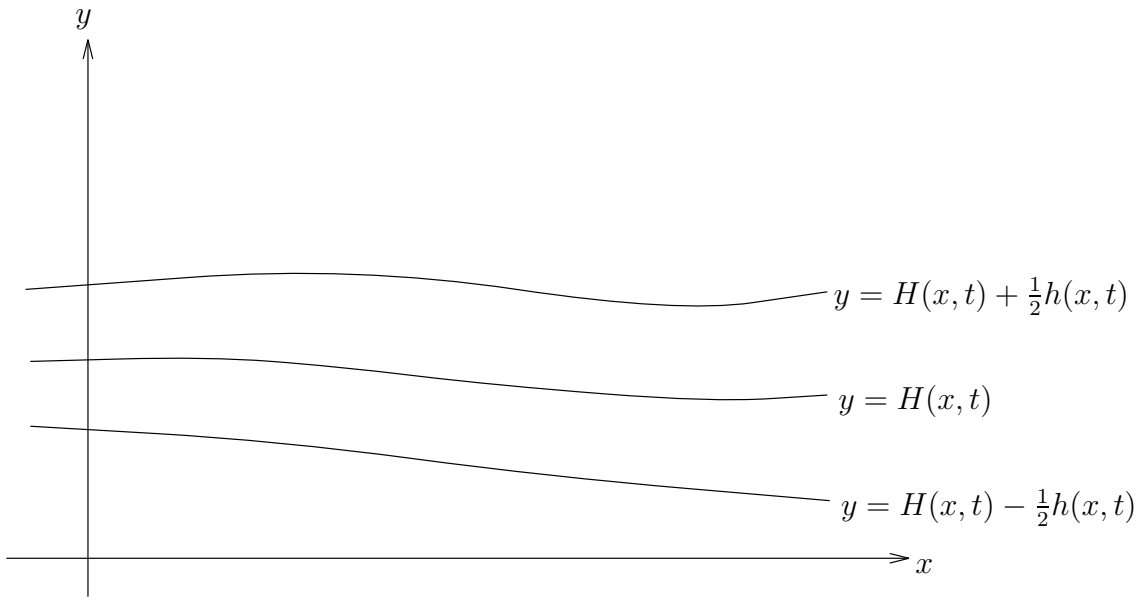

Figure 2.1: A two-dimensional sheet of fluid

2.1 A two–dimensional sheet

We consider the two–dimensional slow flow of a Newtonian fluid of constant viscosity, between two free surfaces given by $y = H(x,t) - \frac{1}{2}h(x,t)$ and $y = H(x,t) + \frac{1}{2}h(x,t)$ (see figure 2.1). Thus $H(x,t)$ is the equation of the centre–line of the sheet, and $h(x,t)$ is its thickness. We suppose that the sheet is slender and that its centre–line is almost straight. Thus if L is a typical length in the x-direction, $H/L \ll 1$ and $h/L \ll 1$. The flow is governed by the two-dimensional Stokes equations.

$$u_x + v_y = 0, \tag{2.1}$$

$$p_x = \mu(u_{xx} + u_{yy}), \tag{2.2}$$

$$p_y = \mu(v_{xx} + v_{yy}). \tag{2.3}$$

On the two free surfaces we have the kinematic condition, and the condition of zero stress.

$$v = H_t \pm \tfrac{1}{2}h_t + u\left(H_x \pm \tfrac{1}{2}h_x\right) \quad \text{on } y = H \pm \tfrac{1}{2}h, \tag{2.4}$$

$$(-p + 2\mu u_x)\left(H_x \pm \tfrac{1}{2}h_x\right) = \mu(u_y + v_x) \quad \text{on } y = H \pm \tfrac{1}{2}h, \tag{2.5}$$

$$\mu(u_y + v_x)\left(H_x \pm \tfrac{1}{2}h_x\right) = (-p + 2\mu v_y) \quad \text{on } y = H \pm \tfrac{1}{2}h. \tag{2.6}$$

Suitable initial and boundary conditions for these equations are: given H and h at $t = 0$, and given u and v at the two ends of the sheet.

2.1.1 Nondimensionalisation and scaling

We suppose that typical lengths and velocities for the flow are L and U in the x-direction, and ϵL and ϵU in the y-direction, where $\epsilon \ll 1$. We consider a time-scale over which the fluid is moved a distance of order L in the x-direction, i.e. L/U. Thus we nondimensionalise as follows.

$$\begin{aligned} x = Lx', \quad & y = \epsilon L y', \\ u = Uu', \quad & v = \epsilon U v', \\ H = \epsilon L H', \quad & h = \epsilon L h', \\ t = (L/U)t', \quad & p = (\mu U/L)p'. \end{aligned}$$

This yields the nondimensional, scaled equations (dropping primes)

$$u_x + v_y = 0, \tag{2.7}$$

$$\epsilon^2 p_x = \epsilon^2 u_{xx} + u_{yy}, \tag{2.8}$$

$$p_y = \epsilon^2 v_{xx} + v_{yy}, \tag{2.9}$$

$$v = H_t \pm \tfrac{1}{2}h_t + u\left(H_x \pm \tfrac{1}{2}h_x\right) \quad \text{on } y = H \pm \tfrac{1}{2}h, \tag{2.10}$$

$$\epsilon^2(-p + 2u_x)\left(H_x \pm \tfrac{1}{2}h_x\right) = u_y + \epsilon^2 v_x \quad \text{on } y = H \pm \tfrac{1}{2}h, \tag{2.11}$$

$$(u_y + \epsilon^2 v_x)\left(H_x \pm \tfrac{1}{2}h_x\right) = -p + 2v_y \quad \text{on } y = H \pm \tfrac{1}{2}h\ . \tag{2.12}$$

2.1.2 Asymptotic expansions

We seek solutions in the form of asymptotic expansions in powers of the small parameter ϵ^2:

$$u \sim u_0 + \epsilon^2 u_1 + \epsilon^4 u_2 + \ldots, \quad v \sim v_0 + \epsilon^2 v_1 + \epsilon^4 v_2 + \ldots, \quad \textit{etc.}$$

We substitute these into equations (2.7) to (2.12) and equate like powers of ϵ^2.

2.1.3 Leading–order solution

The only $O(1)$ term in equation (2.8) reveals that

$$u_{0_{yy}} = 0,$$

with the boundary conditions from (2.11)

$$u_{0_y} = 0, \quad \text{on } y = H_0 \pm \tfrac{1}{2}h_0.$$

This problem for u_0 is homogeneous, and admits the nonunique eigensolution

$$u_0 = u_0(x,t), \tag{2.13}$$

that is, the axial velocity is uniform across the sheet; this type of flow is termed *extensional*. The transverse velocity may then be found from (2.7) :

$$v_0 = f(x,t) - yu_{0_x},$$

where the arbitrary function f is found using the kinematic boundary condition (2.10), which gives

$$f(x,t) = H_{0_t} \pm \tfrac{1}{2}h_{0_t} + \left[u_0\left(H_0 \pm \tfrac{1}{2}h_0\right)\right]_x.$$

Hence

$$v_0 = H_{0_t} + (u_0 H_0)_x - yu_{0_x}, \tag{2.14}$$

and we obtain a relation between u_0 and h_0

$$h_{0_t} + (u_0 h_0)_x = 0, \tag{2.15}$$

which represents conservation of mass. The leading–order pressure may be found from (2.7), (2.9) and (2.12),

$$p_0 = -2u_{0_x}, \tag{2.16}$$

so that the leading–order dimensionless axial stress

$$(\sigma_{xx})_0 = -p_0 + 2u_{0_x} = 4u_{0_x}. \tag{2.17}$$

We now have to consider the $O(\epsilon^2)$ terms in the expansions in order to derive a closed system of equations for the leading–order variables $h_0(x,t)$, $u_0(x,t)$ and $H_0(x,t)$. Equation (2.8) gives

$$u_{1_{yy}} = -3u_{0_{xx}}$$

with boundary conditions from (2.11)[1],

$$u_{1_y} = 4u_{0_x}\left(H_{0_x} \pm \tfrac{1}{2}h_{0_x}\right) - H_{0_{xt}} - (u_0H_0)_{xx} + u_{0_{xx}}\left(H_0 \pm \tfrac{1}{2}h_0\right) \quad \text{on } y = H_0 \pm \tfrac{1}{2}h_0.$$

Note that in this problem for u_1, the operator is the same as that in the problem for u_0, though in this case there is an inhomogeneous right–hand side. As there exist eigenfunction solutions for u_0, the Fredholm alternative implies that no solutions for u_1 will exist unless an orthogonality condition is satisfied. In this case it is trivial to note that

$$\int_{H_0-\frac{1}{2}h_0}^{H_0+\frac{1}{2}h_0} u_{1_{yy}}\, dy = \left[u_{1_y}\right]_{H_0-\frac{1}{2}h_0}^{H_0+\frac{1}{2}h_0}$$

and hence

$$(4h_0u_{0_x})_x = 0, \tag{2.18}$$

which represents an axial force balance. We can then solve for u_{1_y}, giving

$$u_{1_y} = [4H_0u_{0_x} - H_{0_t} - (u_0H_0)_x]_x - 3yu_{0_{xx}}. \tag{2.19}$$

Then (2.7) gives

$$v_{1_{yy}} = [H_{0_t} + (u_0H_0)_x - 4H_0u_{0_x}]_{xx} + 3yu_{0_{xxx}}, \tag{2.20}$$

(2.9) gives

$$p_{1_y} = [2H_{0_t} + 2(u_0H_0)_x - 4H_0u_{0_x}]_{xx} + 2yu_{0_{xxx}}, \tag{2.21}$$

and the boundary condition (2.12) reveals

$$-p_1 + 2v_{1_y} = 4\left(H_{0_x} \pm \tfrac{1}{2}h_{0_x}\right)\left[(H_0u_{0_x})_x - u_{0_{xx}}\left(H_0 \pm \tfrac{1}{2}h_0\right)\right] \quad \text{on } y = H_0 \pm \tfrac{1}{2}h_0.$$

Then integration of $-p_{1_y}+2v_{1_{yy}}$ between the two free surfaces gives a third leading–order equation, which reduces to

$$(4h_0u_{0_x}H_{0_x})_x = 0, \tag{2.22}$$

[1]Note that we have omitted the identically zero term which arises from the expansion of H and h, namely $u_{0_{yy}}(H_1 \pm \frac{1}{2}h_1)$. In general, terms of this type must be included.

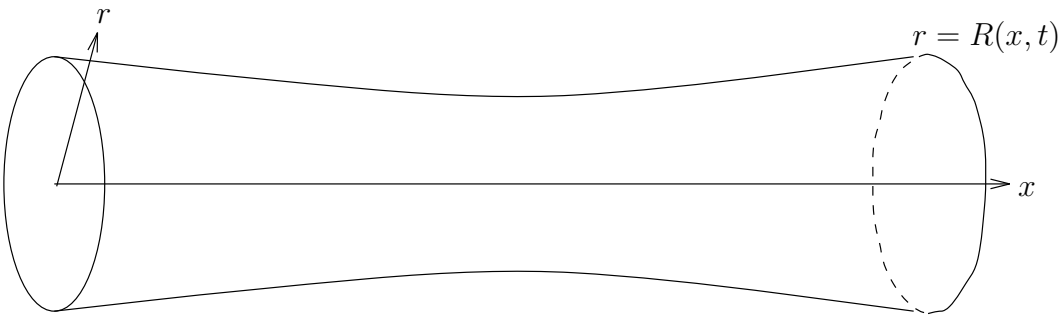

Figure 2.2: An axisymmetric fibre

a lateral force balance.

We have left the factor 4 in (2.18) and (2.22) to emphasise the so–called "Trouton ratio" which is 4 for a two–dimensional Newtonian sheet. The significance is that $4h_0u_{0_x}$ is the leading–order dimensionless tension in the sheet (see equation (2.17)). We shall see later how this ratio depends crucially on the geometry under consideration.

Equations (2.15) and (2.18) form a hyperbolic system for the sheet thickness and the axial velocity, often known as the *Trouton Model*. Their solution is discussed in section 2.4.

Equations (2.18) and (2.22) tells us that so long as the tension in the sheet is nonzero, the sheet's centre–line is straight to leading–order, and without loss of generality[2], we may take

$$H_0 = 0. \tag{2.23}$$

2.2 An axisymmetric fibre

We now consider the motion of a slender, axisymmetric, inertia–free viscous fibre. The fibre may best be described using cylindrical polar coordinates: we take the x-axis to lie along the axis of the fibre and denote by r the radial distance from this axis, which we assume to be much less than a typical length in the x-direction. See

[2]This is because of the property of Stokes flow with a stress–free free surface that an arbitrary rigid–body motion may be added to the flow.

figure 2.2 for a definition sketch. We denote by u and v the fluid velocities in the x- and r-directions respectively. The Stokes equations, after nondimensionalisation and scaling analogous to those employed in the previous section, may be written in the form

$$v_r + \frac{v}{r} + u_x = 0, \tag{2.24}$$

$$p_r = v_{rr} + \frac{v_r}{r} - \frac{v}{r^2} + \epsilon^2 v_{xx}, \tag{2.25}$$

$$\epsilon^2 p_x = u_{rr} + \frac{u_r}{r} + \epsilon^2 u_{xx}. \tag{2.26}$$

We describe the free surface of the fibre by $r = R(x,t)$. The dimensionless kinematic and zero–stress boundary conditions may then be written as

$$v = R_t + uR_x \quad \text{on } r = R, \tag{2.27}$$

$$-p + 2v_r = R_x(u_r + \epsilon^2 v_x) \quad \text{on } r = R, \tag{2.28}$$

$$u_r + \epsilon^2 v_x = \epsilon^2 R_x(-p + 2u_x) \quad \text{on } r = R. \tag{2.29}$$

We proceed as in the previous section to seek solutions in the form of asymptotic expansions in powers of ϵ^2; the details of the analysis may be found in Dewynne, Ockendon & Wilmott (1989). As in the last section, it is necessary to continue up to $O(\epsilon^2)$ in the expansions in order to close the leading–order equations. These are

$$A_{0_t} + (u_0 A_0)_x = 0, \tag{2.30}$$

representing conservation of mass and

$$(3A_0 u_{0_x})_x = 0, \tag{2.31}$$

an axial force balance, where $A_0 = \pi R_0^2$ is the leading–order cross–sectional radius of the fibre. As in the previous section, we have left in the Trouton ratio, which is 3 for an axisymmetric fibre.

2.3 General comments

We note the following properties of equations (2.15), (2.18) and (2.22) for a two–dimensional sheet, and (2.30) and (2.31) for an axisymmetric fibre which will crop up in many of the more complicated models to follow.

- In our theory, it is the slender region which is of interest, and the passive space in which it moves is largely ignored. There is also an interesting class of problems, in a sense complementary to those considered in this thesis, in which it is the slender region which is passive, and its effect on some larger outer flow which is of interest, see for example Morgan (1994).

- It is implicit in our nondimensionalisation and scaling that we are seeking disturbances of the free surface whose amplitude is of the same order as the thickness of the fibre or sheet, and whose wavelength is much longer. We shall be considering motions of this kind throughout this thesis, though there are other self–consistent scalings which can be employed. For example, the analysis by Benjamin & Mullin (1988), of the buckling of a layer of viscous fluid subjected to shear, is based on the assumption that disturbances to the free surfaces have a wavelength of the same order as the thickness of the fluid sheet and an amplitude which is much less. The relationship between their work and ours is very similar to the relationship between the theory of Stokes surface waves and shallow water theory in inviscid flow.

- Only even powers of ϵ appear in the nondimensionalised equations. This enables us to seek solutions which are asymptotic expansions in powers of ϵ^2, rather than powers of ϵ. We shall see in subsequent chapters that this will not always be the case.

- It is necessary to proceed to $O(\epsilon^2)$ in the asymptotic expansions in order to derive a closed system of equations for the leading–order variables. The leading–order equations and boundary conditions are homogeneous, and admit eigensolutions which are nonunique. The higher order unknowns satisfy inhomogeneous versions of the leading–order problems which, by the Fredholm alternative, will have no solutions unless certain orthogonality conditions are met. It is these solvability conditions which provide us with a closed system of equations for the leading–order unknowns.

- The Trouton ratio is 3 for an axisymmetric fibre and 4 for a two–dimensional sheet. This ratio may be thought of as the ratio between the extensional viscosity and the shear viscosity, where the extensional viscosity is the constant

of proportionality between the tension in the fibre or sheet and its rate of extension. We shall discuss this change from 3 to 4 in some detail in chapter 8.

- The leading–order equations of section 2.1 predict that the centre–line of the sheet is straight. Hence we are unable to satisfy the initial condition of a given H at $t = 0$, except in the exceptional case that the sheet is straight initially. This implies that the solution for H is a singular perturbation in t whose outer solution is $H = 0$ to leading order. In order to study the evolution of an initially curved centre–line, we must consider the inner solution for H, and hence use a timescale shorter than L/U. We shall discuss the use of shorter timescales in chapter 3.

- If the ends of the fluid sheet are not pulled apart, but are pushed together, then in theory equations (2.15), (2.18) and (2.22) should still apply. However, it is clear experimentally that in this case an initially curved centre–line certainly will not straighten, and hence equation (2.22) is false. The assumption that the centre–line is nearly straight ($H/L \ll 1$) becomes invalid before times of order L/U are achieved, so the equations of section 2.1 cease to apply. Hence it is also necessary to consider a shorter timescale in order to study the "buckling" behaviour of a fluid sheet under compression.

2.4 Solution of the Trouton Model

Consider the system

$$h_t + (uh)_x = 0, \tag{2.32}$$

$$hu_x = T(t), \tag{2.33}$$

where $T(t)$ is the tension, scaled with the Trouton viscosity. Typical initial and boundary conditions for these equations are

$$h(x, 0) = h_0(x), \tag{2.34}$$

$$u(0, t) = 0, \quad u(l(t), t) = \dot{l}(t), \tag{2.35}$$

where without loss of generality, we have assumed that one end of the fibre (or sheet) is fixed and the other end is pulled so that the fibre length is a known function $l(t)$.

Dewynne, Ockendon & Wilmott (1989) showed that a first integral of these equations may be found by a partial hodograph transformation. We choose instead to employ Lagrangian coordinates ξ and τ defined by

$$x_\tau = u(x(\xi,\tau),\tau), \quad x(\xi,0)=\xi, \quad t=\tau. \tag{2.36}$$

Then equation (2.32) gives

$$h_\tau + \frac{h}{x_\xi}u_\xi = 0,$$

which may be integrated, using the fact that $u = x_\tau$, to give

$$\frac{\partial x}{\partial \xi} = \frac{h_0(\xi)}{h(\xi,\tau)}. \tag{2.37}$$

Substitution from (2.32) into (2.33) gives an equation for h:

$$h(\xi,\tau) = h_0(\xi) - f(\tau), \tag{2.38}$$

where

$$\dot{f}(\tau) = T(\tau), \quad f(0)=0. \tag{2.39}$$

The arbitrary function f is found by specifying the length of the fibre:

$$l(\tau) = \int_0^1 \frac{h_0(\xi)\,d\xi}{h_0(\xi)-f(\tau)} \;=\; 1 + f(\tau)\int_0^1 \frac{d\xi}{h_0(\xi)-f(\tau)}. \tag{2.40}$$

Once f is known, h is given by (2.38) and x by

$$x(\xi,\tau) = \int_0^\xi \frac{h_0(\xi')\,d\xi'}{h_0(\xi')-f(\tau)}. \tag{2.41}$$

Two consequences of this analysis which were also noted by Dewynne, Ockendon & Wilmott (1989) are that the difference in thickness between any two material points of the fibre is maintained as the fibre stretches, and that the solution at any time depends only on the instantaneous length of the fibre; there is no dependence on the history of the stretching of the fibre. However, this Lagrangian description of the flow also makes it clear that at least one conjecture made by Dewynne, Ockendon & Wilmott (1989) is incorrect: the Trouton model does *not* predict the

formation of shocks when the fibre is put under compression. The two families of characteristics of the system are given by $x = \text{const.}$ and by putting $\xi = \text{const.}$ in (2.41). A shock is formed if two or more of the second family of characteristics meet at a point in the (x, t)-plane. The envelope of these characteristics is found by differentiating (2.41) with respect to ξ while holding x and τ constant, resulting in

$$\frac{h_0(\xi)}{h_0(\xi) - f(\tau)} = 0. \tag{2.42}$$

In the compression problem, f is a decreasing function of τ; (2.42) shows that the characteristics all converge as $f \to -\infty$, which corresponds to the two ends of the fibre meeting and the thickness going to infinity.

2.4.1 Can the fibre break ?

From the equation (2.40) for the length of the fibre it is immediately clear that the thickness of the fibre can never go to zero while the length remains finite unless there is a cusp in the initial thickness h_0. This has been noted by Dewynne, Ockendon & Wilmott (1989) and by Wilmott (1989). Indeed, if the initial thickness has a minimum at some point $\xi = b$ for b between 0 and 1, then $\xi = b$ will continue to be a minimum as the fibre is stretched and the asymptotic behaviour of (2.40) as $f \to h_0(b)$ shows that the minimum thickness $h_m = h(b, \tau)$ satisfies

$$h_m \sim \frac{2\pi^2 h_0(b)^2}{h_0''(b) l^2} \text{ as } l \to \infty. \tag{2.43}$$

(Compare with the case of uniform thickness, in which $h \sim 1/l$).

Now consider the more general case in which h_0 has its least value at an interior point $\xi = b$, whereat the local behaviour of h_0 is given by

$$h_0(\xi) \sim h_0(b) + |\alpha(\xi - b)|^n + o(|\xi - b|^n) \text{ as } \xi \to b, \;\; n > 0.$$

Now the asymptotic behaviour of l as the fibre becomes close to breaking depends on whether $n > 1$ (and the fibre is smooth), $n = 1$ (when h_0' is discontinuous at

$\xi = b$) or $n < 1$ (when there is a cusp in h_0 at $\xi = b$);

$$\left.\begin{aligned} n > 1, \quad & l \sim \frac{2\Gamma(1+\frac{1}{n})\Gamma(1-\frac{1}{n})h_0(b)}{\alpha} h_m^{\frac{(1-n)}{n}} + O(1) \\ n = 1, \quad & l \sim \frac{2h_0(b)}{\alpha} \log\left(\frac{1}{h_m}\right) + O(1) \\ n < 1, \quad & l \sim \int_0^1 \frac{h_0(\xi)\, d\xi}{h_0(\xi) - h_0(b)} + o(1) \end{aligned}\right\} \text{ as } h_m \to 0. \tag{2.44}$$

Hence the leading–order behaviour of the least thickness as the length becomes large is

$$h_m \sim \left(\frac{2\Gamma(1+\frac{1}{n})\Gamma(1-\frac{1}{n})h_0(b)}{\alpha l}\right)^{\frac{n}{n-1}}, \tag{2.45}$$

for $n > 1$ or

$$h_m \sim \text{const.} \exp\left(-\frac{\alpha l}{2h_0(b)}\right), \tag{2.46}$$

in the special case $n = 1$. (Note that (2.45) converges to the uniform thickness solution in the limit as $n \to \infty$). For $n < 1$ the minimum thickness becomes zero at a finite value of the length, given by

$$l_c = \int_0^1 \frac{h_0(\xi)\, d\xi}{h_0(\xi) - h_0(b)}. \tag{2.47}$$

However we should note that in the cases where the thickness is not smooth initially our equations are unlikely to be valid. This is because firstly our assumption that h_x is small used in deriving the model (see section 2.1) will be contravened, and secondly, surface tension, which we have neglected, is likely to become important in the neighbourhood of non–smooth points. We shall discuss the inclusion of surface tension and other real–fluid effects in the following section.

2.5 Extensions to the Trouton model

2.5.1 A two–dimensional sheet with inertia, surface tension and gravity

The methods of section 2.1 may be applied to the more general case when inertia, surface tension and gravity are significant, by considering the full Navier–Stokes

equations in place of the Stokes equations and applying a surface tension stress condition at the free surfaces. However, in order to proceed with the asymptotic expansions, it is necessary to prescribe the orders of magnitude of the relevant dimensionless parameters, namely the Reynolds number, capillary number and Stokes number, given by

$$Re = \frac{\rho U L}{\mu} \ , \ Ca = \frac{\mu U}{\gamma} \ , \ St = \frac{\rho L^2 g}{\mu U} \ , \tag{2.48}$$

respectively, where L and U are a typical length and velocity, ρ, μ and γ are the fluid's density, viscosity and surface tension coefficient, and g is the acceleration due to gravity.

We scale the above parameters in such a way that viscous stresses, inertia, surface tension and gravity are all balanced in the equations. In this way, as many effects as possible are incorporated in the model; situations where some effects dominate over others may then be considered by letting the appropriate parameters tend to zero or infinity as appropriate.

To this end, we suppose the Reynolds number is of order one as are the dimensionless body forces in the x- and y-directions, denoted by

$$g_x = St \cos\alpha \ , \ g_y = \frac{St}{\epsilon} \sin\alpha, \tag{2.49}$$

where α is the angle between the x-axis and the direction of gravity. The restriction that g_y be $O(1)$ may be interpreted as a measure of the relative velocity required of the two ends of the sheet in order to ensure that it is only deflected by a distance of order ϵL, namely

$$\frac{\rho g L^2 \sin\alpha}{\epsilon \mu} = O(U).$$

If α is $O(\epsilon)$ then both gravity components will be important; if it is $O(1)$ then the restriction noted above dictates that g_x be $O(\epsilon)$, and hence negligible to leading order[3]. We note that Re and St will typically be much smaller than one for most processes in the glass industry; however, the figures given in the Introduction suggest that both parameters may be non–negligible in extreme cases.

[3]Note that similar considerations apply, for example, to the well–known theory for a thin layer of viscous fluid driven by gravity down a sloping surface, namely that the normal component of gravity is negligible to leading order unless the slope is of order ϵ.

There are two scalings of potential interest for the surface tension coefficient. First, let us suppose that

$$\tilde{\gamma} = \frac{\epsilon}{Ca} = O(1). \tag{2.50}$$

Then surface tension dominates the behaviour of the centre–line; the leading–order equations give (dropping subscripts)

$$\tilde{\gamma} H_{xx} = 0. \tag{2.51}$$

(This is an example where making some of the leading–order boundary conditions inhomogeneous means that more information can be obtained from the leading–order equations.) The usual conservation–of–mass equation is also obtained,

$$h_t + (uh)_x = 0, \tag{2.52}$$

as well as an axial momentum balance with extra contributions due to surface tension, inertia and gravity,

$$(4hu_x)_x + \frac{\tilde{\gamma}}{2} h h_{xxx} = Re\, h(u_t + uu_x) - g_x h. \tag{2.53}$$

This model is valid for an extremely slender film dominated by surface tension, for example a lamella in a foam (as in Ida & Miksis (1994)). The approximate figures given in the Introduction suggest that in a glass manufacturing process the capillary number will in general be much greater than $O(\epsilon)$. Hence, if we are to model such a process we should rescale the surface tension coefficient:

$$\gamma^* = \frac{1}{\epsilon Ca} = O(1). \tag{2.54}$$

With the new scaling, the conservation–of–mass equation (2.52) is retained and the surface tension term drops out of the axial momentum balance, leaving

$$(4hu_x)_x = Re\, h(u_t + uu_x) - g_x h. \tag{2.55}$$

The behaviour of the centre–line is now given by a balance between the tension in the sheet, the inertia of the fluid, and the transverse component of gravity:

$$(Re\, hu^2 - 4hu_x - \gamma^*) H_{xx} + 2Re\, huH_{xt} + Re\, hH_{tt} = g_y h - g_x h H_x. \tag{2.56}$$

The inclusion of inertia at this order has a dramatic effect on the behaviour of the centre–line. Equation (2.56) has discriminant $Re\,h(4hu_x + \gamma^*)$ and hence is hyperbolic for $4hu_x + \gamma^* > 0$ (when the sheet is under tension) and elliptic for $4hu_x + \gamma^* < 0$ (when the sheet is under compression). This contrasts strongly with the inertia–free theory (2.22), where the centre–line behaviour is independent of the tension in the sheet, so long as the tension is nonzero.

As noted above, for most of the industrial process we shall be considering, the Reynolds number is much less than $O(1)$. However, (2.56) suggests that inertia terms will still become important when a suitable short timescale (namely $O(Re^{1/2})$) is considered. This will be discussed further in chapter 3.

2.5.2 An axisymmetric viscous fibre with inertia, surface tension and gravity

We now extend the theory of section 2.2 to take account of inertia, surface tension and gravity acting in the direction of the x-axis. As in the previous subsection we must make some assumptions about the orders of magnitude of the relevant dimensionless groups. In order to balance all the desired effects, we suppose that the Reynolds number and Stokes number are $O(1)$, as is the dimensionless surface tension coefficient

$$\gamma^* = \frac{1}{\epsilon Ca}.$$

The leading–order equations are then (dropping subscripts)

$$(R^2)_t + (uR^2)_x = 0, \tag{2.57}$$

$$(3R^2u_x)_x = Re\,R^2(u_t + uu_x) - St\,R^2 - \gamma^* R_x. \tag{2.58}$$

Of the additional effects, surface tension is the most important in many practical applications such as fibre tapering. If we neglect inertia and gravity in the above equations and rewrite them using the Lagrangian description of section 2.4 (setting $h = R^2$) we obtain

$$R_\tau = \frac{\gamma^* R - T(\tau)}{6R}, \tag{2.59}$$

$$x(\xi,\tau) = \int_0^\xi \frac{R_0^2(\xi')\,d\xi'}{R^2(\xi',\tau)}, \tag{2.60}$$

where $R_0(\xi)$ is the initial fibre radius and the arbitrary function T is found by specifying the length of the fibre

$$l(\tau) = x(1, \tau). \tag{2.61}$$

This problem may be solved numerically with relative ease; differentiation of (2.61) with respect to τ gives an expression for T in terms of the drawing speed $V = \dot{l}$,

$$T(\tau) = \frac{3V + \gamma^* \int_0^1 (R_0^2/R^3)\, d\xi}{\int_0^1 (R_0^2/R^4)\, d\xi}. \tag{2.62}$$

Hence T may be found once R is known, and then R may be updated using (2.59). The output of such a numerical scheme is shown in figure 2.3.

The most important feature which is introduced into the model by the inclusion of surface tension is the possibility that the fibre may break in finite time without an initial cusp. However it is clear from (2.60) and (2.61) that if R is to become zero for finite l, a cusp must be formed. This will now be shown to be possible by reference to a specific example in which (2.59) can be integrated.

Suppose the fibre is pulled in such a way that the tension is proportional to the minimum radius R_m, say $T = cR_m$. Then (2.59) gives

$$R_m = \frac{(c - \gamma^*)}{6}(\tau^* - \tau) \ , \ T = \frac{c(c - \gamma^*)}{6}(\tau^* - \tau), \tag{2.63}$$

where τ^* is the time at which the fibre breaks. With this $T(\tau)$, (2.59) may be integrated to give

$$[6R + c(\tau^* - \tau)]^c [6R - (c - \gamma^*)(\tau^* - \tau)]^{c - \gamma^*} = f(\xi), \tag{2.64}$$

for some arbitrary function f defined by the initial conditions. Our aim is to choose f in such a way that R is smooth for all $\tau < \tau^*$ while l remains finite as $\tau \to \tau^*$. At $\tau = \tau^*$, when R_m becomes zero, R is given by

$$R(\xi, \tau^*) = \frac{1}{6}[f(\xi)]^{\frac{1}{2c - \gamma^*}}, \tag{2.65}$$

while the leading–order behaviour of R for all $\tau < \tau^*$ is given by

$$R \sim \frac{(c - \gamma^*)(\tau^* - \tau)}{6} + \frac{1}{6}\left(\frac{f}{((2c - \gamma^*)(\tau^* - \tau))^c}\right)^{\frac{1}{c - \gamma^*}} + O(f^{\frac{1}{c - \gamma^*} + 1}) \tag{2.66}$$

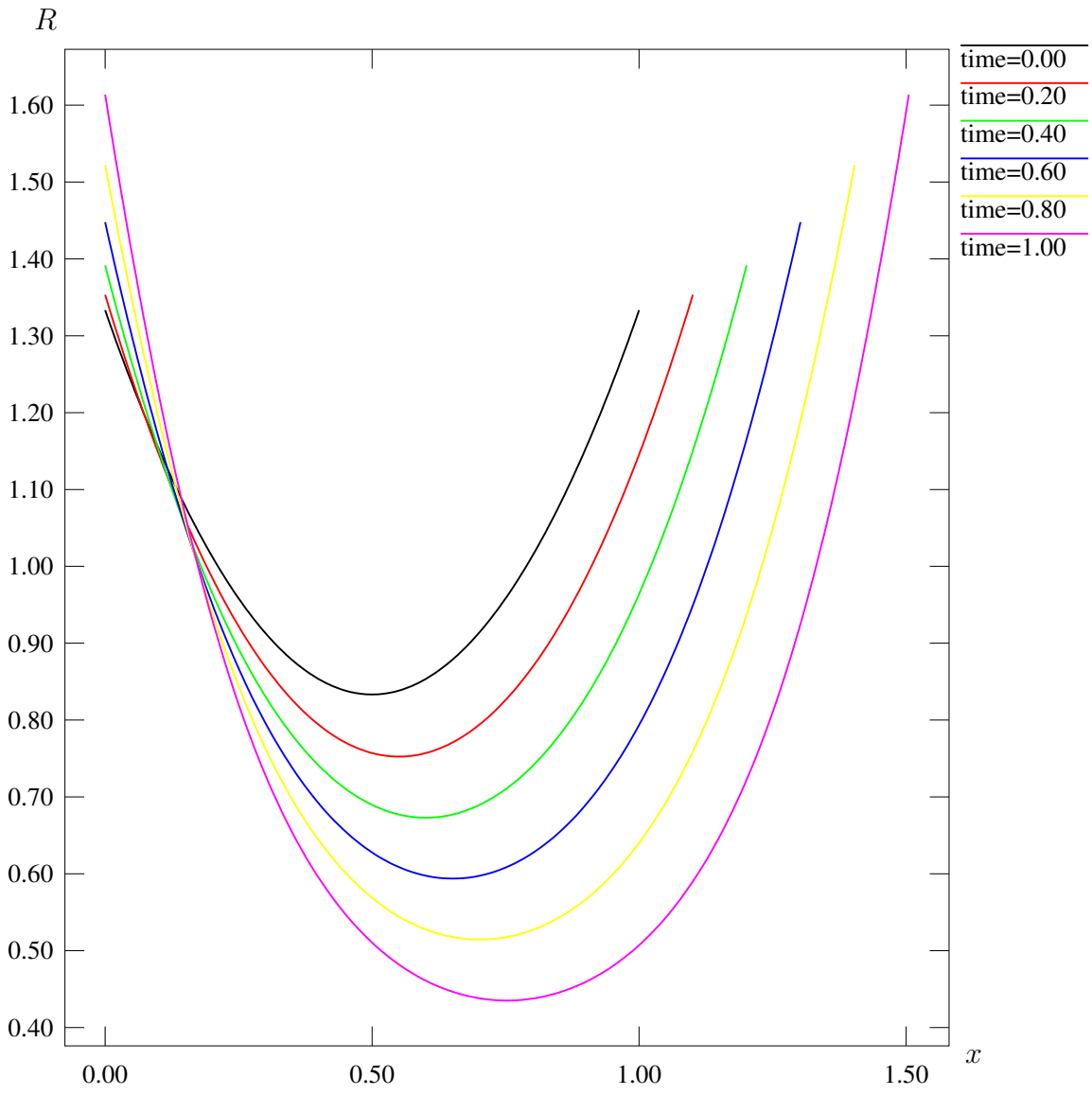

Figure 2.3: The radius of a stretching fibre with surface tension; $R_0(x) = (x^2 - x)/2 + 4/3, \quad l(t) = 1 + t/2$.

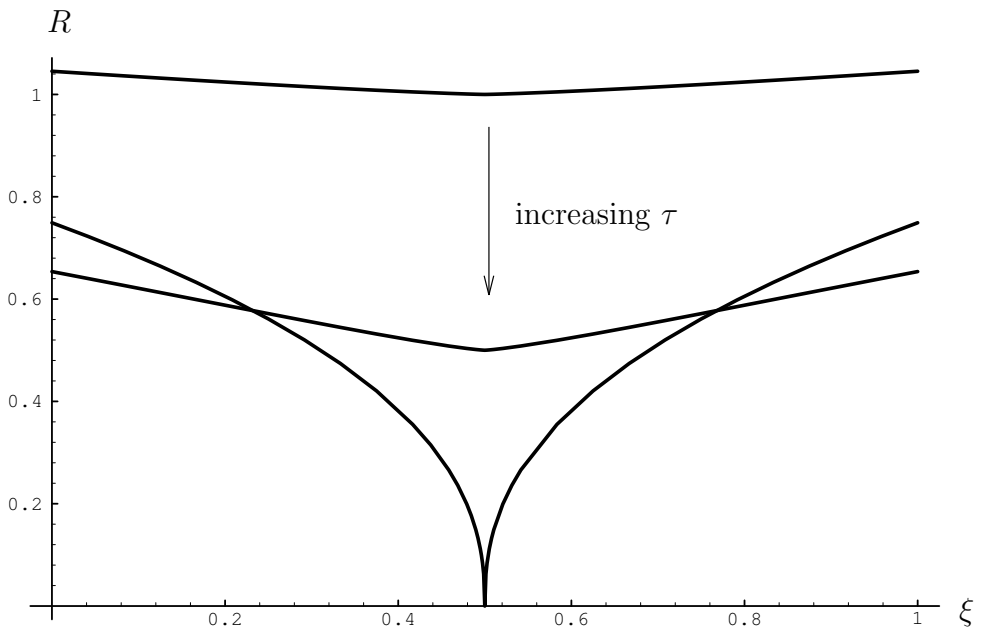

Figure 2.4: The formation of a cusp in an axisymmetric fibre

for small f. Consider, for example, the case

$$f = |\xi - b|^{\alpha},$$

which gives

$$R \sim R_m + \frac{1}{6}\left(\frac{1}{[(2c-\gamma^*)(\tau^*-\tau)]}\right)^{\frac{c}{c-\gamma^*}} |\xi - b|^{\frac{\alpha}{c-\gamma^*}} \tag{2.67}$$

as the leading–order behaviour for R as $\xi \to b$ for $\tau < \tau^*$, and when $\tau = \tau^*$,

$$R(\xi, \tau^*) = \frac{1}{6}|\xi - b|^{\frac{\alpha}{2c-\gamma^*}}. \tag{2.68}$$

Hence it is possible for $1/R^2$ to be integrable when R_m becomes zero, while R is smooth for all smaller times by choosing c and α such that

$$\frac{2\alpha}{2c-\gamma^*} < 1 \text{ and } \frac{\alpha}{c-\gamma^*} > 1. \tag{2.69}$$

These combine to give

$$\frac{c}{\gamma^*} - 1 < \frac{\alpha}{\gamma^*} < \frac{c}{\gamma^*} - \frac{1}{2}, \tag{2.70}$$

where $c > \gamma^*$. A simple example is $\gamma^* = 1$, $c = 2$, in which case (2.64) is a cubic for R, the solution of which may be found explicitly. The formation of the cusp in such a case is shown in figure 2.4.

Note that, though R_ξ becomes unbounded as the cusp is formed,

$$R_x = \frac{R^2 R_\xi}{R_0^2} = \frac{(R^3)_\xi}{3R_0^2},$$

may well remain finite as $R_m \to 0$; in our example it is easily seen to be zero. However, since the fluid velocity is given by

$$X_\tau = \int_0^\xi \frac{(T - \gamma^* R)\, d\xi}{3R^4},$$

if $(R^3)_\xi$ is to remain finite as $R_m \to 0$ the velocity must become infinite. This implies that, locally at least, inertia effects should be included in the analysis. Such a local analysis has been carried out by Eggers (1993) by looking for similarity solutions of (2.57) and (2.58).

2.5.3 The break–up of a two–dimensional sheet with surface tension

In section 2.5.2, we showed that surface tension effects can cause the break–up of an axisymmetric fibre by causing a cusp to be formed in the Lagrangian description of its free surface. We shall now discuss briefly, but not solve, the corresponding problem for a two–dimensional sheet.

It is clear physically that a much larger surface tension coefficient is required to have a significant effect than for a fibre as the curvatures are much smaller. Hence we consider the first scaling employed in section 2.5.1, and set

$$\tilde{\gamma} = \frac{\epsilon}{Ca} = O(1).$$

Then, neglecting inertia and gravity, (2.52) and (2.53) can be written in the form

$$h_t + (uh)_x = 0, \quad 4hu_x + \tfrac{1}{4}\tilde{\gamma}(2hh_{xx} - h_x^2) = T(t), \tag{2.71}$$

where T is the tension in the sheet. As in section 2.4, we assume without loss of generality that one end of the sheet is fixed, and specify the length of the sheet as a function of time:

$$u(0,t) = 0, \quad u(l(t),t) = \dot{l}.$$

We also have to specify h at the two ends of the sheet and at $t = 0$. We now pose the question: can h go to zero at a point on the sheet while l remains finite ?

This problem may be simplified via the transformation (motivated by consideration of the Lagrangian transformation of the last section)

$$\zeta = \int_0^x h(x',t)\,dx', \quad \tau = t, \tag{2.72}$$

after which h is found to satisfy

$$8(h^{-3/2})_\tau + \tilde{\gamma}(h^{3/2})_{\zeta\zeta} = 3T(\tau)h^{-5/2}, \tag{2.73}$$

while x is given by

$$x = \int_0^\zeta \frac{d\zeta}{h}. \tag{2.74}$$

Without loss of generality, suppose the ends of the sheet are given by $\zeta = 0$ and $\zeta = 1$. Then the initial and boundary conditions required to solve this problem are: h at $\tau = 0$ and at $\zeta = 0, 1$, and the length of the sheet $l(\tau) = x(1,\tau)$. For the sheet to break, h must go to zero with a cusp, *i.e.* like $|\zeta - \zeta_0|^\alpha$ where $0 < \alpha < 1$, so that l remains finite. Alternatively, setting $Z = h^{-3/2}$, the problem becomes

$$Z_\tau + \frac{\tilde{\gamma}}{8}\left(\frac{1}{Z}\right)_{\zeta\zeta} = \frac{3T(\tau)}{8}Z^{5/3}. \tag{2.75}$$

We now ask, for smooth initial Z, reasonable T and end conditions for Z at $\zeta = 0, 1$, can Z blow up at a single point ζ_0 like $|\zeta - \zeta_0|^{-3\alpha/2}$ where $0 < \alpha < 1$; if so, then surface tension effects can cause the sheet to break. However, since the mathematical or numerical analysis of nonlinear diffusion equations like (2.75) often requires some subtle estimates and transformations, we do not attempt to answer this question here.

2.5.4 The twisting of an axisymmetric fibre

The theory of section 2.2 may easily be extended to allow for the twisting of the fibre about its axis. One simply has to employ the full Navier–Stokes equations and free–surface conditions in cylindrical polar coordinates, without setting the rotational velocity to zero but neglecting all θ–derivatives. This results in the introduction of another dimensionless parameter into the problem: if Ω is a typical angular velocity and U and L are as before, then the Strouhal number,

$$S = \frac{\epsilon \Omega L}{U}, \tag{2.76}$$

measures the relative importance of twisting compared to stretching. Most authors who have considered the twisting of fibres (for example Dewynne, Ockendon & Wilmott (1992), Dewynne, Howell & Wilmott (1994), Bechtel *et al.* (1994)) have implicitly assumed that S is of order ϵ. If this scaling is adopted, the equation for the twist of the fibre about its axis decouples from the stretching equations. In fact u and R are given by (2.57) and (2.58), and the angular velocity ω of the fibre about its axis satisfies

$$(R^4\omega_x)_x = Re\, R^2[(R^2\omega)_t + u(R^2\omega)_x]. \tag{2.77}$$

Bechtel *et al.* (1992) considered the twisting and stretching of more general viscoelastic fibres, assuming $S = O(\epsilon)$, and found that there could be coupling between twisting and stretching via higher–order terms in that, if the relative rate of twisting of the two ends of the fibre is large enough, higher–order terms in the asymptotic expansions may become comparable with the leading–order terms. We shall now demonstrate with our simpler Newtonian rheology that this coupling may be seen explicitly in the leading–order equations by rescaling the Strouhal number; we shall now consider the case where S is of order one. In this case, the equations of motion are found to be

$$\left.\begin{aligned} &(R^2)_t + (uR^2)_x = 0 \\ &(3R^2u_x)_x = Re\, R^2(u_t + uu_x) + St\, R^2 - \gamma^* R_x - \tfrac{1}{4} Re\, S^2 (R^4\omega^2)_x \\ &(R^4\omega)_x = Re\, R^2[(R^2\omega)_t + u(R^2\omega)_x] \end{aligned}\right\}. \tag{2.78}$$

We see that there is indeed coupling, provided $Re\,S^2$ is large enough. It is notable that the examples given by Bechtel *et al.* (1994) in which "torsional coupling" was found to be significant were exactly those in which the parameter $Re\,S^2$ was non–negligible.

2.6 Conclusions

In section 2.2 we have derived a system of partial differential equations governing the stretching of an axisymmetric viscous fibre – often known as the Trouton model. In section 2.1 we have shown that the same system of equations may be used to model a two–dimensional sheet of viscous fluid, and that the centre–line of such a sheet must be straight to leading order, with the scalings used. In section 2.3 we have noted the important points in these two models which have implications for the more complicated models to follow.

In section 2.4 we have described how the general solution of the Trouton model may be written down by using Lagrangian coordinates, and hence have shown that a purely viscous axisymmetic fibre can only be broken in finite time if there is a cusp in the initial cross–sectional area. In section 2.5 we have described how the Trouton model may be extended to account for the effects of inertia, surface tension and gravity. In particular, we have shown that

- the inclusion of inertia in the equations for a two–dimensional sheet results in a partial differential equation for the centre–line which changes type depending on whether the sheet is under tension or compression,
- the inclusion of surface tension effects in the equations for an axisymmetric fibre gives equations which admit the possibility of break–up,
- if a certain dimensionless parameter is big enough, there is coupling between twisting and stretching of an axisymmetric viscous fibre.

In the next chapter we shall show how the evolution of the centre–line of a two–dimensional sheet which is not initially straight may be described by rescaling the

equations over a suitable short timescale.

Chapter 3

Short timescale analyses

In this chapter we discuss the response of two–dimensional viscous sheets over timescales shorter then the L/U timescale we employed in chapter 2. Because of the restriction to a strictly two–dimensional geometry, the analysis is relatively straightforward; in the remaining chapters we shall make conjectures about the probable short–timescale behaviour in more complicated geometries using the two–dimensional case as a guide.

In section 3.1 we discuss the short timescale dynamics of an inertia–free two–dimensional sheet. This enables us to formulate a complete description of the evolution of such a sheet as it straightens under tension or buckles under compression. This theory is due to Buckmaster, Nachman & Ting (1975), which we shall refer to as BNT.

In section 3.2 we show that the inclusion of inertia effects, even if they are rather small, may invalidate the theory of BNT and lead to a model which exhibits radically different behaviour from that predicted by BNT. We then show, in section 3.3, that the two theories can be reconciled by rescaling distance along the sheet as well as time.

3.1 Two–dimensional Stokes flow

3.1.1 Timescale L/U

Recall the equations derived in section 2.1 for the motion of a two–dimensional, inertia–free viscous sheet whose curvature is of order ϵ/L over the time–scale L/U, where L is a typical length and U a typical pulling speed. These comprise the Trouton model for the sheet thickness h and axial velocity u, along with an equation that predicts that so long as u is not constant, the centre–line of the sheet, given by $y = H(x,t)$, must be straight, so that without loss of generality we may take $H = 0$. As we noted in section 2.3, this implies that the solution for H is a singular perturbation in t, the outer solution of which is $H = 0$; in order to study the evolution of a centre–line which is not straight initially, we must consider a timescale shorter than L/U. As found by BNT, the required timescale is $\epsilon^2 L/U$.

3.1.2 Timescale $\epsilon^2 L/U$

We now rescale the Stokes equations and boundary conditions (2.7) to (2.12) using the new timescale by setting

$$t = \epsilon^2 \tau. \tag{3.1}$$

The kinematic boundary condition (2.10) implies that we should also rescale the transverse velocity v by setting

$$v = \epsilon^{-2} V. \tag{3.2}$$

After these rescalings, (2.7) to (2.12) take the form

$$\epsilon^2 u_x + V_y = 0, \tag{3.3}$$

$$\epsilon^2 p_x = \epsilon^2 u_{xx} + u_{yy}, \tag{3.4}$$

$$\epsilon^2 p_y = \epsilon^2 V_{xx} + V_{yy}, \tag{3.5}$$

$$V = H_\tau \pm \tfrac{1}{2} h_\tau + \epsilon^2 u \left(H_x \pm \tfrac{1}{2} h_x \right) \quad \text{on } y = H \pm \tfrac{1}{2} h, \tag{3.6}$$

$$\epsilon^2 (-p + 2u_x) \left(H_x \pm \tfrac{1}{2} h_x \right) = u_y + V_x \quad \text{on } y = H \pm \tfrac{1}{2} h, \tag{3.7}$$

$$\epsilon^2 (u_y + V_x) \left(H_x \pm \tfrac{1}{2} h_x \right) = -\epsilon^2 p + 2V_y \quad \text{on } y = H \pm \tfrac{1}{2} h \ . \tag{3.8}$$

Our method is, as usual, to expand the dependent variables in powers of the small parameter ϵ^2. As previously it is necessary to proceed to higher order in the expansions in order to close the leading–order equations. The Stokes equations and boundary conditions at leading order reveal that the transverse velocity v is independent of y. Hence the kinematic boundary condition gives (dropping subscripts)

$$v = H_\tau, \tag{3.9}$$

and

$$h_\tau = 0, \tag{3.10}$$

that is, the thickness of the sheet does not change with time. The leading–order axial velocity is given by

$$u = \bar{u}(x, \tau) + H_{x\tau}(H - y), \tag{3.11}$$

so that the leading–order flow is *not* extensional with the present scalings. The linear dependence of u on y leads to *bending* stresses in the sheet. With the scalings employed in section 2.1 we found that the dominant stress in the sheet was due to stretching; the bending stress was negligible to leading order. With the present scalings we find that stretching and bending stresses both play a part in the leading–order equations.

The solvability conditions for the $O(\epsilon^2)$ equations give the axial stress balance,

$$4h(\bar{u}_x + H_x H_{x\tau}) = T(\tau), \tag{3.12}$$

which represents the tension in the sheet. Continuing to $O(\epsilon^4)$ in the analysis leads to the following equation for the centre–line of the sheet:

$$T(\tau)H_{xx} = \frac{1}{3}[h^3(H_{xx\tau})]_{xx}. \tag{3.13}$$

BNT obtained equivalent equations by employing curvilinear coordinates fixed in the sheet. As we are only considering sheets with small curvature here, we have chosen to employ fixed Cartesian coordinates which simplify the analysis.

Over this short timescale the ends of the sheet do not move to leading order, and hence the end conditions for H may be applied at $x = 0$ and $x = 1$. If these end

conditions are homogeneous then (3.13) can be solved by means of eigenfunction expansions:

$$H = \sum_{n=1}^{\infty} A_n f_n(x) \exp\left(-\frac{3}{\lambda_n^2}\int_0^{\tau} T(\tau')d\tau'\right), \tag{3.14}$$

where f_n and λ_n are the eigenfunctions and eigenvalues of the o.d.e.

$$(h^3 f_n'')'' = \lambda_n^2 f_n'', \tag{3.15}$$

with the given homogeneous boundary conditions at $x = 0$ and $x = 1$. It is simple to establish that for reasonable h, the λ_n^2 are real and positive and that the f_n' are orthogonal and complete, so that the coefficients A_n may be found by Fourier analysis of $H_x(x, 0)$. For example, in the case considered by BNT in which $h = 1$ and $H = H_x = 0$ at the two ends of the sheet, we obtain

$$f_n(x) = 2\sin(\lambda_n x) - \lambda_n \cos(\lambda_n x) - 2\lambda_n x + \lambda_n, \tag{3.16}$$

where the eigenvalues are the solutions of

$$\frac{\lambda_n}{2} = \tan\left(\frac{\lambda_n}{2}\right), \tag{3.17}$$

in agreement with the solution given by BNT. This separable solution implies that if the sheet is under compression ($T < 0$) then the solution grows exponentially in time and is dominated by the lowest mode, while if the sheet is under tension ($T > 0$) the solution decays exponentially, with the highest mode decaying slowest.

For cases where the boundary conditions imposed on H are inhomogeneous, (3.13) can still be solved by Laplace transform; this has been carried out by Wilmott (1989). The behaviour of the solutions which result is qualitatively similar to that of the separable solutions described above.

3.1.3 Large displacements

By considering a short timescale we have resolved the apparent paradox which we encountered in section 2.1, namely that the centre–line of the sheet was found to be straight to leading order. Equation (3.13) describes how an initially curved (but only by a distance of order ϵL) sheet will straighten under tension or buckle under

compression over a timescale $\epsilon^2 L/U$. In the former case, the theory of section 2.1 becomes valid over a timescale L/U while in the latter case it is invalid as the displacement of the centre–line becomes large. Hence, in order to complete the picture, we shall now consider the dynamics of a two–dimensional sheet of non–negligible curvature.

The simplest way to derive the leading–order equations of motion is to employ curvilinear coordinates fixed in the sheet. Such a derivation was performed in BNT and found to result in an equation identical to (5.79), which we shall encounter in the context of a curved viscous fibre which is constrained to move in a plane. We shall now describe briefly how equivalent equations may be derived using fixed Cartesian coordinates. The advantage of such an approach is that the boundary conditions take a simpler form in a fixed coordinate system; the disadvantage is that a great deal more algebra is involved.

We start with the two–dimensional Stokes equations and stress–free boundary conditions given in (2.1) to (2.6). We then perform the following transformation,

$$y = H(\tilde{x},\tilde{t}) + \tilde{y}, \quad v = H_{\tilde{t}} + uH_{\tilde{x}} + \tilde{v}, \quad x = \tilde{x}, \quad t = \tilde{t}, \tag{3.18}$$

which results in the chain rules

$$\frac{\partial}{\partial t} = \frac{\partial}{\partial \tilde{t}} - H_{\tilde{t}}\frac{\partial}{\partial \tilde{y}}, \quad \frac{\partial}{\partial x} = \frac{\partial}{\partial \tilde{x}} - H_{\tilde{x}}\frac{\partial}{\partial \tilde{y}}, \quad \frac{\partial}{\partial y} = \frac{\partial}{\partial \tilde{y}}. \tag{3.19}$$

After making the above transformation the leading–order equations of section 2.1 can be derived via the scalings

$$\begin{aligned} \tilde{x} &= L\tilde{x}', & \tilde{y} &= \epsilon L\tilde{y}', \\ u &= Uu', & \tilde{v} &= \epsilon U\tilde{v}', \\ H &= \epsilon LH', & h &= \epsilon Lh', \\ t &= (L/U)t', & p &= (\mu U/L)p'. \end{aligned}$$

Here, we are interested in large displacements of the centre–line and the only change needed to the above scalings is to nondimensionalise H with L instead of ϵL. Then we proceed as usual to expand the unknowns in powers of ϵ (see the footnote on page 84 for a discussion of when a series in powers of ϵ^2 is or is

not appropriate). It is necessary to continue the expansions up to $O(\epsilon^2)$ and the algebra is fairly unpleasant so we proceed directly to the leading–order equations which result. These are (dropping primes and tildes)

$$h_t + (uh)_x = 0, \tag{3.20}$$

$$H_x(H_{xt} + uH_{xx}) + u_x(1 + H_x^2) = 0, \tag{3.21}$$

$$\left[\frac{h^3}{3(1+H_x^2)^2}\left(\frac{H_{xt}+uH_{xx}}{1+H_x^2}\right)_x\right]_{xx} = T(t)H_{xx}, \tag{3.22}$$

where the arbitrary function T can be associated with the tension in the sheet. In the case where H is of order ϵL in dimensional variables, T is an order of magnitude larger than the left–hand side of (3.22), and hence the leading–order equation $H_{xx} = 0$ is recovered. Notice that the short timescale equation (3.13) can be obtained by linearising these equations for small H.

Equations (3.20), (3.21) and (3.22) take a more familiar form when recast in the curvilinear coordinates employed by BNT. We denote by α the angle made by the centre–line of the sheet with a fixed horizontal axis, and by s arc length along the centre–line, so that

$$H_x = \tan\alpha, \quad \frac{\partial}{\partial s} = \cos\alpha\frac{\partial}{\partial x}.$$

We also note that h is the thickness of the sheet, *as measured in the y-direction*; the thickness of the sheet as measured in the normal direction is given by

$$\tilde{h} = h\cos\alpha.$$

Hence (3.20) and (3.21) combine to give

$$\tilde{h}_t = 0, \tag{3.23}$$

(here $\partial/\partial t$ represents differentiating with respect to t while holding s constant) so that there is no stretching of the sheet to leading order, and (3.22) becomes

$$\left(\tilde{h}^3\alpha_{st}\right)_s = F(t)\cos\alpha + G(t)\sin\alpha. \tag{3.24}$$

This is the so–called "viscida" equation derived by BNT. If the time–derivative on the left–hand side were not present it would be identical to the elastica equation of linear elasticity. It is highly nonlinear and in general must be solved by numerical means.

3.1.4 Summary

The theory of inertia–free two–dimensional viscous sheets may be summarised as follows.

- A sheet of $O(\epsilon L)$ thickness and $O(L)$ displacement, when put under tension by moving its ends with a relative speed of order U, will straighten over a timescale $O(L/U)$, *without stretching*. The motion of the sheet will be governed by (3.24).
- When the displacement reaches $O(\epsilon L)$, the sheet will subsequently straighten over a timescale $O(\epsilon^2 L/U)$, again without stretching. The displacement of the centre–line will be given by (3.13), which predicts that the smallest wavelength modes are the slowest to decay.
- Once the sheet has straightened, it will stretch over a timescale $O(L/U)$, satisfying the Trouton model.
- When a nearly straight sheet (with thickness and displacement both of order ϵL) is compressed by moving its ends towards each other with relative speed U, it will buckle over a timescale $O(\epsilon^2 L/U)$. During the motion, there will be no stretching, the governing equation will be (3.13) and the longest wavelength modes will dominate.
- When the displacement of the centre–line becomes of order L, the buckling will continue over a timescale L/U, there will be no stretching, and the motion of the sheet will be governed by (3.24).

For example, to model the buckling of an initially nearly straight sheet under given end conditions, one would first solve the linear problem (3.13). The dominant behaviour of this solution as $\tau \to \infty$ would then be used as the initial condition for a numerical integration of (3.24). This is the approach which was adopted by BNT.

Note that (3.13) and (3.22) are both invariant under the transformation $\{\tau \to -\tau, T \to -T\}$. Hence the model predicts that the motion of the sheet is reversible.

One aspect of this is that short–wavelength displacements grow the most slowly during buckling and take the longest time to decay during straightening of the sheet. In practice, or indeed during a numerical integration of the equations over a long time interval, short–wavelength disturbances will be lost during straightening because of dampening effects and the lowest buckling mode will dominate during compression, so this mathematical reversibility will be of academic interest.

3.2 Inertia effects

We shall now describe the dramatic effect that the incorporation of inertia effects has on the theory of the previous section. The inclusion of inertia results in the introduction of a dimensionless parameter, the Reynolds number Re, into the problem. We may expect the behaviour of our model to depend critically on the size of the Reynolds number compared to our small parameter ϵ. We shall consider three representative examples: $Re = O(1)$, $Re = O(\epsilon^2)$ and $Re = O(\epsilon^4)$.

3.2.1 $Re = O(1)$

We have already considered this case in section 2.5, where the leading–order equations were found to be (neglecting other effects)

$$h_t + (uh)_x = 0, \quad (4hu_x)_x = Re\, h(u_t + uu_x), \tag{3.25}$$

with the decoupled equation for H,

$$(Re\, hu^2 - 4hu_x)H_{xx} + 2Re\, huH_{xt} + Re\, hH_{tt} = 0. \tag{3.26}$$

These equations are much more difficult to solve than the standard Trouton model. However, several general statements may be made about the properties which are introduced due to inertia effects:

- more initial conditions are required by this system than in the inertia–free case;

- the short timescale analysis of section (3.1.2) is redundant if the Reynolds number is this large; indeed, (3.26) suggests that any short timescale analysis will simply give $H_{tt} = 0$ as the governing equation for the centre–line;

- the equations no longer have the reversibility properties noted at the end of section 3.1.4; indeed, the equation for the centre–line changes type from hyperbolic to elliptic depending on whether the sheet is under tension ($u_x > 0$) or compression ($u_x < 0$);

- the hyperbolic case will give rise to wave–like behaviour, while the elliptic case is ill–posed in the sense of Hadamard, leading to blow–up with the linearised growth rate becoming unbounded as the spatial wavenumber tends to infinity.

For the industrial processes described in the Introduction, the Reynolds number is usually much less than $O(1)$. However, (3.26) implies that inertia effects will still enter the model over a timescale $t = O(Re^{1/2})$.

3.2.2 $Re = O(\epsilon^2)$

We shall now consider the case, relevant to many processes, in which Re is of order ϵ^2. In this case, inertia plays no part in the leading–order equations over the timescale L/U, and the equations of section 2.1 are recovered. As in section 3.1, we would like to consider a short timescale in order to model the evolution of a sheet which is not straight initially. However, with the present scaling of the Reynolds number, the timescale $t = O(\epsilon^2)$ used in section 3.1.2 is no longer relevant; the timescale over which viscous and inertia effects are balanced is $t = O(\epsilon)$.

We put

$$Re = \epsilon^2 Re',$$

assuming $Re' = O(1)$, and nondimensionalise the two–dimensional Navier–Stokes equations and stress–free boundary conditions according to

$$x = Lx', \qquad y = \epsilon L y',$$

$$u = Uu', \qquad \tilde{v} = Uv',$$
$$H = \epsilon L H', \quad h = \epsilon L h',$$
$$t = (\epsilon L/U)t', \quad p = (\mu U/L)p',$$

where the scaling for v is motivated by the kinematic boundary condition. After applying these scalings, we drop primes and seek solutions in the form of asymptotic expansions in powers of ϵ. The analysis is relatively straightforward, and results in the leading–order equations (dropping subscripts)

$$h_t = 0, \quad 4hu_x = T(t), \quad T(t)H_{xx} = Re' h H_{tt}. \tag{3.27}$$

The dependence of the type of the centre–line equation on the sign of T is clear. As in section 3.1.2, the end conditions for H are applied at $x = 0$ and $x = 1$, since the ends of the sheet do not move over this timescale to leading order. If these conditions are homogeneous, the solution for H can be expanded in the form

$$H = \sum_{n=1}^{\infty} f_n(x) \left(a_n g_{1,n}(t) + b_n g_{2,n}(t) \right), \tag{3.28}$$

where f_n are the eigenfunctions of the Stürm–Liouville equation

$$f_n'' + \lambda_n^2 Re' h f_n = 0, \tag{3.29}$$

which satisfy the given conditions at $x = 0$ and $x = 1$, and $g_{1,n}$ and $g_{2,n}$ are the two linearly independent solutions of

$$g_n'' + \lambda_n^2 T g_n = 0. \tag{3.30}$$

The coefficients a_n and b_n are found by Fourier analysis of $H(x, 0)$ and $H_t(x, 0)$.

Consider, for example, the steady state solution of (2.15), (2.18) and (2.22), namely

$$h = h_0 e^{-cx}, \quad T = \text{ const.}, \quad H = 0.$$

We can examine the response of the centre–line to small disturbances over our short timescale by substituting for h and T into (3.27). Assume the end conditions are $H = 0$ at $x = 0$ and $x = 1$, and without loss of generality, so long as T is positive,

we may suppose the equations are scaled in such a way that $h_0 = T = 1$. Then the general solution for H is

$$H = \sum_{n=1}^{\infty} \left(J_0(\gamma_n) Y_0(\gamma_n e^{-\frac{c}{2}x}) - J_0(\gamma_n e^{-\frac{c}{2}x}) Y_0(\gamma_n) \right) \left(a_n \cos(\omega_n t) + b_n \sin(\omega_n t) \right), \tag{3.31}$$

where the eigenvalues γ_n are the roots of

$$J_0(\gamma_n) Y_0(\gamma_n e^{-\frac{c}{2}}) - J_0(\gamma_n e^{-\frac{c}{2}}) Y_0(\gamma_n) = 0,$$

and $\omega_n = c\gamma_n/(2\sqrt{Re})$. If T is negative, the oscillatory terms in t become exponentials and the pathological behaviour alluded to earlier is clear: the growth rate of the modes becomes unbounded as their wavelength goes to zero. We will discuss in section 3.3 how this blow–up is prevented from occurring in practice.

3.2.3 $Re = O(\epsilon^4)$

We shall now examine the case in which $Re = O(\epsilon^4)$ so that the inertial timescale of $Re^{1/2}$ is the same as the ϵ^2 timescale used in section 3.1.2. We put

$$Re = \epsilon^4 Re^*,$$

and employ the same nondimensionalisations as those in section 3.1.2. The result is, as may have been anticipated, equations similar to those of section 3.1.2 with an additional term due to inertia. These are

$$h_\tau = 0, \tag{3.32}$$

$$4h(\bar{u}_x + H_x H_{x\tau}) = T(\tau), \tag{3.33}$$

$$T(\tau) H_{xx} = \frac{1}{3}[h^3 (H_{xx\tau})]_{xx} + Re^* h H_{\tau\tau}. \tag{3.34}$$

We shall not discuss the solution of these equations, but simply make the observation that if the Reynolds number is not less than $O(\epsilon^4)$ then inertia effects cannot be ignored when considering the short timescale behaviour of a fluid sheet. The ball–park figures given in the Introduction suggest that for many industrial processes the relevant Reynolds number lies somewhere between $O(\epsilon^4)$ and $O(1)$.

3.2.4 Summary

Let us summarise the models for slender, nearly flat, two–dimensional viscous sheets we have presented so far in this chapter.

- If inertia is neglected, the usual L/U timescale predicts the centre–line of the sheet is straight.
- If inertia is neglected, the straightening of a sheet under tension or buckling of a sheet under compression takes place over a timescale $\epsilon^2 L/U$ and is governed by (3.13). The problem with this model is
  - Re must be extremely small for inertia to be negligible.
- If $Re \geq O(\epsilon^4)$ then inertia cannot be neglected when the timescale $Re^{1/2}L/U$ is considered. Typical evolution equations which govern the short time behaviour are (3.26) and (3.27). The problem with these equations is:
  - the equations are ill–posed if the sheet is under compression, and predict pathological behaviour as the sheet buckles.

3.3 Short lengthscales and timescales

In this section we shall discuss how elements of the inertia–free theory and the theory incorporating inertia may be combined to make sense of the unphysical pathological behaviour which is predicted when the sheet is put under compression. Notice that the ill–posed equations (3.26) and (3.27) when $T < 0$ predict the dominance of short lengthscale displacements as the sheet buckles. If x is rescaled to examine such a short lengthscale, we may expect the $[h^3(H_{xx\tau})]_{xx}$ term of equation (3.13) to become important and hence regularise the equation.

This motivates us in the case $T < 0$ to examine the consequences of rescaling x as well as t. To determine the important length– and timescales, we start by considering the simplified paradigm centre–line equation, motivated by (3.34),

$$TH_{xx} = \frac{\epsilon^2}{3} H_{xxxxt} + ReH_{tt}, \tag{3.35}$$

where we have assumed that, over the length– and timescales we will be considering, variations in h and T may be neglected. We find the linear growth rates by looking for a solution of the form

$$H = H_0 e^{ikx+\lambda t},$$

which, on substitution into (3.35) gives

$$\lambda = \frac{-\epsilon^2 k^4 \pm k\sqrt{\epsilon^4 k^6 - 36 Re\, T}}{6Re}. \tag{3.36}$$

Here, λ is the linear growth rate and $k = L/\tilde{L} > 1$, where L is the length of the sheet and $\tilde{L}$ is the lengthscale of the disturbance. When $T < 0$, there is always one positive root for λ, so that all modes grow exponentially. However, the growth rate tends to zero like $-3T/(\epsilon^2 k^2)$ as $k \to \infty$, and there is a maximum value for λ, and hence a dominant lengthscale, given by

$$\frac{\tilde{L}}{L} \sim O(\epsilon^{2/3} Re^{-1/6}), \tag{3.37}$$

with linear growth rate

$$\lambda \sim O(\epsilon^{-2/3} Re^{-1/3}). \tag{3.38}$$

Notice that if $Re < O(\epsilon^4)$ then this length is greater than the length of the sheet and so the dominant lengthscale is L, with the corresponding linear growth rate of order ϵ^{-2}; this agrees with the inertia–free theory of section 3.1.2. However, if $Re > O(\epsilon^4)$ then (3.37) and (3.38) give the lengthscale of the disturbances whose amplitude grows the fastest and the timescale over which they grow. This dominant lengthscale increases as the Reynolds number decreases, while the corresponding timescale decreases.

Note that, while $\tilde{L}$ is the appropriate lengthscale for disturbances to the centre–line $y = H$, variations in h and u still take place over a lengthscale L. Hence in general, it is necessary to perform a two–lengthscale analysis.

As a simple example, consider the case (chosen to make the scalings as simple as possible) in which $Re = O(\epsilon)$. This means that over the usual lengthscale and timescale inertia does not enter the leading–order equations, which are hence identical to those of section 2.1. If only time is rescaled, over the inertial timescale

$Re^{1/2} \sim \epsilon^{1/2}$, then leading–order equations identical to those obtained in section 3.1.2 (for $Re = O(\epsilon^2)$) result. The centre–line equation is ill–posed if the sheet is under compression.

Using the ideas of this section, we may rescale both x and t; from (3.37), the appropriate new lengthscale is given by $\tilde{L}/L = \epsilon^{1/2}$, and the short timescale implied by (3.38) is $t = O(\epsilon L/U)$. Hence we set $Re = \epsilon\tilde{Re}$ and scale the Navier–Stokes equations via the following nondimensionalisations:

$$\begin{aligned} x &= Lx', & y &= \epsilon L y', \\ u &= Uu', & v &= Uv', \\ H &= \epsilon L H', & h &= \epsilon L h', \\ t &= (\epsilon L/U)t', & p &= (\mu U/L)p'. \end{aligned}$$

We also introduce a short lengthscale, denoted by

$$\xi = \epsilon^{-1/2}x,$$

and, in order to perform a two–lengthscale analysis, treat x and ξ as independent, so that partial x-derivatives become:

$$\frac{\partial}{\partial x} = \frac{1}{L}\left(\frac{\partial}{\partial \tilde{x}} + \frac{1}{\epsilon^{1/2}}\frac{\partial}{\partial \xi}\right).$$

After these rescalings, we expand the Navier–Stokes equations in powers of $\epsilon^{1/2}$. After some algebra, the centre–line is found to satisfy

$$TH_{\xi\xi} = \left(\frac{h^3}{3}H_{\xi\xi t}\right)_{\xi\xi} + \tilde{Re}\, hH_{tt}, \tag{3.39}$$

where the tension T is a function of x and t, while the thickness h is a function only of x and ξ.

This example demonstrates how, by rescaling x as well as t, elements of the inertia–free theory and of the theory including inertia can be combined, and hence the catastrophic change of type caused by the inclusion of inertia can be avoided.

3.4 Conclusions

We have shown that, by considering a timescale of order $\epsilon^2 L/U$ as well as the standard timescale of L/U, a complete, self–consistent model can be formulated to describe the buckling under compression or straightening and stretching under tension of a two–dimensional inertia–free fibre. Indeed, such a model was derived by Buckmaster, Nachman & Ting (1975). However, we have also shown that inertia effects may invalidate this model even when the Reynolds number is relatively small, since their importance increases over short timescales. In order to provide a self–consistent model which includes inertia effects we have found that it is necessary to introduce a new short lengthscale, dependent on the size of the Reynolds number, as well as a short timescale.

Note that in many practical situations it is not necessary to know the details of the short–timescale dynamics. For example, in order to model fibre tapering, we only need to know that the fibre will instantaneously straighten when it is placed under tension; the manner in which it does so is largely irrelevant. As this is also true for most of the more complicated models to follow, we shall not pursue short timescale analyses in the remaining chapters, though we shall make some conjectures about what the results of such analyses might be.

Chapter 4

Nonaxisymmetric viscous fibres

In section 2.2 we derived the Trouton model for the cross–sectional area and axial velocity of an axisymmetric viscous fibre. In this chapter we relax the assumption that the fibre be axisymmetric and find that it is still possible to derive leading–order extensional equations governing the evolution of the fibre shape as it stretches and twists. The methods we employ are similar to those used by Dewynne, Ockendon & Wilmott (1992), referred to hereafter as DOW '92, for Stokes flow with a stress–free boundary. A brief summary of the results in that paper is given below.

- Each cross–section of the fibre preserves its shape, while undergoing rotation and uniform scaling in size.
- The cross–sectional area and axial velocity satisfy the Trouton model (with Trouton ratio 3).
- The centre–line of the fibre (defined to be the line joining the centres of mass of the fibre cross–sections) is straight to leading order (c.f. section 2.1).
- There is a decoupled equation governing the twist of the fibre about its centre–line. This equation involves rather complicated integrals across the fibre cross–section and so is recast in Lagrangian variables so that the integrals need only be calculated once.

We shall extend this work to include the effects of inertia, surface tension and gravity. As in section 2.5 we have to make some assumptions about the relative sizes of

the relevant dimensionless parameters before we can proceed with the asymptotic analysis. In this problem, there is a particularly delicate balance between surface tension and viscosity effects. In section 4.2 we suppose that the surface tension coefficient is small enough that the property noted above, that each cross–section preserves its shape, is retained. We then find that the analysis of DOW '92 may be followed fairly closely with the addition of new terms in the equations due to the new effects. However, with this scaling, we discover that surface tension effects do not enter the leading–order equations at all, see Dewynne, Howell & Wilmott (1994).

To take account of fibres where surface tension is important, in section 4.3 we consider larger values of the surface tension coefficient, which means that the shape–preserving property described above is lost. Indeed the cross–sectional shape of the fibre evolves under surface tension, which makes it tend to minimise its surface area. In general this leads to a much harder problem, in which a number of boundary value problems have to be solved at each time–step as the cross–sectional shape evolves. However, we are able to show in section 4.4 that the problem for the evolution of the cross–section is very similar to the two–dimensional sintering problem considered by Hopper (1990) and Richardson (1992). By using the ideas of these two papers, we find that the cross–sectional shape can be described by means of a conformal map which depends on time and distance along the fibre.

4.1 Equations of motion and boundary conditions

The fluid flow is governed by the Navier–Stokes equations

$$\rho[\boldsymbol{u}_t + (\boldsymbol{u}.\nabla)\boldsymbol{u}] = -\nabla p + \mu\nabla^2\boldsymbol{u} + \rho\boldsymbol{g}, \quad \nabla.\boldsymbol{u} = 0, \tag{4.1}$$

where ρ and μ are the fluid density and viscosity (assumed constant), p and $\boldsymbol{u}$ are the pressure and fluid velocity, and $\boldsymbol{g}$ is the acceleration due to gravity. We suppose the free surface of the fibre is given by $G(x, y, z, t) = 0$. Then the kinematic and surface tension boundary conditions may be written

$$G_t + \boldsymbol{u}.\nabla G = 0, \quad \boldsymbol{\sigma}.\nabla G = -\gamma\kappa\nabla G \quad \text{on } G = 0. \tag{4.2}$$

Here, γ is the surface tension coefficient, κ is the mean curvature of the free surface and $\boldsymbol{\sigma}$ is the stress tensor, given for an incompressible Newtonian fluid by

$$\boldsymbol{\sigma} = \begin{pmatrix} -p + 2\mu u_x & \mu(u_y + v_x) & \mu(u_z + w_x) \\ \mu(v_x + u_y) & -p + 2\mu v_y & \mu(v_z + w_y) \\ \mu(w_x + u_z) & \mu(w_y + v_z) & -p + 2\mu w_z \end{pmatrix}.$$

Initially we must specify the fibre shape and the fluid velocity. The problem is then closed by prescribing the velocities of the two ends of the fibre. Thinking of a situation where the ends are attached to rigid planes perpendicular to the x-axis we put

$$\boldsymbol{u} = \boldsymbol{u}_1^* \text{ at } x = s_1(t), \quad \boldsymbol{u} = \boldsymbol{u}_2^* \text{ at } x = s_2(t), \tag{4.3}$$

where $x = s_i(t)$ are the two ends of the fibre. Note that if $\boldsymbol{u}_i^*(t) = (u_i, v_i, w_i)$ then $u_i = \dot{s}_i$; v_i and w_i describe lateral translation and twist applied at the ends.

In nondimensionalising the equations we utilise the slenderness of the fibre.

$$(x, y, z) = L(\bar{x}, \epsilon\bar{y}, \epsilon\bar{z}), \quad t = \frac{L}{U}\bar{t},$$

$$\boldsymbol{u} = U(\bar{u}, \epsilon\bar{v}, \epsilon\bar{w}) \quad \text{and} \quad p = \frac{\mu U}{L}\bar{p}.$$

Here U is a typical pulling speed, L the initial length of the fibre and ϵ the slenderness parameter (the ratio of a typical radius to a typical length) which is small. Note that by using these scalings we are also implicitly assuming that the fibre is nearly straight, and choose the x-axis to lie approximately along its centre–line (see figure 4.1 for a definition sketch). For cases where the curvature of the centre–line is not small, a fixed Cartesian coordinate system fails to capture the geometry of the fibre, and curvilinear coordinates fixed in the fibre are desirable. This forms the subject of the next chapter.

Henceforth we shall drop overbars. The relevant dimensionless parameters are the Reynolds number, capillary number and Stokes number, given by

$$Re = \frac{\rho U L}{\mu}, \quad Ca = \frac{\mu U}{\gamma}, \quad St = \frac{\rho L^2 g}{\mu U}. \tag{4.4}$$

As in section 2.1 we suppose that gravity acts at an angle α to the x-axis, and denote its components by

$$g_x = St\cos\alpha, \quad g_y = \frac{St}{\epsilon}\sin\alpha.$$

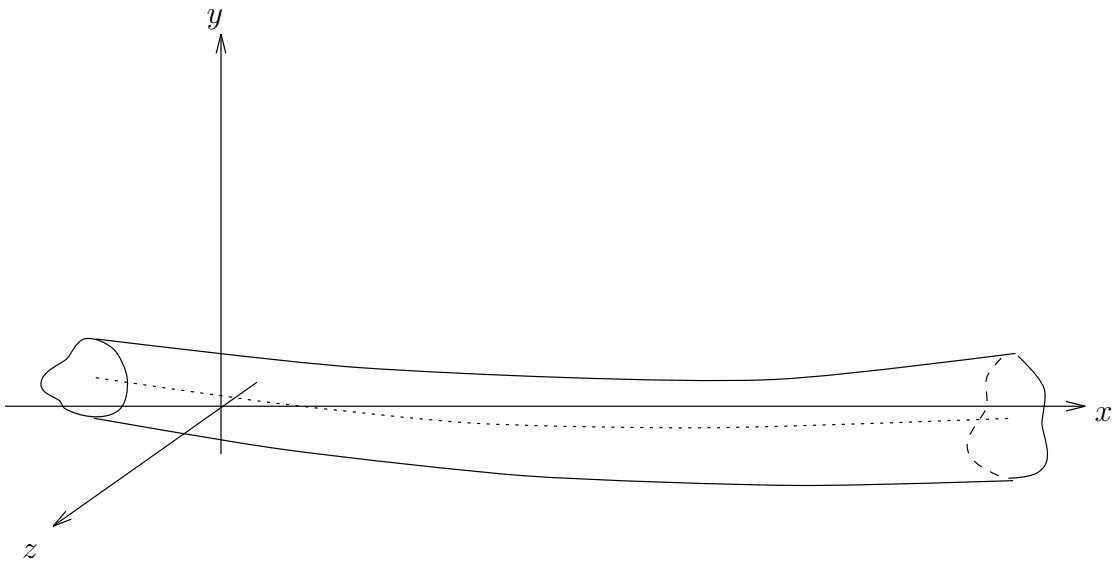

Figure 4.1: Definition sketch for a slender fibre

Throughout this chapter we assume that the Reynolds number and Stokes number are $O(1)$ so that viscous stresses, inertia and gravity are all balanced. In the following section we assume that the capillary number is $O(\epsilon^{-3})$ so that surface tension effects only enter the equations at $O(\epsilon^2)$. However, in sections 4.3 and 4.4 we consider the case where $Ca = O(\epsilon^{-1})$ and surface tension enters the equations at leading order. The rough estimates for the scalings appropriate to the glass industry given in the Introduction suggest that, depending on the exact process under consideration, the capillary number could be anywhere between 10^3 and 10^{10}, so that these two scalings are both potentially of interest.

Having scaled the dimensionless parameters suitably the procedure is, as in the previous chapter, to expand the leading–order unknowns in powers of the slenderness parameter ϵ, typically $u \sim u_0 + \epsilon^2 u_1 + \epsilon^4 u_2 + \ldots$, and equate terms of the same order.

In deriving the leading–order equations we shall be utilising the following transport theorems, introduced in DOW '92.

$$\frac{\partial}{\partial t}\int\int_A \phi \, dydz = \int\int_A \frac{\partial \phi}{\partial t} dxdy - \oint_{\partial A} \frac{G_t \phi \, ds}{(G_y^2 + G_z^2)^{1/2}}, \tag{4.5}$$

$$\frac{\partial}{\partial x}\int\int_A \phi \, dydz = \int\int_A \frac{\partial \phi}{\partial x} dxdy - \oint_{\partial A} \frac{G_x \phi \, ds}{(G_y^2 + G_z^2)^{1/2}}, \tag{4.6}$$

$$\int\int_A \frac{\partial \phi}{\partial y} dydz = \oint_{\partial A} y \frac{(G_y \phi_y + G_z \phi_z) ds}{(G_y^2 + G_z^2)^{1/2}} - \int\int_A y(\phi_{yy} + \phi_{zz}) dydz, \tag{4.7}$$

$$\int\int_A \frac{\partial \phi}{\partial z} dydz = \oint_{\partial A} z \frac{(G_y \phi_y + G_z \phi_z) ds}{(G_y^2 + G_z^2)^{1/2}} - \int\int_A z(\phi_{yy} + \phi_{zz}) dydz. \tag{4.8}$$

Here A is any cross-sectional slice of the fibre (with area $A(x,t)$) and $\phi(x,y,z,t)$ is any twice continuously differentiable function.

4.2 Fibres with low surface tension

Making the assumption outlined above about the size of the capillary number, we substitute for the dimensionless surface tension coefficient

$$\gamma' = \frac{1}{\epsilon^3 Ca} = O(1).$$

The analysis of the equations with this scaling is described in Dewynne, Howell & Wilmott (1994), so we shall omit many of the details here.

4.2.1 Leading–order equations

Consider the leading–order equations of motion and boundary conditions.

$$u_{0_x} + v_{0_y} + w_{0_z} = 0, \tag{4.9}$$

$$u_{0_{yy}} + u_{0_{zz}} = 0, \tag{4.10}$$

$$v_{0_{yy}} + v_{0_{zz}} = p_{0_y}, \tag{4.11}$$

$$w_{0_{yy}} + w_{0_{zz}} = p_{0_z}, \tag{4.12}$$

$$G_{0_t} + u_0 G_{0_x} + v_0 G_{0_y} + w_0 G_{0_z} = 0 \ \text{ on } G_0 = 0, \tag{4.13}$$

$$G_{0_y} u_{0_y} + G_{0_z} u_{0_z} = 0 \ \text{ on } G_0 = 0, \tag{4.14}$$

$$G_{0_x} u_{0_y} + G_{0_y}(-p_0 + 2v_{0_y}) + G_{0_z}(v_{0_z} + w_{0_y}) = 0 \ \text{ on } G_0 = 0, \tag{4.15}$$

$$G_{0_x} u_{0_z} + G_{0_y}(v_{0_z} + w_{0_y}) + G_{0_z}(-p_0 + 2w_{0_z}) = 0 \ \text{ on } G_0 = 0. \tag{4.16}$$

The homogeneous problem for the leading–order axial velocity, (4.10) and (4.14), admits the eigensolution

$$u_0 = u_0(x,t), \tag{4.17}$$

so to leading order the flow is extensional.

We apply the transport theorems (4.5) and (4.6) to the leading–order kinematic condition (4.13) and hence obtain the conservation of mass equation

$$A_{0_t} + (u_0 A_0)_x = 0, \tag{4.18}$$

where A_0 is the leading–order cross–sectional area,

$$A_0 = \int\int_{A_0} dydz. \tag{4.19}$$

Similarly, the leading–order cross–flow problem (4.9), (4.11) and (4.12) with boundary conditions (4.15) and (4.16) admits the eigensolution

$$p_0 = -u_{0_x}, \tag{4.20}$$

$$v_0 = -\frac{u_{0_x}}{2} y + a(x,t)z + b(x,t), \tag{4.21}$$

$$w_0 = -\frac{u_{0_x}}{2} z - a(x,t)y + c(x,t). \tag{4.22}$$

Note that the leading–order dimensionless axial stress $(\sigma_{xx})_0 = -p_0 + 2u_{0_x}$ is given by $3u_{0_x}$, and the Trouton ratio is therefore 3 (c.f. section 2.2).

The arbitrary functions a, b and c represent rotation and translation in the y- and z-directions. The first terms on the right-hand sides of (4.21) and (4.22) represent a uniform scaling of the cross-sectional area. Equations (4.21) and (4.22), along with (4.13), imply that to leading order, each cross-section retains its original shape while undergoing rigid body translation and rotation and an affine scaling in size. Once u_0, a, b and c are known, the evolution of the fibre shape is determined by (4.13).

We can interpret b and c in terms of the motion of the centre–line of the fibre as follows. Define

$$\boldsymbol{r}^*(x,t) = \begin{pmatrix} y^*(x,t) \\ z^*(x,t) \end{pmatrix} = \frac{1}{A_0} \int\int_{A_0} \begin{pmatrix} y \\ z \end{pmatrix} dydz, \tag{4.23}$$

that is, $\boldsymbol{r} = \boldsymbol{r}^*$ is the line joining the centres of mass of the fibre cross–sections. The transport theorems (4.5) and (4.6) and the continuity equation (4.9) then give the identity

$$\boldsymbol{r}^*_t + u_0 \boldsymbol{r}^*_x = \frac{1}{A_0} \int\int_{A_0} \begin{pmatrix} v_0 \\ w_0 \end{pmatrix} dydz. \tag{4.24}$$

Now we substitute in the functional forms of v and w to obtain

$$\begin{aligned} b &= y_t^* + u_0 y_x^* + \frac{u_{0_x}}{2} y^* - a z^*, \\ c &= z_t^* + u_0 z_x^* + \frac{u_{0_x}}{2} z^* + a y^*, \end{aligned} \tag{4.25}$$

so that v_0 and w_0 are given by

$$\begin{aligned} v_0 &= y_t^* + u_0 y_x^* - \frac{u_{0_x}}{2}(y - y^*) + a(z - z^*), \\ w_0 &= z_t^* + u_0 z_x^* - \frac{u_{0_x}}{2}(z - z^*) - a(y - y^*). \end{aligned} \tag{4.26}$$

In order to resolve the indeterminacy remaining in u_0, A_0 and the arbitrary functions a, y^* and z^*, we now have to consider the equations and boundary conditions at $O(\epsilon^2)$.

$$u_{1_x} + v_{1_y} + w_{1_z} = 0, \tag{4.27}$$

$$Re\,(u_{0_t} + u_0 u_{0_x}) = g_x + 2u_{0_{xx}} + u_{1_{yy}} + u_{1zz}, \tag{4.28}$$

$$Re\,(v_{0_t} + u_0 v_{0_x} + v_0 v_{0_y} + w_0 v_{0_z}) = g_y - p_{1_y} + v_{0_{xx}} + v_{1_{yy}} + v_{1_{zz}}, \tag{4.29}$$

$$Re\,(w_{0_t} + u_0 w_{0_x} + v_0 w_{0_y} + w_0 w_{0_z}) = -p_{1_z} + w_{0_{xx}} + w_{1_{yy}} + w_{1_{zz}}, \tag{4.30}$$

$$3G_{0_x} u_{0_x} + G_{0_y}(u_{1_y} + v_{0_x}) + G_{0_z}(u_{1_z} + w_{0_x}) = 0 \ \text{ on } G_0 = 0, \tag{4.31}$$

$$G_{0_x}(u_{1_y} + v_{0_x}) + G_{0_y}(-p_1 + 2v_{1_y}) + G_{0_z}(v_{1_z} + w_{1_y}) = -\gamma' \kappa_0 G_{0_y} \ \text{ on } G_0 = 0, \tag{4.32}$$

$$G_{0_x}(u_{1_z} + w_{0_x}) + G_{0_y}(v_{1_z} + w_{1_y}) + G_{0_z}(-p_1 + 2w_{1_z}) = -\gamma' \kappa_0 G_{0_z} \ \text{ on } G_0 = 0. \tag{4.33}$$

Note that the $O(\epsilon^2)$ kinematic boundary condition is not required, and that G_1 does not appear at this order.

Assuming G_0 is known, the $O(\epsilon^2)$ axial velocity u_1 is determined up to an arbitrary function of x and t by (4.28) with boundary condition (4.31). The solvability condition for this Neumann problem gives a relation between A_0 and u_0, which we recognise as an axial force balance,

$$(3A_0 u_{0_x})_x = Re\, A_0 (u_{0_t} + u_0 u_{0_x}) - g_x A_0. \tag{4.34}$$

Equations (4.18) and (4.34) form a closed system for A_0 and u_0 which is the same as that obtained for an axisymmetric fibre with inertia and gravity in section 2.5.

4.2.2 Motion of the centre–line

We now proceed in a similar fashion to use solvability conditions for equations (4.29) and (4.30) with boundary conditions (4.32) and (4.33) to derive equations for the remaining unknowns a, y^* and z^*. We omit the details which may be found in Dewynne, Howell & Wilmott (1994). Integration of (4.29) and (4.30) over the cross–section and use of the transport theorems (4.5) to (4.8) leads to

$$Re\, A_0 \left(\frac{\partial}{\partial t} + u_0 \frac{\partial}{\partial x} \right)^2 \boldsymbol{r}^* = 3(A_0 u_{0_x} \boldsymbol{r}^*_x)_x + g_y A_0 \boldsymbol{j} - \gamma' \oint_{\partial A_0} \kappa_0 \hat{\boldsymbol{n}}\, ds, \tag{4.35}$$

where $\hat{\boldsymbol{n}}$ is the two-dimensional normal to the cross–sectional slice,

$$\hat{\boldsymbol{n}} = \frac{1}{(G_{0_y}^2 + G_{0_z}^2)^{1/2}} \begin{pmatrix} G_{0_y} \\ G_{0_z} \end{pmatrix}. \tag{4.36}$$

Now we note that to find the leading–order curvature κ_0 it is only necessary to calculate the curvature of the boundary of the cross–section, ∂A_0; the dependence on x only comes in at higher order. It is then a trivial exercise to show that the integral multiplying the surface tension coefficient in (4.35) is identically zero for any smooth surface. Hence (4.35) simplifies to the following equation for the fibre centre–line:

$$(Re\, u_0^2 - 3u_{0_x}) \boldsymbol{r}^*_{xx} + 2Re\, u_0 \boldsymbol{r}^*_{xt} + Re\, \boldsymbol{r}^*_{tt} = g_y \boldsymbol{j} - g_x \boldsymbol{r}^*_x. \tag{4.37}$$

Notice the strong analogy between this equation and that for the centre–line of a two–dimensional sheet (2.56), with a change in the Trouton ratio from 4 to 3. As noted in section 2.5 the equation changes type from hyperbolic to elliptic depending on whether the fibre is under tension or compression, contrasting with the inertia–free model derived by DOW '92 which predicts that the centre–line is straight in either case. As the elliptic problem is ill–posed, leading to instability or blow–up, the inclusion of inertia terms gives a new mechanism for the irreversibility of the fibre–drawing process. We shall discuss this analogy between nonaxisymmetric fibres and two–dimensional sheets further at the end of the next chapter.

4.2.3 Rotation of the fibre

It remains to find an equation for a which represents the angular speed at which the fibre rotates about its centre–line. We do this by taking moments of (4.29) and (4.30) and consider the term

$$\int\int_{A_0} y(w_{1_{yy}} + w_{1_{zz}}) - z(v_{1_{yy}} + v_{1_{zz}})\, dydz.$$

Again we find that the term due to surface tension is identically zero, and the resulting equation reduces to

$$Re\,[(\mathcal{I}a)_t + (u_0\mathcal{I}a)_x] = \frac{\partial}{\partial x}\left\{\mathcal{I}a_x + \int\int_{A_0}\left((z-z^*)u_{1_y} - (y-y^*)u_{1_z}\right) dydz\right\}, \tag{4.38}$$

where $\mathcal{I}$ is the moment of inertia of the cross–section about its centre–line, that is

$$\mathcal{I} = \int\int_{A_0}\left((y-y^*)^2 + (z-z^*)^2\right)\, dydz. \tag{4.39}$$

Since u_1 is given up to an arbitrary function of x and t by (4.28) and (4.31), (4.38) determines a in principle. However in practice, solving for a will be complicated by the fact that it is necessary to solve the Neumann problem for u_1 at each time–step. As observed by DOW '92, because of the shape–preserving property noted earlier, this problem can be circumvented by transforming to scaled Lagrangian variables so that u_1 need only be found once, at $t = 0$.

4.2.4 Lagrangian description

We shall now recast the problem in terms of Lagrangian variables similar to those introduced by DOW '92. We set

$$\begin{aligned}
x &= X(\xi,\tau),\\
y^*(x,t) &= Y^*(\xi,\tau) = \eta^*\cos\theta + \zeta^*\sin\theta,\\
z^*(x,t) &= Z^*(\xi,\tau) = \zeta^*\cos\theta - \eta^*\sin\theta,\\
y &= Y(\xi,\eta,\zeta,\tau) = Y^* + \mathcal{A}(\xi,\tau)^{1/2}(\eta\cos\theta + \zeta\sin\theta),\\
z &= Z(\xi,\eta,\zeta,\tau) = Z^* + \mathcal{A}(\xi,\tau)^{1/2}(\zeta\cos\theta - \eta\sin\theta),\\
t &= \tau,
\end{aligned} \tag{4.40}$$

where $\mathcal{A}(\xi,\tau) = A_0(X(\xi,\tau),\tau)$ and θ, X, Y and Z are defined by

$$\begin{aligned}
\theta_\tau &= a(X(\xi,\tau),\tau) = \alpha(\xi,\tau), \quad \theta(0) = 0, \text{ say,} \\
X_\tau &= u_0(X(\xi,\tau),\tau), \quad X(\xi,0) = \xi, \\
Y_\tau &= v_0(X(\xi,\tau), Y(\xi,\eta,\zeta,\tau), Z(\xi,\eta,\zeta,\tau),\tau), \quad Y(\xi,\eta,\zeta,0) = \eta^*(\xi,0) + \mathcal{A}(\xi,0)^{1/2}\eta, \\
Z_\tau &= w_0(X(\xi,\tau), Y(\xi,\eta,\zeta,\tau), Z(\xi,\eta,\zeta,\tau),\tau), \quad Z(\xi,\eta,\zeta,0) = \zeta^*(\xi,0) + \mathcal{A}(\xi,0)^{1/2}\zeta.
\end{aligned}$$

If a Lagrangian description of the leading-order free surface is given by $\mathcal{G} = 0$, the kinematic condition (4.13) gives $\mathcal{G}_\tau = 0$ so that we may take

$$\mathcal{G}(\xi,\eta,\zeta) = G(x,y,z,0). \tag{4.41}$$

Our equations (4.18) and (4.34) governing A_0 and u_0, translated into Lagrangian variables may be integrated twice as in section 2.4 to give

$$X_\xi = \frac{\mathcal{A}_0(\xi)}{\mathcal{A}(\xi,\tau)}, \tag{4.42}$$

$$3\mathcal{A}_\xi + \mathcal{A}_0(Re\, X_\tau - g_x\tau) = 3\mathcal{A}_0' + Re\, \mathcal{A}_0 X_\tau(\xi,0), \tag{4.43}$$

where $\mathcal{A}_0(\xi) = \mathcal{A}(\xi,0)$ is the initial cross–sectional area. The equation for the centre–line (4.37) becomes

$$Re\, \mathcal{A}_0 Y^*_{\tau\tau} = -\frac{\partial}{\partial\xi}\left(\frac{3\mathcal{A}_\tau Y^*_\xi}{X_\xi}\right) + g_y\mathcal{A}_0, \quad Re\, \mathcal{A}_0 Z^*_{\tau\tau} = -\frac{\partial}{\partial\xi}\left(\frac{3\mathcal{A}_\tau Z^*_\xi}{X_\xi}\right). \tag{4.44}$$

We now transform the problem for u_1 given by (4.28) and (4.31) into Lagrangian variables, setting

$$u_1 = \mathcal{A}\left(\tilde{u} + \frac{1}{4}(\eta^2+\zeta^2)(Re\, u_{0_\tau} - g_x - 2u_{0_{xx}})\right)$$
$$+\frac{\mathcal{A}^{1/2}\eta}{X_\xi^2}\left(\frac{5u_{0_\xi}}{2}(\eta_\xi^* + \theta_\xi\zeta^*) - X_\xi(\eta_\xi^* + \theta_\xi\zeta^*)_\tau\right)$$
$$+\frac{\mathcal{A}^{1/2}\zeta}{X_\xi^2}\left(\frac{5u_{0_\xi}}{2}(\zeta_\xi^* - \theta_\xi\eta^*) - X_\xi(\zeta_\xi^* - \theta_\xi\eta^*)_\tau\right), \tag{4.45}$$

so that $\tilde{u}$ satisfies

$$\tilde{u}_{\eta\eta} + \tilde{u}_{\zeta\zeta} = 0,$$
$$\mathcal{G}_\eta\tilde{u}_\eta + \mathcal{G}_\zeta\tilde{u}_\zeta = -\frac{3u_{0_\xi}}{X_\xi^2}\mathcal{G}_\xi + \left(\frac{3u_{0_\xi}\theta_\xi}{X_\xi^2} - \frac{\alpha_\xi}{X_\xi}\right)(\zeta\mathcal{G}_\eta - \eta\mathcal{G}_\zeta) \quad \text{on } \mathcal{G}=0. \tag{4.46}$$

As in DOW '92, we may write $\tilde{u}$ as a combination of two functions, both independent of τ,

$$\tilde{u} = -\left(\frac{3u_{0_\xi}}{X_\xi^2}\right)\tilde{u}_1 + \left(\frac{3u_{0_\xi}\theta_\xi}{X_\xi^2} - \frac{\alpha_\xi}{X_\xi}\right)\tilde{u}_2, \tag{4.47}$$

where $\tilde{u}_1$ and $\tilde{u}_2$ satisfy the Neumann problems

$$\tilde{u}_{1_{\eta\eta}} + \tilde{u}_{1_{\zeta\zeta}} = 0, \quad \tilde{u}_{1_\eta}\mathcal{G}_\eta + \tilde{u}_{1_\zeta}\mathcal{G}_\zeta = \mathcal{G}_\xi \ \text{ on } \mathcal{G}=0, \tag{4.48}$$

and

$$\tilde{u}_{2_{\eta\eta}} + \tilde{u}_{2_{\zeta\zeta}} = 0, \quad \tilde{u}_{2_\eta}\mathcal{G}_\eta + \tilde{u}_{2_\zeta}\mathcal{G}_\zeta = \zeta\mathcal{G}_\eta - \eta\mathcal{G}_\zeta \ \text{ on } \mathcal{G}=0, \tag{4.49}$$

the same problems as those found in DOW '92 when neglecting inertia and gravity. These problems need only be solved once, using the initial shape of the free surface, given by $G(x,y,z,0)=0$. Then the following time independent integrals, which depend solely on the initial shape of the fibre, must be calculated:

$$\tilde{\mathcal{I}} = \int\int_{\mathcal{A}_0}(\eta^2+\zeta^2)\,d\eta d\zeta, \tag{4.50}$$

$$I_1 = \int\int_{\mathcal{A}_0}\left(\eta\tilde{u}_{1_\zeta} - \zeta\tilde{u}_{1_\eta}\right)d\eta d\zeta, \tag{4.51}$$

$$I_2 = \int\int_{\mathcal{A}_0}\left(\eta\tilde{u}_{2_\zeta} - \zeta\tilde{u}_{2_\eta}\right)d\eta d\zeta. \tag{4.52}$$

Substitution of the expression (4.45) for u_1 into (4.38) then gives an equation for $\theta(\xi,\tau)$, the angle through which the fibre twists, using the fact that $\alpha = \theta_\tau$:

$$\frac{\partial}{\partial\xi}\left\{\frac{\mathcal{A}}{X_\xi}\left((I_2+\tilde{\mathcal{I}})\mathcal{A}\theta_{\xi\tau} + 3I_2\mathcal{A}_\tau\theta_\xi - 3I_1\mathcal{A}_\tau\right)\right\} = Re\tilde{\mathcal{I}}\left(\mathcal{A}\theta_\tau\right)_\tau. \tag{4.53}$$

Note the inhomogeneous term $-3I_1\mathcal{A}_\tau$ on the left-hand side of (4.53). So long as this term is non-zero, the fibre will be forced to twist even if no twist is applied at the ends. This p.d.e. for θ is of mixed hyperbolic–parabolic type, with characteristic directions given by $\tau = \text{const.}$ and a repeated root $\xi = \text{const.}$

In summary, the leading–order cross–sectional area and axial velocity satisfy the generalised Trouton model (4.18) and (4.34), which using a Lagrangian formulation may be integrated twice to give (4.42) and (4.43). The motion of the centre–line is governed by the decoupled equations (4.37), which become (4.44) in the Lagrangian formulation. Then to solve for the twist of the fibre about its axis, it is necessary to solve the two Neumann problems (4.48) and (4.49) and then calculate the integrals $\tilde{\mathcal{I}}$, I_1 and I_2, which are functions only of ξ and depend on the initial shape of the fibre. Once these are known, θ is given by equation (4.53). We shall now consider an example where the initial geometry of the fibre is simple enough that the integrals may be found explicitly.

4.2.5 Example — fibres with elliptical cross–section

Suppose the surface of the fibre is given initially by

$$G(x,y,z,0) = \left(\frac{y-y_0^*(x)}{\alpha(x)}\right)^2 + \left(\frac{z-z_0^*(x)}{\beta(x)}\right)^2 - 1 = 0.$$

Here (y_0^*, z_0^*) is the initial position of the centre-line; α and β are given positive functions. The initial cross–sectional area of the fibre, $\mathcal{A}_0 = \pi\alpha\beta$ so that the Lagrangian description of the free surface is

$$\mathcal{G}(\xi,\eta,\zeta) = \pi\alpha(\xi)\beta(\xi)\left[\left(\frac{\eta}{\alpha(\xi)}\right)^2 + \left(\frac{\zeta}{\beta(\xi)}\right)^2\right] - 1 = 0.$$

We can solve (4.48) and (4.49) explicitly, giving

$$\tilde{u}_1 = \frac{1}{4}\left(\frac{\beta'}{\beta} - \frac{\alpha'}{\alpha}\right)(\eta^2 - \zeta^2), \quad \tilde{u}_2 = \left(\frac{\beta^2-\alpha^2}{\beta^2+\alpha^2}\right)\eta\zeta, \tag{4.54}$$

so that

$$\tilde{\mathcal{I}} = \frac{\pi}{4\alpha\beta}(\alpha^2+\beta^2), \quad I_1 = 0, \quad I_2 = -\frac{\pi(\alpha^2-\beta^2)^2}{4\alpha\beta(\alpha^2+\beta^2)}. \tag{4.55}$$

Consider for example the case where there is no stretching at all, so that $u_0 = g_x = g_y = 0$. Then $X = \xi$, $\mathcal{A} = \pi\alpha\beta$, and (4.53) becomes

$$\frac{\partial}{\partial\xi}\left(\frac{\alpha^3\beta^3}{\alpha^2+\beta^2}\theta_{\xi\tau}\right) = \frac{Re(\alpha^2+\beta^2)\alpha\beta}{4}\theta_{\tau\tau}. \tag{4.56}$$

This is clearly a diffusion equation for θ_τ; changes in the rate of rotation of the ends of the fibre will diffuse along the fibre.

Apply boundary conditions $\theta(0,\tau) = 0$, $\theta(1,\tau) = \Theta(\tau)$ and $\theta(\xi,0) = 0$. Then the solution is

$$\theta = \frac{\int_0^\xi h(s)\,ds}{\int_0^1 h(s)\,ds}\Theta + \sum_{n=1}^{\infty} f_n(\xi)e^{-k_n^2\tau}\int_0^\tau (B_n - A_n\Theta'(s))e^{k_n^2 s}ds, \tag{4.57}$$

where

$$h(s) = \frac{\alpha(s)^2+\beta(s)^2}{\alpha(s)^3\beta(s)^3}$$

and f_n and k_n are the eigenvectors and eigenvalues of the Stürm-Liouville problems

$$\left(\frac{\alpha^3\beta^3}{\alpha^2+\beta^2}f_n'\right)' + \frac{k_n^2 Re(\alpha^2+\beta^2)\alpha\beta}{4}f_n = 0,$$

$$f_n(0) = f_n(1) = 0, \tag{4.58}$$

assumed to be normalised such that

$$\int_0^1 (\alpha^2+\beta^2)\alpha\beta f_n^2\,ds = 1.$$

The constants A_n and B_n are given by

$$A_n = \left\{\int_0^1 (\alpha(s)^2+\beta(s)^2)\alpha(s)\beta(s)f_n(s)\int_0^s h(t)\,dtds\right\} \Big/ \left\{\int_0^1 h(t)\,dt\right\},$$

$$B_n = \int_0^1 (\alpha(s)^2+\beta(s)^2)\alpha(s)\beta(s)f_n(s)\theta_\tau(s,0)\,ds.$$

For example, consider a fibre of uniform elliptical cross-section, spinning with uniform angular velocity and then brought to rest by fixing its two ends. In this case, α and β are constants, $\Theta = 0$ and $\theta_\tau(\xi,0) = 1$, and the solution is

$$\theta = \frac{Re(\alpha^2+\beta^2)^2}{\pi^3\alpha^2\beta^2}\sum_{n=0}^{\infty}\frac{\sin[(2n+1)\pi\xi]}{(2n+1)^3}\left[1-\exp\left(-\frac{4\pi^2\alpha^2\beta^2n^2\tau}{Re(\alpha^2+\beta^2)^2}\right)\right]. \tag{4.59}$$

A plot of the evolution of such a fibre is given in figure 4.2.

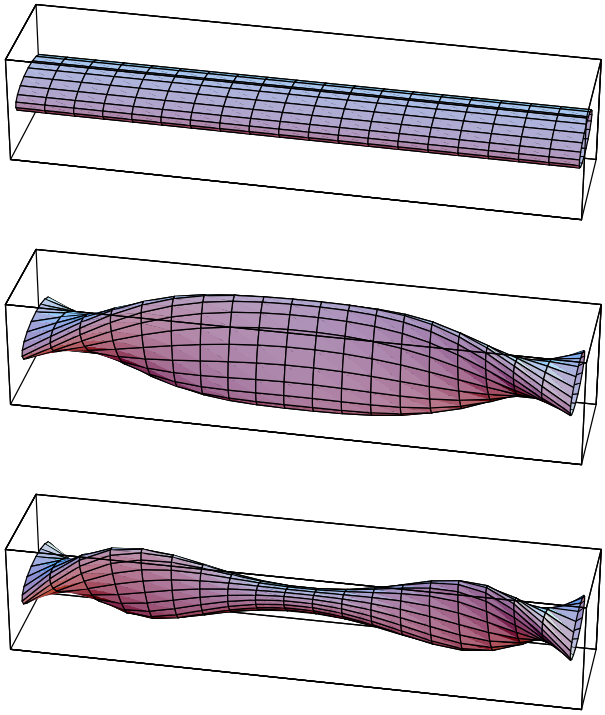

Figure 4.2: The twisting of a uniform elliptic fibre

4.3 Fibres with higher surface tension

In the previous section we considered the dynamics of a viscous fibre of arbitrary cross–section, restricting our attention to cases in which surface tension effects are small enough that the shape of each fibre cross–section is preserved. We found that in the cases we have considered surface tension does not in fact affect the leading–order behaviour of the fibre at all. Hence, in order to model fibres for which surface tension is an important effect, we are forced to abandon this shape–preserving property; indeed the cross–sectional shape will evolve under the action of surface tension and probably tend towards a circle.

We now rescale the surface tension coefficient assuming it is an order of magnitude higher than in the last section:

$$\gamma^* = \frac{1}{\epsilon Ca} = O(1). \tag{4.60}$$

The leading–order Navier–Stokes equations and kinematic boundary condition (4.9) to (4.13) are unchanged, as is the x-component of the dynamic boundary condition (4.14). Hence the Neumann problem for u_0 is unchanged, and yields an

extensional flow as before,

$$u_0 = u_0(x,t). \tag{4.61}$$

Similarly, the derivation of the conservation of mass equation follows exactly as in the previous section, giving

$$A_{0_t} + (u_0 A_0)_x = 0. \tag{4.62}$$

Surface tension now enters the cross–flow components of the dynamic boundary condition, and (4.15) and (4.16) are replaced by (making use of (4.61))

$$G_{0_y}(-p_0 + 2v_{0_y}) + G_{0_z}(v_{0_z} + w_{0_y}) = -\gamma^* \kappa_0 G_{0_y} \quad \text{on } G_0 = 0, \tag{4.63}$$

$$G_{0_y}(v_{0_z} + w_{0_y}) + G_{0_z}(-p_0 + 2w_{0_z}) = -\gamma^* \kappa_0 G_{0_z} \quad \text{on } G_0 = 0. \tag{4.64}$$

In section (4.2) we found it was possible to find a general solution of the leading–order problem for v_0 and w_0 in terms of arbitrary functions a, b and c. Now that surface tension effects enter the problem at leading–order, this is no longer possible; the solution for u_0 and v_0 depends strongly on the shape of the cross–section through the boundary conditions (4.63) and (4.64).

Using (4.61) we write (4.11) and (4.12) in the form

$$(-p_0 + 2v_{0_y})_y + (v_{0_z} + w_{0_y})_z = 0,$$

$$(v_{0_z} + w_{0_y})_y + (-p_0 + 2w_{0_z})_z = 0,$$

so that we may use an Airy stress function $\mathfrak{A}$, in terms of which

$$\begin{aligned} -p_0 + 2v_{0_y} &= \mathfrak{A}_{zz}, \\ v_{0_z} + w_{0_y} &= -\mathfrak{A}_{yz}, \\ -p_0 + 2w_{0_z} &= \mathfrak{A}_{yy}. \end{aligned} \tag{4.65}$$

The problem for $\mathfrak{A}$ is[1]

$$\left.\begin{aligned} \hat{\nabla}^4 \mathfrak{A} &= 0 && \text{in } A_0, \\ \mathfrak{A} &= 0 \\ \frac{\partial \mathfrak{A}}{\partial \hat{n}} &= -\gamma^* \end{aligned}\right\} \quad \text{on } \partial A_0, \tag{4.66}$$

[1]Note that $\mathfrak{A}$ is only defined up to a linear function of y and z. This means that physical boundary conditions for $\mathfrak{A}$ will in general involve some arbitrary constants which can be chosen to simplify the boundary conditions as much as possible. For example, at a stress–free boundary, the most general boundary condition is that $\hat{\nabla}\mathfrak{A}$ is constant on the boundary. However, this constant vector may be chosen to be zero, resulting in $\partial\mathfrak{A}/\partial\hat{n} = 0$, $\mathfrak{A}$ = const.. Finally, this constant may also be taken to be zero, resulting in the standard stress–free boundary condition: $\mathfrak{A}$ and its normal derivative both being zero.

where $\hat{\nabla}^2$ is the two–dimensional Laplacian $\partial^2/\partial y^2 + \partial/\partial z^2$, and $\hat{\boldsymbol{n}}$ is the two–dimensional normal to the cross–section; $\hat{\boldsymbol{n}} = (G_{0_y}^2 + G_{0_z}^2)^{-1/2}(0, G_{0_y}, G_{0_z})$. If G_0 is known then $\mathfrak{A}$ is given uniquely by (4.66). However, in general this boundary value problem for $\mathfrak{A}$ must be solved anew at each time–step as the cross–section evolves. Once $\mathfrak{A}$ is known, the leading–order pressure and transverse velocity gradients are given by

$$\begin{aligned} p_0 &= -\tfrac{1}{2}(\mathfrak{A}_{yy} + \mathfrak{A}_{zz}) - u_{0_x}, \\ v_{0_y} &= \tfrac{1}{4}(\mathfrak{A}_{zz} - \mathfrak{A}_{yy}) - \tfrac{1}{2}u_{0_x}, \\ w_{0_z} &= \tfrac{1}{4}(\mathfrak{A}_{yy} - \mathfrak{A}_{zz}) - \tfrac{1}{2}u_{0_x}, \end{aligned} \tag{4.67}$$

where

$$v_{0_z} + w_{0_y} = -\mathfrak{A}_{yz}. \tag{4.68}$$

As noted before, v_0 and w_0 are only given up to an arbitrary rigid–body motion by these equations. To determine them uniquely it is necessary to proceed to higher order to find three equations governing the lateral motion of the cross–section and its rotation.

The problem for the first–order axial velocity is

$$u_{1_{yy}} + u_{1_{zz}} = Re\,(u_{0_t} + u_0 u_{0_x}) + p_{0_x} - u_{0_{xx}} - g_x,$$

$$u_{1_y} G_{0_y} + u_{1_z} G_{0_z} = G_{0_x}(p_0 - 2u_{0_x} - \gamma^* \kappa_0) - G_{0_y} v_{0_x} - G_{0_z} w_{0_x} \quad \text{on } G_0 = 0. \tag{4.69}$$

Assuming G_0 is known, this Neumann problem defines u_1 up to an arbitrary function of x and t. By using the boundary conditions (4.66) for $\mathfrak{A}$, the solvability condition for (4.69) may be reduced to

$$(3A_0 u_{0_x})_x = Re\, A_0(u_{0_t} + u_0 u_{0_x}) - g_x A_0 + \frac{\gamma^*}{2}\frac{\partial}{\partial x}\oint_{\partial A_0} ds + \gamma^* \oint_{\partial A_0} \frac{\kappa_0 G_{0_x} ds}{(G_{0_y}^2 + G_{0_z}^2)^{1/2}}. \tag{4.70}$$

Denoting by S the circumference of the cross–section, it may be shown that the final integral in this equation is equal to $-S_x$, so that the axial stress balance is given by

$$(3A_0 u_{0_x})_x = Re\, A_0(u_{0_t} + u_0 u_{0_x}) - g_x A_0 - \frac{\gamma^*}{2} S_x. \tag{4.71}$$

As an example of the effect which surface tension has in this equation, in the next section we shall consider the case in which the cross–section of the fibre is circular.

In such a case, (4.71) reduces to (2.58) for an axisymmetric fibre. As was shown in section 2.5 an important effect introduced through the inclusion of surface tension in this simple case is the possibility that the fibre may break up in finite time.

Now we consider the first–order cross–flow. The equations for v_1, w_1 and p_1, namely (4.27), (4.29) and (4.30), are unchanged, but the boundary conditions (4.32) and (4.33) become

$$G_{0_x}(u_{1_y}+v_{0_x})+G_{0_y}(-p_1+2v_{1_y})+G_{0_z}(v_{1_z}+w_{1_y}) = -\gamma^*\kappa_1 G_{0_y} \quad \text{on } G_0=0, \tag{4.72}$$

$$G_{0_x}(u_{1_z}+w_{0_x})+G_{0_y}(v_{1_z}+w_{1_y})+G_{0_z}(-p_1+2w_{1_z}) = -\gamma^*\kappa_1 G_{0_z} \quad \text{on } G_0=0, \tag{4.73}$$

where κ_1 is the first–order perturbation to the curvature of the free surface. Integration of (4.29) and (4.30) over the cross–section with the new boundary conditions gives the lateral force balance; as above we use the boundary conditions satisfied by $\mathfrak{A}$ to write the surface tension terms in a form which depends only on the shape of the cross–section:

$$\begin{aligned}
&(Re\,u_0^2-3u_{0_x})\boldsymbol{r}^*_{xx}+2Re\,u_0\boldsymbol{r}^*_{xt}+Re\,\boldsymbol{r}^*_{tt}-g_y\boldsymbol{j}+g_x\boldsymbol{r}^*_x\\
&\quad=-\frac{\gamma^*}{A_0}\left\{\frac{1}{2}\boldsymbol{r}^*_{xx}S+\boldsymbol{r}^*_xS_x+\frac{1}{2}\frac{\partial^2}{\partial x^2}\oint_{\partial A_0}(\boldsymbol{r}-\boldsymbol{r}^*)ds\right.\\
&\qquad\left.+\frac{\partial}{\partial x}\oint_{\partial A_0}\frac{(\boldsymbol{r}-\boldsymbol{r}^*)\kappa_0 G_{0_x}ds}{(G_{0_y}^2+G_{0_z}^2)^{1/2}}+\oint_{\partial A_0}\kappa_1\hat{\boldsymbol{n}}\,ds\right\}.
\end{aligned} \tag{4.74}$$

An equation for the twist of the fibre is found as before by taking moments of the transverse velocity equations (4.29) and (4.30) before integrating over the cross–section. This yields

$$\begin{aligned}
&\frac{\partial}{\partial x}\int\int_{A_0}\Big((y-y^*)(w_{0_x}+u_{1_z})-(z-z^*)(v_{0_x}+u_{1_y})\Big)\,dydz\\
&=Re\,A_0(L_t+u_0L_x)+\gamma^*\oint_{\partial A_0}\frac{\kappa_1((y-y^*)G_{0_z}-(z-z^*)G_{0_y})ds}{(G_{0_y}^2+G_{0_z}^2)^{1/2}},
\end{aligned} \tag{4.75}$$

where L is the scaled angular momentum of the cross–section,

$$L=\frac{1}{A_0}\int\int_{A_0}((y-y^*)w_0-(z-z^*)v_0)\,dydz. \tag{4.76}$$

Hence in general the problem must be solved as follows. Given the shape of the cross–section at some time, the axial velocity u_0 may be found from (4.71). Then

(4.66) must be solved for the stress function $\mathfrak{A}$, in terms of which v_0 and w_0 are given up to an arbitrary rigid–body motion by (4.67). The rigid–body translation is given by (4.74) and the rotation by (4.75), which also requires the solution of the Neumann problem (4.69) for u_1. Once u_0, v_0 and w_0 have been found, the evolution of the cross–section is given by the kinematic boundary condition (4.13).

Unlike section 4.2, changing to Lagrangian variables will not significantly simplify this solution procedure as the shape–preserving property found in that section has been lost due to higher surface tension effects. However, we shall now consider a simple example in which the the cross–section is circular — when surface tension effects are important, this will certainly be the case after some time. Then in section 4.4 we shall show how the evolution of a more general cross–section may be found by analogy with the two–dimensional sintering problem considered by Hopper (1990) and Richardson (1992).

4.3.1 A fibre with circular cross–section

Suppose

$$G_0(x,y,z,t) = (y - y^*(x,t))^2 + (z - z^*(x,t))^2 - R_0(x,t)^2, \tag{4.77}$$

so that $\kappa_0 = 1/R_0$. Then (4.66) may be solved explicitly to give

$$\mathfrak{A} = \frac{\gamma^*}{2R_0}\left(R_0^2 - (y-y^*)^2 - (z-z^*)^2\right), \tag{4.78}$$

so that the general solution for p_0, v_0 and w_0 is

$$\begin{aligned} p_0 &= \frac{\gamma^*}{R_0} - u_{0_x}, \\ v_0 &= y_t^* + u_0 y_x^* - \tfrac{1}{2}u_{0_x}(y-y^*) + a(z-z^*), \\ w_0 &= z_t^* + u_0 z_x^* - \tfrac{1}{2}u_{0_x}(z-z^*) - a(y-y^*), \end{aligned} \tag{4.79}$$

where, as before, y^* and z^* are the coordinates of the centre–line of the fibre and a represents rotation of the fibre about its centre–line.

Likewise, for this simple geometry, the problem (4.69) may be solved explicitly, giving

$$\begin{aligned} u_1 &= \tfrac{1}{4}\left((y-y^*)^2+(z-z^*)^2\right)\left(u_{0_{xx}}+\tfrac{6R_{0_x}u_{0_x}}{R_0}\right) \\ &+ (y-y^*)\left(\tfrac{3}{2}u_{0_x}y^*_x - y^*_{xt} - u_0 y^*_{xx} + a z^*_x\right) \\ &+ (z-z^*)\left(\tfrac{3}{2}u_{0_x}z^*_x - z^*_{xt} - u_0 z^*_{xx} - a y^*_x\right), \end{aligned} \tag{4.80}$$

where an arbitrary but irrelevant function of x and t has been omitted.

Substituting for the circumference of the circular cross–section into (4.71) gives an axial force balance which is the same as that obtained for an axisymmetric fibre in section 2.5,

$$(3R_0^2 u_{0_x})_x = Re\, R_0^2(u_{0_t} + u_0 u_{0x}) - g_x\, R_0^2 - \gamma^* R_{0_x}. \tag{4.81}$$

Using the simple geometry, we may simplify the lateral force balance (4.74) to give

$$\begin{aligned} &(Re\, u_0^2 - 3u_{0_x})\boldsymbol{r}^*_{xx} + 2Re\, u_0 \boldsymbol{r}^*_{xt} + Re\, \boldsymbol{r}^*_{tt} - g_y \boldsymbol{j} + g_x \boldsymbol{r}^*_x \\ &\qquad = -\frac{\gamma^*}{R_0^2}\left(R_{0_x}\boldsymbol{r}^*_x + \frac{1}{\pi}\oint_{\partial A_0} \kappa_1 \hat{\boldsymbol{n}}\, ds\right). \end{aligned} \tag{4.82}$$

To evaluate the line integral, suppose

$$G(x,y,z,t) = (y - y^*(x,t))^2 + (z - z^*(x,t))^2 - R(x,t)^2, \tag{4.83}$$

and expand y^*, z^* and R in powers of ϵ^2. Then we find that the curvature of the free surface at a point $(x, y^* + R\cos\theta, z^* + R\sin\theta)$ is given by

$$\begin{aligned} \kappa \sim \frac{1}{\epsilon R_0} + \frac{\epsilon}{4R_0^2}\Big\{ &-4R_1 - 2R_0 R_{0_x}^2 - 4R_0^2 R_{0_{xx}} - 4R_0 R_{0_x}(y^*_x \cos\theta + z^*_x \sin\theta) \\ &+ R_0 y^{*2}_x (1 - 3\cos 2\theta) + R_0 z^{*2}_x (1 + 3\cos 2\theta) - 6R_0 y^*_x z^*_x \sin 2\theta \\ &- 4R_0^2 (y^*_{xx}\cos\theta + z^*_{xx}\sin\theta)\Big\} + O(\epsilon^3). \end{aligned}$$

Put $\kappa \sim \epsilon^{-1}\kappa_0 + \epsilon\kappa_1 + \ldots$, then the line integral in (4.82) evaluates to

$$\oint_{\partial A_0} \kappa_1 \hat{\boldsymbol{n}}\, ds = -\pi \frac{\partial}{\partial x}\begin{pmatrix} R_0 y^*_x \\ R_0 z^*_x \end{pmatrix},$$

so that the centre–line equation becomes

$$(Re\, u_0^2 - 3u_{0_x} - \gamma^* R_0^{-1})\boldsymbol{r}^*_{xx} + 2Re\, u_0 \boldsymbol{r}^*_{xt} + Re\, \boldsymbol{r}^*_{tt} = g_y \boldsymbol{j} - g_x \boldsymbol{r}^*_x. \tag{4.84}$$

The effect of surface tension is to add a term to the tension in the fibre. The discriminant of this p.d.e. is now $Re(3u_{0_x}+\gamma^* R_0^{-1})$, so that it can remain hyperbolic while undergoing compression ($u_{0_x} < 0$) if $\gamma^* R_0^{-1}$ is large enough.

Since we have an explicit solution for u_1, we can derive an equation for the rate of twist a from (4.75) without resorting to Lagrangian variables. Not surprisingly, given the symmetry of the cross–section in this case, surface tension has no effect on the twisting of the fibre, which is governed by

$$(R_0^4 a_x)_x = Re\, R_0^2 \left((R_0^2 a)_t + u_0 (R_0^2 a)_x \right). \tag{4.85}$$

Note that this agrees with (2.77) for an axisymmetric fibre.

In conclusion, in the case where we assume the fibre is of circular cross–section, the radius, axial velocity and twist of the fibre satisfy equations identical to those found for an axisymmetric fibre in section 2.5. The difference here is that the fibre is not assumed to be straight; its centre–line satisfies (4.84), on which surface tension has a stabilising effect, tending to counteract the change of type from hyperbolic to elliptic described in section 4.2.

We shall now discuss what progress may be made when the fibre has a more general cross–sectional shape.

4.4 The quasi–two–dimensional sintering problem

In the previous section we derived equations governing the axial velocity and cross–sectional area ((4.62) and (4.71)) and lateral translation (4.74) of a nonaxisymmetric fibre, in which the surface tension terms are simple functions of the shape of the cross–section (though the equation for the twist of the fibre (4.75) requires the solution of two boundary value problems (4.66) and (4.69)). Hence the solution procedure is simplified considerably if the evolution of the cross–sectional shape can be determined. We shall now show that for many simple geometries of practical interest, the problem of determining the evolution of the cross–sectional shape may be reduced to the solution of a couple of first–order p.d.e.'s in x and t.

Consider the problem for the leading–order cross flow (4.9), (4.11), (4.12) with dynamic boundary conditions (4.63) and (4.64) and kinematic boundary condition (4.13). We now subtract the general solution found in section 4.2 where surface tension was not present at this order, setting

$$\begin{aligned} v_0 &= y_t^* + u_0 y_x^* - \tfrac{1}{2}u_{0_x}(y-y^*) + a(z-z^*) + \tilde{v}, \\ w_0 &= z_t^* + u_0 z_x^* - \tfrac{1}{2}u_{0_x}(z-z^*) - a(y-y^*) + \tilde{w}, \\ p_0 &= -u_{0_x} + \tilde{p}. \end{aligned} \tag{4.86}$$

As a result of this definition, $\tilde{v}$ and $\tilde{w}$ satisfy

$$\int\int_{A_0} \begin{pmatrix} \tilde{v} \\ \tilde{w} \end{pmatrix} dydz = 0, \tag{4.87}$$

and we may choose a to account for the net rotation of the cross–section so that

$$\int\int_{A_0} ((y-y^*)\tilde{w} - (z-z^*)\tilde{v})\, dydz = 0. \tag{4.88}$$

Hence, with this choice of a, with respect to the tilded variables the cross–section has no linear or angular momentum.

In terms of the new variables, the cross–flow problem becomes

$$\begin{aligned} \tilde{v}_y + \tilde{w}_z &= 0, \\ \tilde{p}_y &= \tilde{v}_{yy} + \tilde{v}_{zz}, \\ \tilde{p}_z &= \tilde{w}_{yy} + \tilde{w}_{zz}, \\ G_{0_y}(-\tilde{p} + 2\tilde{v}_y) + G_{0_z}(\tilde{v}_z + \tilde{w}_y) &= -\gamma^*\kappa_0 G_{0_y} \quad \text{on } \partial A_0, \\ G_{0_y}(\tilde{v}_z + \tilde{w}_y) + G_{0_z}(-\tilde{p} + 2\tilde{w}_z) &= -\gamma^*\kappa_0 G_{0_z} \quad \text{on } \partial A_0, \end{aligned} \tag{4.89}$$

which is identical to the problem of two–dimensional Stokes flow with a surface tension–driven boundary, though the kinematic condition is more complicated:

$$\begin{aligned} G_{0_t} + \tilde{v}G_{0_y} + \tilde{w}G_{0_z} = -u_0 G_{0_x} - (y_t^* + u_0 y_x^*)G_{0_y} - (z_t^* + u_0 z_x^*)G_{0_z} \\ + \frac{1}{2}u_{0_x}\Big((y-y^*)G_{0_y} + (z-z^*)G_{0_z}\Big) + a\Big((y-y^*)G_{0_z} - (z-z^*)G_{0_y}\Big) \quad \text{on } \partial A_0. \end{aligned} \tag{4.90}$$

For two–dimensional Stokes flow with a free boundary driven by surface tension, the arbitrary rigid–body motion may be eliminated so that the right–hand side of

(4.90) is identically zero. Hopper (1990) showed that in many cases, exact solutions of this problem may be found in terms of a time–dependent conformal map from a unit circle to the boundary of the cross–section ∂A_0. Richardson (1992) reached the same conclusion in a different way, and gave a general procedure for constructing such solutions whenever the shape of the cross–section may be obtained from the unit disc by a rational conformal map. We shall show how the analysis of Richardson (1992) may be applied to our more general problem where the right–hand side of (4.90) is not identically zero. Where his analysis results in ordinary differential equations for the time–dependent coefficients of the conformal map, we shall obtain partial differential equations for the coefficients which depend on time t and distance along the fibre x. Otherwise, our analysis follows Richardson's closely; we shall therefore refer the reader to his paper for most of the details and confine ourselves to pointing out the important differences brought about by the new kinematic condition.

The incompressibility condition implies that the cross–flow velocity may be described using a stream function ψ,

$$\tilde{v} = \psi_z, \quad \tilde{w} = -\psi_y. \tag{4.91}$$

The stream function satisfies the biharmonic equation and hence may be written in the form

$$\psi = -\mathrm{Im}\left[\bar{\mathcal{Z}}\phi(\mathcal{Z}) + \chi(\mathcal{Z})\right], \tag{4.92}$$

where ϕ and χ are holomorphic functions of $\mathcal{Z} = y + iz$ for (y, z) in A_0. In terms of these, the velocities and pressure are given by

$$\tilde{v} + i\tilde{w} = \phi(\mathcal{Z}) - \mathcal{Z}\bar{\phi}'(\bar{\mathcal{Z}}) + \bar{\chi}'(\bar{\mathcal{Z}}), \tag{4.93}$$

$$\tilde{p} = -4\,\mathrm{Re}\left[\phi'(\mathcal{Z})\right]. \tag{4.94}$$

We suppose the cross–section A_0 may be mapped from the unit disc $|\zeta| < 1$ by a conformal map Ω, which will depend on x and t. For simplicity we shall first eliminate rotation and translation of A_0, and hence set

$$\mathcal{Z} = y + iz = y^* + iz^* + \Omega(\zeta; x, t)e^{-i\alpha(x,t)}, \tag{4.95}$$

where α satisfies

$$\alpha_t + u_0 \alpha_x = a. \tag{4.96}$$

Henceforth, the dependence of Ω on x and t will be implicit: we shall denote $\Omega_\zeta(\zeta; x, t)$ by $\Omega'(\zeta)$. Following Richardson, we write

$$\left(\Omega'(\zeta)\bar{\Omega}'(\zeta^{-1})\right)^{-1/2} = F_+(\zeta) - F_-(\zeta), \tag{4.97}$$

where $F_+(\zeta)$ is holomorphic for $|\zeta| \leq 1$, $F_-(\zeta)$ is holomorphic for $|\zeta| \geq 1$, and $F_-(\zeta) \to 0$ as $\zeta \to \infty$. We shall be employing the symmetries of F_+ and F_- given by Richardson's equation (2.15). Defining

$$\Phi(\zeta) = \phi(\mathcal{Z}(\zeta)), \quad \mathcal{X}(\zeta) = \chi'(\mathcal{Z}(\zeta)), \tag{4.98}$$

the dynamic boundary conditions (Richardson's equation (2.18)) may be written in the form

$$e^{i\alpha}\Phi(\zeta) + \frac{\gamma^*}{2}\zeta F_+(\zeta)\Omega'(\zeta) = -(y^* + iz^* + \Omega(\zeta)e^{-i\alpha})\frac{\bar{\Phi}'(\zeta^{-1})}{\bar{\Omega}'(\zeta^{-1})}$$

$$-e^{i\alpha}\bar{\mathcal{X}}(\zeta^{-1}) + \frac{\gamma^*}{2}\zeta F_-(\zeta)\Omega'(\zeta) \quad \text{on } |\zeta| = 1. \tag{4.99}$$

In translating the kinematic boundary condition (4.90) into our complex variable notation, note that the free surface $G_0 = 0$ is given parametrically by

$$y + iz = Y(\theta; x, t) + iZ(\theta; x, t) = y^*(x, t) + iz^*(x, t) + \Omega(e^{i\theta}; x, t)e^{-i\alpha(x,t)}. \tag{4.100}$$

We can transpose our previous notation into parametric form via

$$\hat{\boldsymbol{n}} = \frac{1}{(G_{0_y}^2 + G_{0_z}^2)^{1/2}} \begin{pmatrix} G_{0_y} \\ G_{0_z} \end{pmatrix} = \frac{1}{(Y_\theta^2 + Z_\theta^2)^{1/2}} \begin{pmatrix} Z_\theta \\ -Y_\theta \end{pmatrix}, \tag{4.101}$$

and

$$\begin{aligned} G_{0_x} + G_{0_y}Y_x + G_{0_z}Z_x &= 0, \\ G_{0_t} + G_{0_y}Y_t + G_{0_z}Z_t &= 0, \end{aligned} \tag{4.102}$$

where

$$\begin{aligned} Y_\theta + iZ_\theta &= ie^{i(\theta-\alpha)}\Omega'(e^{i\theta}; x, t), \\ Y_x + iZ_x &= y_x^* + iz_x^* + (\Omega_x - i\alpha_x\Omega)e^{-i\alpha}, \\ Y_t + iZ_t &= y_t^* + iz_t^* + (\Omega_t - i\alpha_t\Omega)e^{-i\alpha}. \end{aligned} \tag{4.103}$$

Hence our kinematic boundary condition (4.90) may be written

$$\mathrm{Re}\left\{\frac{1}{\zeta\Omega'(\zeta)}\left[2\Phi(\zeta)e^{i\alpha}-(\Omega_t+u_0\Omega_x+\tfrac{1}{2}u_{0_x}\Omega)\right]+\gamma^*F_+(\zeta)\right\}$$

$$=\frac{\gamma^*}{2}F_+(0)\quad\text{on }|\zeta|=1, \tag{4.104}$$

which is identical to Richardson's kinematic boundary condition (top of p. 199) if $\alpha = u_0 = 0$. In both of his examples, Richardson has shapes which are symmetric about the y-axis, and he utilises this in simplifying his kinematic condition. The equivalent assumption in our formulation is that our cross–section be symmetric about some axis which rotates with angular speed a. Enforcing that this symmetry is preserved ensures that the angular momentum of the cross–section with respect to our rotating frame is zero, as required by (4.88). This assumption of symmetry implies that without loss of generality we may take $\Omega(\zeta;x,t)$ and $\Phi(\zeta)e^{i\alpha}$ both to be real whenever ζ is real (these agree with Richardson if $\alpha = 0$). We shall also assume that the centre–line (y^*, z^*) is everywhere *inside* the cross–section, so that, as in Richardson, we may take $\Omega(0;x,t) = 0$ for all x and t.

After making these assumptions, the argument given by Richardson also holds here and tells us that the function in curly brackets on the left–hand side of (4.104) is a real constant equal to the one on the right–hand side, and hence our equivalent of Richardson's equation (2.19) is

$$\Omega_t+u_0\Omega_x+\frac{u_{0_x}}{2}\Omega=2\Phi(\zeta)e^{i\alpha}+\frac{\gamma^*}{2}\zeta\Omega'(\zeta)\left(2F_+(\zeta)-F_+(0)\right). \tag{4.105}$$

Hence, our solution procedure is identical to that proposed by Richardson. Given a rational function Ω whose coefficients depend on x and t, equating singularities on either side of (4.99) gives an expression for its left–hand side: another rational function with coefficients which depend on those of Ω. This function may then be substituted into the right–hand side of (4.105), and equating singularities on either side of this equation gives a system of partial differential equations for the coefficients of Ω.

We shall demonstrate this by means of a simple example of particular interest in the manufacture of optical fibre couplers.

4.4.1 The coupling of two equal cylinders

Richardson considers the coalescence of two unequal cylinders in his section 4. For simplicity, we restrict ourselves to the simpler example in which the cylinders are equal. Hence we put

$$\Omega = C\left(\frac{1}{1-b\zeta} - \frac{1}{1+b\zeta}\right) = \frac{2Cb\zeta}{1-b^2\zeta^2}, \tag{4.106}$$

where b and C are functions of x and t. This corresponds to a cross–section which approaches a disc as $b \to 0$, $C \to \infty$, and two equal discs touching at the origin as $b \to 1-$, $C \to 0$ in an appropriate manner. The area of the cross–section is given by

$$A_0 = 4\pi C^2 b^2 \frac{(1+b^4)}{(1-b^4)^2}. \tag{4.107}$$

The analysis in Richardson's section 4 may be followed closely, and results in the following equations for the coefficients b and C:

$$\begin{aligned} b_t + u_0 b_x &= \frac{\gamma^* b}{2}\left(F_+(0) - 2F_+(b)\right), \\ C_t + u_0 C_x + \frac{u_{0_x}}{2} C &= \frac{\gamma^* C}{2}\left(F_+(0) - 2F_+(b)\right)\left(1 - \frac{2(1+3b^4)}{(1-b^8)}\right). \end{aligned}$$

Here,

$$2F_+(b) - F_+(0) = \frac{(1-b^4)}{4\pi Cb}\int_0^{2\pi} \frac{d\theta}{(1+b^4+2b^2\cos(2\theta))^{1/2}} = \frac{(1-b^4)}{\pi Cb} K(b^2),$$

where K denotes an elliptic integral of the first kind. Elimination of this quantity between the two equations for b and C gives the conservation of mass equation (which we have already derived by other means),

$$A_{0_t} + (u_0 A_0)_x = 0, \tag{4.108}$$

while the evolution of the shape of the cross–section is given by

$$b_t + u_0 b_x = \gamma^* b K(b^2)\left(\frac{1+b^4}{\pi A_0}\right)^{1/2}. \tag{4.109}$$

The third relation between A_0, b and u_0 is given by (4.71), where the circumference of the cross–section is

$$S = (1-b^2)\left(\frac{A_0}{\pi(1+b^4)}\right)^{1/2} \int_0^{2\pi} \frac{(1+b^4+2b^2\cos(2\theta))^{1/2}}{(1+b^4-2b^2\cos(2\theta))}\, d\theta. \tag{4.110}$$

4.4.2 The twisting problem

Once the shape of the cross–section is known as a function of x and t, the integrals in the lateral force balance (4.74) may be calculated. Also, the problem for the twist of the fibre (4.75) may be simplified as follows. Given the shape of the cross–section at a given time, one must solve the Neumann problems

$$\begin{cases} \tilde{u}_{1_{yy}} + \tilde{u}_{1_{zz}} = 0, \\ \tilde{u}_{1_y} G_{0_y} + \tilde{u}_{1_z} G_{0_z} = (y - y^*) G_{0_z} - (z - z^*) G_{0_y} \ \text{ on } G_0 = 0, \end{cases} \tag{4.111}$$

$$\begin{cases} \tilde{u}_{2_{yy}} + \tilde{u}_{2_{zz}} = 0, \\ \tilde{u}_{2_y} G_{0_y} + \tilde{u}_{2_z} G_{0_z} = A_0 G_{0_x} + \frac{1}{2} A_{0_x} \left((y - y^*) G_{0_y} + (z - z^*) G_{0_z} \right) \ \text{ on } G_0 = 0, \end{cases} \tag{4.112}$$

$$\begin{cases} \tilde{u}_{3_{yy}} + \tilde{u}_{3_{zz}} = 0, \\ \tilde{u}_{3_y} G_{0_y} + \tilde{u}_{3_z} G_{0_z} = A_0 \kappa_0 G_{0_x} + \frac{1}{2} S_{0_x} \left((y - y^*) G_{0_y} + (z - z^*) G_{0_z} \right) \ \text{ on } G_0 = 0, \end{cases} \tag{4.113}$$

and then evaluate the integrals

$$I_i = \int\int_{A_0} \left((y - y^*) \tilde{u}_{i_z} - (z - z^*) \tilde{u}_{i_y} \right) dydz, \quad i = 1, 2, 3, \tag{4.114}$$

$$I_4 = \int\int_{A_0} \left((y - y^*) \mathfrak{A}_{xz} - (z - z^*) \mathfrak{A}_{xy} \right) dydz, \tag{4.115}$$

and the moment of inertia defined as before

$$\mathcal{I} = \int\int_{A_0} \left((y - y^*)^2 + (z - z^*)^2 \right) dydz.$$

Using the properties of $\mathfrak{A}$, I_4 may be simplified to an integral which depends only on the shape of the cross–section, so that it is not necessary to solve the biharmonic equation to find $\mathfrak{A}$ explicitly:

$$I_4 = -\gamma^* \int_0^\pi \frac{(Z_\theta Y_x - Y_\theta Z_x)}{(Y_\theta^2 + Z_\theta^2)^{1/2}} \left((Y - y^*) Y_\theta + (Z - z^*) Z_\theta \right) d\theta. \tag{4.116}$$

Then the integral on the left–hand side of (4.75) is given by

$$\begin{aligned} &\int\int_{A_0} \left((y - y^*)(w_{0_x} + u_{1_z}) - (z - z^*)(v_{0_x} + u_{1_y}) \right) dydz \\ &\qquad = a_x (I_1 - \mathcal{I}) - \frac{3 u_{0_x}}{A_0} I_2 - \frac{\gamma^*}{2 A_0} I_3 - \frac{1}{2} I_4. \end{aligned} \tag{4.117}$$

Also, from the definition of a, the scaled axial component of angular momentum L is given by

$$L = -\frac{a}{A_0} \mathcal{I}. \tag{4.118}$$

In theory, these integrals may be evaluated as functions of the time– and space–dependent coefficients in the conformal map Ω. However, these functions will in general be extremely complicated; we shall not pursue the matter further here.

4.5 Conclusions

The work of this chapter falls into two main categories. In section 4.2 we showed how the work of Dewynne, Ockendon & Wilmott (1992) may be extended with relative ease to include the effects of inertia and gravity so long as surface tension effects are relatively small. The result is a generalised Trouton model for the axial velocity and cross–sectional area, along with decoupled equations for the lateral motion of the centre–line of the fibre and the twist of the fibre about its centre–line. The centre–line equation (4.37) is of particular interest since it changes type from hyperbolic to elliptic depending on whether the fibre is under tension or compression. This contrasts with the inertia–free model of Dewynne, Ockendon & Wilmott (1992) in which the behaviour of the centre–line is independent of the tension in the fibre.

In section 4.3 we considered fibres for which surface tension is an important effect. In this case the problem is in general much harder as it is necessary to solve a number of boundary value problems over the fibre cross–section, the shape of which is not known in advance. However, in section 4.4 we showed that in many cases of practical interest, the problem for the evolution of the shape of the fibre cross–section may be reduced to the solution of a system of first–order p.d.e.'s, by analogy with the two–dimensional sintering problem considered by Hopper (1990) and Richardson (1992).

Throughout this chapter we have assumed that the curvature of the fibre is small, so that it may effectively be described using a fixed Cartesian coordinate system. In the next chapter we shall consider fibres whose curvature is large, so that it is necessary to employ a curvilinear coordinate system which moves with the fibre.

Chapter 5

Highly curved viscous fibres

In the previous chapter we found leading–order extensional equations governing the motion of a nonaxisymmetric viscous fibre. By assuming that the curvature of the fibre was small, we were able to use a fixed Cartesian coordinate system. In this chapter we shall be modelling a fibre whose curvature is not small, and to describe the slender geometry effectively we shall employ curvilinear coordinates defined relative to the centre–line of the fibre. We shall only consider Stokes flow with body forces, though inertia and surface tension effects could be included in the analysis by incorporating some of the ideas of chapters 4 and 7.

This work is an extension of the work of Buckmaster, Nachman & Ting (1975), referred to hereafter as BNT, who derived equations governing the motion of a purely two–dimensional sheet of viscous fluid without body forces. We generalise this to allow for more general three–dimensional motion, to consider the effects of body forces and to show how the cross–sectional shape of the fibre affects its dynamics.

We find that the nature of the leading–order extensional solution depends crucially on the relative order of magnitude of the body forces and the viscous stresses. Initially we consider a situation in which the body forces are relatively small. We then find (as did BNT) that to leading order the fibre is not stretched during the motion; it is only bent and twisted. The equations governing this bending and twisting are generalisations of the equations derived by BNT and are similar to

the equations governing the equilibrium of elastic rods.

We then consider larger body forces and find that there is a leading–order balance between the forces acting on the fibre and the tension in the fibre. In this case there certainly is stretching of the fibre and the equations of BNT are clearly inappropriate. This second scenario bears a similarity to the "two–dimensional bottle" problem which will be described in chapter 7.

In section 5.1 we define the orthogonal coordinate system which is employed throughout the chapter. The Stokes equations and free surface boundary conditions are given using this coordinate system in section 5.2.

Assuming the body forces are relatively small, as described above, the leading–order equations of motion are derived in sections 5.4 and 5.5. They are recast in a rotating coordinate system in section 5.6 so that various integrals need only be evaluated once. A simple example in which the fibre moves in a plane without rotating is considered in section 5.7 and shown to give equations equivalent to those of section 3.1.3.

In section 5.8 we consider the effect of larger body forces acting on the fibre and find that in this case the leading–order behaviour of the fibre is very different from that found by BNT.

5.1 Geometrical Preamble

5.1.1 Modified Serret–Frenet coordinates

Suppose the centre–line of the fibre (defined as in the last chapter to be the line joining the centres of mass of the fibre cross–sections) is given by

$$\boldsymbol{r} = \boldsymbol{r}_c(s,t), \tag{5.1}$$

where s is arc length and t is time. We define the tangent vector as usual

$$\boldsymbol{t} = \frac{\partial \boldsymbol{r}_c}{\partial s}, \tag{5.2}$$

and the principal normal $\boldsymbol{n}$ and binormal $\boldsymbol{b}$ are related to $\boldsymbol{t}$ by the Serret–Frenet formulae (see for example Kreyszig (1959)),

$$\begin{aligned} \frac{\partial \boldsymbol{t}}{\partial s} &= \kappa \boldsymbol{n}, \\ \frac{\partial \boldsymbol{n}}{\partial s} &= -\kappa \boldsymbol{t} + \tau \boldsymbol{b}, \\ \frac{\partial \boldsymbol{b}}{\partial s} &= -\tau \boldsymbol{n}, \end{aligned} \tag{5.3}$$

where κ and τ are the curvature and torsion of the centre–line respectively. Our derivations are simplified by employing coordinates which are rotated with respect to Serret–Frenet coordinates according to the torsion of the centre–line. We define

$$\begin{aligned} \boldsymbol{n}_1 &= \boldsymbol{n}\cos\phi - \boldsymbol{b}\sin\phi, \\ \boldsymbol{n}_2 &= \boldsymbol{n}\sin\phi + \boldsymbol{b}\cos\phi, \end{aligned} \tag{5.4}$$

where

$$\phi(s,t) = \int_0^s \tau(s',t)\, ds'. \tag{5.5}$$

The analogues of the Serret–Frenet formulae for these new unit vectors are

$$\begin{aligned} \frac{\partial \boldsymbol{t}}{\partial s} &= \kappa\left(\boldsymbol{n}_1\cos\phi + \boldsymbol{n}_2\sin\phi\right), \\ \frac{\partial \boldsymbol{n}_1}{\partial s} &= -\kappa \boldsymbol{t}\cos\phi, \\ \frac{\partial \boldsymbol{n}_2}{\partial s} &= -\kappa \boldsymbol{t}\sin\phi. \end{aligned} \tag{5.6}$$

We shall describe a general point in the fibre using coordinates

$$\boldsymbol{r}(s,x_1,x_2,t) = \boldsymbol{r}_c(s,t) + x_1\boldsymbol{n}_1(s,t) + x_2\boldsymbol{n}_2(s,t). \tag{5.7}$$

This coordinate system is orthogonal (a feature not shared by standard Serret–Frenet coordinates), with scaling factors

$$\begin{aligned} l_s &= 1 - \kappa\left(x_1\cos\phi + x_2\sin\phi\right), \\ l_1 &= 1, \\ l_2 &= 1. \end{aligned} \tag{5.8}$$

Also, since x_1 and x_2 are measured relative to the fibre centre–line, they must satisfy

$$\int\int_A \begin{pmatrix} x_1 \\ x_2 \end{pmatrix} dx_1 dx_2 = \boldsymbol{0}, \tag{5.9}$$

where A is any cross–section of the fibre.

5.1.2 Velocity of the centre–line

The centre–line of the fibre is free to move with time; we resolve its velocity onto the $\boldsymbol{t}$-, $\boldsymbol{n}_1$- and $\boldsymbol{n}_2$-directions:

$$\frac{\partial \boldsymbol{r}_c}{\partial t} = \boldsymbol{v} = v_s \boldsymbol{t} + v_1 \boldsymbol{n}_1 + v_2 \boldsymbol{n}_2. \tag{5.10}$$

Successive differentiation of this equation with respect to s reveals three equations linking v_1, v_2 and v_3 to κ and ϕ:

$$\frac{\partial v_s}{\partial s} = \kappa \left(v_1 \cos\phi + v_2 \sin\phi \right), \tag{5.11}$$

$$\frac{\partial \kappa}{\partial t} = \frac{\partial^2 v_1}{\partial s^2} \cos\phi + \frac{\partial^2 v_2}{\partial s^2} \sin\phi + \frac{\partial}{\partial s}(\kappa v_s), \tag{5.12}$$

$$\frac{\partial}{\partial s}\left(\frac{\partial \phi}{\partial t} - v_s \frac{\partial \phi}{\partial s} + \frac{\partial^2 v_1}{\partial s^2} \frac{\sin\phi}{\kappa} - \frac{\partial^2 v_2}{\partial s^2} \frac{\cos\phi}{\kappa} \right) + \kappa \left(\frac{\partial v_1}{\partial s} \sin\phi - \frac{\partial v_2}{\partial s} \cos\phi \right) = 0, \tag{5.13}$$

and the time derivatives of our unit vectors are given by

$$\frac{\partial \boldsymbol{t}}{\partial t} = \left(\frac{\partial v_1}{\partial s} + \kappa v_s \cos\phi \right) \boldsymbol{n}_1 + \left(\frac{\partial v_2}{\partial s} + \kappa v_s \sin\phi \right) \boldsymbol{n}_2, \tag{5.14}$$

$$\begin{aligned} \frac{\partial \boldsymbol{n}_1}{\partial t} = & -\left(\frac{\partial v_1}{\partial s} + \kappa v_s \cos\phi \right) \boldsymbol{t} \\ & - \left(\frac{\partial \phi}{\partial t} - v_s \frac{\partial \phi}{\partial s} + \frac{\partial^2 v_1}{\partial s^2} \frac{\sin\phi}{\kappa} - \frac{\partial^2 v_2}{\partial s^2} \frac{\cos\phi}{\kappa} \right) \boldsymbol{n}_2, \end{aligned} \tag{5.15}$$

$$\begin{aligned} \frac{\partial \boldsymbol{n}_2}{\partial t} = & -\left(\frac{\partial v_2}{\partial s} + \kappa v_s \sin\phi \right) \boldsymbol{t} \\ & + \left(\frac{\partial \phi}{\partial t} - v_s \frac{\partial \phi}{\partial s} + \frac{\partial^2 v_1}{\partial s^2} \frac{\sin\phi}{\kappa} - \frac{\partial^2 v_2}{\partial s^2} \frac{\cos\phi}{\kappa} \right) \boldsymbol{n}_1. \end{aligned} \tag{5.16}$$

5.2 The Stokes equations and boundary conditions

We denote by $\boldsymbol{u} = (u_s, u_1, u_2)$ the fluid velocities in the $\boldsymbol{t}$, $\boldsymbol{n}_1$ and $\boldsymbol{n}_2$ directions. The Stokes equations in our orthogonal coordinate system take the form

$$\frac{\partial u_s}{\partial s} + \frac{\partial}{\partial x_1}(l_s u_1) + \frac{\partial}{\partial x_2}(l_s u_2) = 0, \tag{5.17}$$

$$\frac{\partial \sigma_{ss}}{\partial s} + \frac{\partial}{\partial x_1}(l_s \sigma_{s1}) + \frac{\partial}{\partial x_2}(l_s \sigma_{s2}) - \kappa \cos\phi \sigma_{s1} - \kappa \sin\phi \sigma_{s2} + \rho l_s f_s = 0, \tag{5.18}$$

$$\frac{\partial \sigma_{s1}}{\partial s} + \frac{\partial}{\partial x_1}(l_s \sigma_{11}) + \frac{\partial}{\partial x_2}(l_s \sigma_{12}) + \kappa \cos\phi \sigma_{ss} + \rho l_s f_1 = 0, \tag{5.19}$$

$$\frac{\partial \sigma_{s2}}{\partial s} + \frac{\partial}{\partial x_1}(l_s \sigma_{12}) + \frac{\partial}{\partial x_2}(l_s \sigma_{22}) + \kappa \sin\phi \sigma_{ss} + \rho l_s f_2 = 0, \tag{5.20}$$

where (f_s, f_1, f_2) is the body force acting on the fibre, and the physical components of stress are given by

$$\sigma_{ss} = -p + \frac{2\mu}{l_s}\left(\frac{\partial u_s}{\partial s} - \kappa(u_1 \cos\phi + u_2 \sin\phi)\right), \tag{5.21}$$

$$\sigma_{11} = -p + 2\mu \frac{\partial u_1}{\partial x_1}, \tag{5.22}$$

$$\sigma_{22} = -p + 2\mu \frac{\partial u_2}{\partial x_2}, \tag{5.23}$$

$$\sigma_{s1} = \frac{\mu}{l_s}\left(l_s \frac{\partial u_s}{\partial x_1} + \frac{\partial u_1}{\partial s} + \kappa u_1 \cos\phi\right), \tag{5.24}$$

$$\sigma_{s2} = \frac{\mu}{l_s}\left(l_s \frac{\partial u_s}{\partial x_2} + \frac{\partial u_2}{\partial s} + \kappa u_2 \sin\phi\right), \tag{5.25}$$

$$\sigma_{12} = \mu\left(\frac{\partial u_1}{\partial x_2} + \frac{\partial u_2}{\partial x_1}\right). \tag{5.26}$$

Suppose the free surface of the fibre is given by $G(s, x_1, x_2, t) = 0$. Then zero–stress boundary conditions on $G = 0$ take the form

$$\frac{\sigma_{ss}}{l_s}\frac{\partial G}{\partial s} + \sigma_{s1}\frac{\partial G}{\partial x_1} + \sigma_{s2}\frac{\partial G}{\partial x_2} = 0, \tag{5.27}$$

$$\frac{\sigma_{s1}}{l_s}\frac{\partial G}{\partial s} + \sigma_{11}\frac{\partial G}{\partial x_1} + \sigma_{12}\frac{\partial G}{\partial x_2} = 0, \tag{5.28}$$

$$\frac{\sigma_{s2}}{l_s}\frac{\partial G}{\partial s} + \sigma_{12}\frac{\partial G}{\partial x_1} + \sigma_{22}\frac{\partial G}{\partial x_2} = 0. \tag{5.29}$$

The convective derivative is given by

$$\frac{D}{Dt} = \frac{\partial}{\partial t} + \left(\boldsymbol{u} - \frac{\partial \boldsymbol{r}_c}{\partial t} - x_1 \frac{\partial \boldsymbol{n}_1}{\partial t} - x_2 \frac{\partial \boldsymbol{n}_2}{\partial t}\right).\nabla, \tag{5.30}$$

and hence the kinematic boundary condition on $G = 0$ may be written

$$\frac{\partial G}{\partial t} + \left(u_s - l_s v_s - x_1 \frac{\partial v_1}{\partial s} - x_2 \frac{\partial v_2}{\partial s}\right)\frac{1}{l_s}\frac{\partial G}{\partial s} + \left(u_1 - v_1 - x_2 \boldsymbol{n}_1 . \frac{\partial \boldsymbol{n}_2}{\partial t}\right)\frac{\partial G}{\partial x_1} + \left(u_2 - v_2 - x_1 \boldsymbol{n}_2 . \frac{\partial \boldsymbol{n}_1}{\partial t}\right)\frac{\partial G}{\partial x_2} = 0. \tag{5.31}$$

5.3 Nondimensionalisation and scaling

In nondimensionalising the equations we suppose the curvature of the fibre is of order L^{-1} and its thickness is of order ϵL, where L is a typical length and ϵ is much smaller than 1. We shall scale the velocity with a typical speed U and allow for varying viscosity, of order M. Hence we nondimensionalise as follows

$$\begin{array}{lll} s = Ls', & x_1 = \epsilon L x_1', & x_2 = \epsilon L x_2', \\ \boldsymbol{r}_c = L\boldsymbol{r}_c', & \boldsymbol{u} = U\boldsymbol{u}', & \boldsymbol{v} = U\boldsymbol{v}', \\ \mu = M\mu', & p = MUL^{-1}p', & t = LU^{-1}t'. \end{array} \tag{5.32}$$

We scale the dimensionless body forces as follows

$$f_s' = \frac{\rho L^2 f_s}{\epsilon MU}, \quad f_1' = \frac{\rho L^2 f_1}{\epsilon MU}, \quad f_2' = \frac{\rho L^2 f_2}{\epsilon MU},$$

and assume these are all order one. We substitute these into the Stokes equations and boundary conditions, drop primes and seek solutions in the form of asymptotic expansions in powers of the slenderness parameter ϵ, typically[1]

$$u_1 \sim u_1^{(0)} + \epsilon u_1^{(1)} + \epsilon^2 u_1^{(2)} + \ldots.$$

5.4 Leading–order equations

For simplicity, we shall suppose $\mu = \mu(s,t)$. The analysis is similar in style to the previous chapter so we shall omit most of the details. Typically, the leading–order Stokes equations and boundary conditions give rise to homogeneous Neumann problems. The indeterminacy in the eigensolutions to these problems is resolved by applying orthogonality conditions to the higher–order equations. We shall employ transport theorems equivalent to those introduced in section 4.1; we shall not bother to write them out again in the new notation.

[1]Note that here it is necessary to consider powers of ϵ while in the previous chapter our expansions were in powers of ϵ^2 (that is we were free to choose all coefficients of odd powers of ϵ to be zero). This is related to the scaling factor $l_s = 1 - \kappa n$ which measures the deviation of our coordinate system from Cartesian. Clearly this is consistent with a series in powers of ϵ^2 in the case $\kappa = O(\epsilon)$ considered in the previous chapter, or indeed the case $\kappa = 0$ considered in chapter 2, but not in the present case $\kappa = O(1)$. We shall employ similar asymptotic expansions in chapter 7 when considering highly curved viscous sheets.

Here, the leading–order equations reveal

$$u_s^{(0)} = u_s^{(0)}(s,t), \tag{5.33}$$

and

$$u_1^{(0)} = v_1^{(0)}, \;\; u_2^{(0)} = v_2^{(0)}. \tag{5.34}$$

Proceeding to higher order, we find that the Stokes equations and zero stress conditions are still homogeneous, allowing the eigensolutions

$$u_s^{(1)} = v_s^{(1)}(s,t) - \left(\frac{\partial v_1^{(0)}}{\partial s} + \kappa^{(0)} u_s^{(0)} \cos\phi^{(0)} \right) x_1 - \left(\frac{\partial v_2^{(0)}}{\partial s} + \kappa^{(0)} u_s^{(0)} \sin\phi^{(0)} \right) x_2, \tag{5.35}$$

$$u_1^{(1)} = v_1^{(1)} + \frac{\partial}{\partial s}\left(v_s^{(0)} - u_s^{(0)} \right) \frac{x_1}{2} + a x_2, \tag{5.36}$$

$$u_2^{(1)} = v_2^{(1)} + \frac{\partial}{\partial s}\left(v_s^{(0)} - u_s^{(0)} \right) \frac{x_2}{2} - a x_1, \tag{5.37}$$

$$p^{(0)} = \frac{\partial}{\partial s}\left(v_s^{(0)} - u_s^{(0)} \right). \tag{5.38}$$

The kinematic boundary condition at order ϵ gives

$$\frac{\partial G^{(0)}}{\partial t} + \left(u_s^{(0)} - v_s^{(0)} \right) \frac{\partial G^{(0)}}{\partial s} + \left(u_1^{(1)} - v_1^{(1)} - x_2 \boldsymbol{n}_1^{(0)} . \frac{\partial \boldsymbol{n}_2^{(0)}}{\partial t} \right) \frac{\partial G^{(0)}}{\partial x_1}$$

$$+ \left(u_2^{(1)} - v_2^{(1)} - x_1 \boldsymbol{n}_2^{(0)} . \frac{\partial \boldsymbol{n}_1^{(0)}}{\partial t} \right) \frac{\partial G^{(0)}}{\partial x_2} = 0. \tag{5.39}$$

Application of the transport theorems to this gives the usual conservation of mass equation

$$\frac{\partial A_0}{\partial t} + \frac{\partial}{\partial s}\left((u_s^{(0)} - v_s^{(0)}) A_0 \right) = 0. \tag{5.40}$$

Continuing to order ϵ^2 in the expansions, the solvability condition for (5.18) with boundary condition (5.27) gives the usual constant tension equation

$$\frac{\partial}{\partial s}\left(3\mu^{(0)} A^{(0)} \frac{\partial}{\partial s}(u_s^{(0)} - v_s^{(0)}) \right) = 0. \tag{5.41}$$

However, the solvability conditions for the transverse stress balances (5.19) and (5.20) with boundary conditions (5.28) and (5.29) give

$$3\mu^{(0)} \kappa^{(0)} \frac{\partial}{\partial s}(u_s^{(0)} - v_s^{(0)}) = 0. \tag{5.42}$$

Hence, either the fibre must be straight to leading order or the tension in the fibre must be zero (compare with the two–dimensional sheet considered in section 2.1). Here, $\kappa^{(0)} = 0$ means that the curvature of the fibre centre–line is order ϵL^{-1}. As we are interested in fibres with large curvature, we are forced to take the second option, and without loss of generality, set

$$u_s^{(0)} = v_s^{(0)}. \tag{5.43}$$

This means that there is *no stretching* of the fibre to leading order. The conservation of mass equation (5.40) simplifies to

$$\frac{\partial A^{(0)}}{\partial t} = 0. \tag{5.44}$$

Indeed, the kinematic boundary condition (5.39) gives

$$\frac{\partial G^{(0)}}{\partial t} + \left(a + \boldsymbol{n}_2^{(0)} . \frac{\partial \boldsymbol{n}_1^{(0)}}{\partial t} \right) \left(x_2 \frac{\partial G^{(0)}}{\partial x_1} - x_1 \frac{\partial G^{(0)}}{\partial x_2} \right) = 0, \tag{5.45}$$

so that the cross–section of the fibre simply rotates with angular speed $a + \boldsymbol{n}_2^{(0)} . \boldsymbol{n}_{1_t}^{(0)}$.

Continuing to order ϵ^2 in the expansions, we find that the first nonzero axial stress terms are given by

$$\begin{aligned}
\sigma_{ss} &\sim 3\epsilon\mu^{(0)} x_1 \left[-\frac{\partial}{\partial s} \left(\frac{\partial v_2^{(0)}}{\partial s} + \kappa^{(0)} v_s^{(0)} \cos\phi^{(0)} \right) + a\kappa^{(0)} \sin\phi^{(0)} \right] \\
&\quad -3\epsilon\mu^{(0)} x_2 \left[-\frac{\partial}{\partial s} \left(\frac{\partial v_1^{(0)}}{\partial s} + \kappa^{(0)} v_s^{(0)} \sin\phi^{(0)} \right) + a\kappa^{(0)} \cos\phi^{(0)} \right] \\
&\quad +\epsilon(\text{ function of } s \text{ and } t\ ) + O(\epsilon^2), \qquad (5.46) \\
\sigma_{s1} &\sim \epsilon\mu^{(0)} \left\{ \frac{\partial u_s^{(2)}}{\partial x_1} + x_2 \left[\kappa^{(0)} \frac{\partial v_1^{(0)}}{\partial s} \sin\phi^{(0)} - \kappa^{(0)} \frac{\partial v_2^{(0)}}{\partial s} \cos\phi^{(0)} + \frac{\partial a}{\partial s} \right] \right\} \\
&\quad +\epsilon(\text{ function of } s \text{ and } t\ ) + O(\epsilon^2), \qquad (5.47) \\
\sigma_{s2} &\sim \epsilon\mu^{(0)} \left\{ \frac{\partial u_s^{(2)}}{\partial x_2} - x_1 \left[\kappa^{(0)} \frac{\partial v_1^{(0)}}{\partial s} \sin\phi^{(0)} - \kappa^{(0)} \frac{\partial v_2^{(0)}}{\partial s} \cos\phi^{(0)} + \frac{\partial a}{\partial s} \right] \right\} \\
&\quad +\epsilon(\text{ function of } s \text{ and } t\ ) + O(\epsilon^2), \qquad (5.48)
\end{aligned}$$

where

$$u_s^{(2)} = \left(\kappa^{(0)} \frac{\partial v_1^{(0)}}{\partial s} \sin\phi^{(0)} - \kappa^{(0)} \frac{\partial v_2^{(0)}}{\partial s} \cos\phi^{(0)} + \frac{\partial a}{\partial s} \right) \tilde{u_s} + (\text{ linear function of } x_1 \text{ and } x_2\ ) \tag{5.49}$$

and $\tilde{u_s}$ satisfies the Neumann problem

$$\frac{\partial^2 \tilde{u_s}}{\partial x_1^2} + \frac{\partial^2 \tilde{u_s}}{\partial x_2^2} = 0, \tag{5.50}$$

$$\frac{\partial \tilde{u_s}}{\partial x_1}\frac{\partial G^{(0)}}{\partial x_1} + \frac{\partial \tilde{u_s}}{\partial x_2}\frac{\partial G^{(0)}}{\partial x_2} = x_1\frac{\partial G^{(0)}}{\partial x_2} - x_2\frac{\partial G^{(0)}}{\partial x_1} \quad \text{on } G^{(0)} = 0. \tag{5.51}$$

We can eliminate all the unknown arbitrary functions of x and t by considering the leading–order components of the bending moments

$$\mathcal{M}_1 = \int\int_A x_1\sigma_{ss}\, dx_1 dx_2, \;\; \mathcal{M}_2 = \int\int_A x_2\sigma_{ss}\, dx_1 dx_2, \tag{5.52}$$

and the torque

$$\mathcal{N} = \int\int_A (x_1\sigma_{s2} - x_2\sigma_{s1})\; dx_1 dx_2. \tag{5.53}$$

These are found to be (dropping superscripts)

$$\begin{aligned}
\mathcal{M}_1 &= 3\epsilon^4\mu\left[-\frac{\partial}{\partial s}\left(\frac{\partial v_1}{\partial s} + \kappa v_s\cos\phi\right) + \kappa a\sin\phi\right]\int\int_A x_1^2\, dx_1 dx_2 \\
&\quad -3\epsilon^4\mu\left[\frac{\partial}{\partial s}\left(\frac{\partial v_2}{\partial s} + \kappa v_s\sin\phi\right) + \kappa a\cos\phi\right]\int\int_A x_1 x_2\, dx_1 dx_2, \qquad (5.54) \\
\mathcal{M}_2 &= 3\epsilon^4\mu\left[-\frac{\partial}{\partial s}\left(\frac{\partial v_1}{\partial s} + \kappa v_s\cos\phi\right) + \kappa a\sin\phi\right]\int\int_A x_1 x_2\, dx_1 dx_2 \\
&\quad -3\epsilon^4\mu\left[\frac{\partial}{\partial s}\left(\frac{\partial v_2}{\partial s} + \kappa v_s\sin\phi\right) + \kappa a\cos\phi\right]\int\int_A x_2^2\, dx_1 dx_2, \qquad (5.55)
\end{aligned}$$

$$\mathcal{N} = \epsilon^4\mu\left(\kappa\frac{\partial v_2}{\partial s}\cos\phi - \kappa\frac{\partial v_1}{\partial s}\sin\phi - \frac{\partial a}{\partial s}\right)\int\int_A\left(x_2\frac{\partial \tilde{u_s}}{\partial x_1} - x_1\frac{\partial \tilde{u_s}}{\partial x_2} + x_1^2 + x_2^2\right)\, dx_1 dx_2. \tag{5.56}$$

5.5 Integrated equations

As in BNT a great deal of algebra may be avoided by using integrated forms of the Stokes equations and boundary conditions as well as the full equations. Integration of (5.18), (5.19) and (5.20) over the cross–section, application of the boundary conditions (5.27), (5.28) and (5.29), and use of the transport theorems gives three equations relating the averaged axial stress components:

$$\frac{\partial}{\partial s}(A\bar{\sigma}_{ss}) + \rho f_s A = \kappa A\bar{\sigma}_{s1}\cos\phi + \kappa A\bar{\sigma}_{s2}\sin\phi, \tag{5.57}$$

$$\frac{\partial}{\partial s}(A\bar{\sigma}_{s1}) + \kappa A\bar{\sigma}_{ss}\cos\phi + \rho f_1 A = 0, \tag{5.58}$$

$$\frac{\partial}{\partial s}(A\bar{\sigma}_{s2}) + \kappa A\bar{\sigma}_{ss}\sin\phi + \rho f_2 A = 0, \tag{5.59}$$

where A is the cross–sectional area of the fibre and

$$\bar{\sigma}_{ij} = \frac{1}{A}\int\int_A \sigma_{ij}\, dx_1 dx_2.$$

Similarly, taking moments of the equations before integrating gives equations for the bending moments $\mathcal{M}_1$ and $\mathcal{M}_2$ and the torque $\mathcal{N}$, namely

$$\frac{\partial \mathcal{M}_1}{\partial s} = A\bar{\sigma}_{s1} + \kappa\mathcal{N}\sin\phi - \rho f_s \int\int_A x_1 l_s\, dx_1 dx_2, \tag{5.60}$$

$$\frac{\partial \mathcal{M}_2}{\partial s} = A\bar{\sigma}_{s2} - \kappa\mathcal{N}\cos\phi - \rho f_s \int\int_A x_2 l_s\, dx_1 dx_2, \tag{5.61}$$

$$\frac{\partial \mathcal{N}}{\partial s} = \kappa\mathcal{M}_2\cos\phi - \kappa\mathcal{M}_1\sin\phi + \rho\int\int_A l_s\left(f_1 x_2 - f_2 x_1\right) dx_1 dx_2. \tag{5.62}$$

Hence we have a total of twelve equations, namely (5.11) to (5.13), (5.57) to (5.62) and (5.54) to (5.56) for the unknowns v_s, v_1, v_2, κ, ϕ, a, $\bar{\sigma}_{ss}$, $\bar{\sigma}_{s1}$, $\bar{\sigma}_{s2}$, $\mathcal{M}_1$, $\mathcal{M}_2$ and $\mathcal{N}$.

5.6 Rotated coordinates

As in the previous chapter, the equations of motion involve a number of integrals over the cross–section of the fibre. By transforming to a suitably rotated coordinate system we may ensure that these integrals need only be calculated once and not at each timestep. Set

$$x_1 = \xi_1\cos\theta + \xi_2\sin\theta, \tag{5.63}$$

$$x_2 = \xi_2\cos\theta - \xi_1\sin\theta, \tag{5.64}$$

where

$$\frac{\partial\theta}{\partial t} = a + \boldsymbol{n}_2.\frac{\partial \boldsymbol{n}_1}{\partial t};\;\; \theta(s,0) = \theta_0(s). \tag{5.65}$$

We may choose θ_0 in such a way that the ξ_1- and ξ_2- axes are the principal axes of the cross–section, and hence the product of inertia with respect to these axes is

zero. One must then simply calculate the time–independent integrals,

$$\begin{aligned} I_1 &= \int\int_{A_0} \xi_1^2 \, d\xi_1 d\xi_2, \\ I_2 &= \int\int_{A_0} \xi_2^2 \, d\xi_1 d\xi_2, \\ I_3 &= \int\int_{A_0} \left(\xi_2 \frac{\partial \tilde{u}_s}{\partial \xi_1} - \xi_1 \frac{\partial \tilde{u}_s}{\partial \xi_2} \right) d\xi_1 d\xi_2, \end{aligned}$$

using the initial cross–section of the fibre A_0. The leading–order bending moments and torque with respect to the rotated axes are given by (dividing through by the extraneous factor of ϵ^4)

$$\mathcal{M}_{\xi_1} = -3\mu I_1 \frac{\partial}{\partial t} \left(\kappa \cos\left(\theta + \phi\right) \right), \tag{5.66}$$

$$\mathcal{M}_{\xi_2} = -3\mu I_2 \frac{\partial}{\partial t} \left(\kappa \sin\left(\theta + \phi\right) \right), \tag{5.67}$$

$$\mathcal{N} = -\mu (I_1 + I_2 + I_3) \frac{\partial^2 \theta}{\partial s \partial t}. \tag{5.68}$$

The nondimensionalised integrated equations of section 5.5 then give

$$\frac{\partial \mathcal{M}_{\xi_1}}{\partial s} + \frac{\partial \theta}{\partial s} \mathcal{M}_{\xi_2} = A\bar{\sigma}_{s\xi_1} + \kappa \mathcal{N} \sin\left(\theta + \phi\right) + f_s \kappa I_1 \cos\left(\theta + \phi\right), \tag{5.69}$$

$$\frac{\partial \mathcal{M}_{\xi_2}}{\partial s} - \frac{\partial \theta}{\partial s} \mathcal{M}_{\xi_1} = A\bar{\sigma}_{s\xi_2} - \kappa \mathcal{N} \cos\left(\theta + \phi\right) + f_s \kappa I_2 \sin\left(\theta + \phi\right), \tag{5.70}$$

$$\begin{aligned} \frac{\partial \mathcal{N}}{\partial s} &= \kappa \mathcal{M}_{\xi_2} \cos\left(\theta + \phi\right) - \kappa \mathcal{M}_{\xi_1} \sin\left(\theta + \phi\right) \\ &\quad + \kappa \left(f_{\xi_2} I_1 \cos\left(\theta + \phi\right) - f_{\xi_1} I_2 \sin\left(\theta + \phi\right) \right), \end{aligned} \tag{5.71}$$

where the axial stress components with respect to the rotating axes satisfy

$$\frac{\partial}{\partial s}(A\bar{\sigma}_{s\xi_1}) + \frac{\partial \theta}{\partial s} A\bar{\sigma}_{s\xi_2} + \kappa A\bar{\sigma}_{ss} \cos\left(\theta + \phi\right) + f_{\xi_1} A = 0, \tag{5.72}$$

$$\frac{\partial}{\partial s}(A\bar{\sigma}_{s\xi_2}) - \frac{\partial \theta}{\partial s} A\bar{\sigma}_{s\xi_1} + \kappa A\bar{\sigma}_{ss} \sin\left(\theta + \phi\right) + f_{\xi_2} A = 0, \tag{5.73}$$

$$\frac{\partial}{\partial s}(A\bar{\sigma}_{ss}) + f_s A = \kappa A\bar{\sigma}_{s\xi_1} \cos\left(\theta + \phi\right) + \kappa A\bar{\sigma}_{s\xi_2} \sin\left(\theta + \phi\right). \tag{5.74}$$

Equations (5.72) to (5.74) in theory determine $A\bar{\sigma}_{ss}$, $A\bar{\sigma}_{s\xi_1}$ and $A\bar{\sigma}_{s\xi_2}$ in terms of κ, θ and ϕ. Then (5.69) to (5.71) form three equations for κ, θ and ϕ.

Equations (5.69) to (5.74) are identical to the equations of equilibrium for a slender elastic rod; see for example Love (1927). The difference between our problem and the corresponding one in linear elasticity is the time derivatives in the definitions of $\mathcal{M}_{\xi_1}$, $\mathcal{M}_{\xi_2}$, and $\mathcal{N}$ in (5.66) to (5.68).

5.7 The "viscida" equation

We shall now consider a viscous fibre which is constrained to move in a plane, and which does not rotate about its centre–line. This is the slow viscous flow equivalent of the "elastica" problem in elasticity. It has been considered by BNT for purely two–dimensional Stokes flow; this was described in section 3.1 and we shall see that their equation is a special case of our theory.

We put $\theta = \phi = 0$ in equations (5.66) to (5.74). For simplicity we shall also neglect all body forces. As the fibre does not twist our rotated coordinate system is redundant for this simple example. We find that $\bar{\sigma}_{s2} = \mathcal{M}_2 = \mathcal{N} = 0$ and that

$$\mathcal{M}_1 = -3\mu I_1 \frac{\partial \kappa}{\partial t}, \tag{5.75}$$

$$\frac{\partial \mathcal{M}_1}{\partial s} = A\bar{\sigma}_{s1}, \tag{5.76}$$

$$\frac{\partial}{\partial s}(A\bar{\sigma}_{s1}) + \kappa A\bar{\sigma}_{ss} = 0, \tag{5.77}$$

$$\frac{\partial}{\partial s}(A\bar{\sigma}_{ss}) - \kappa A\bar{\sigma}_{s1} = 0. \tag{5.78}$$

As the fibre lies in a plane, we can put $\kappa = \partial\alpha/\partial s$, where α is the angle between the centre–line of the fibre and some fixed axis. Then the above equations combine to give

$$\frac{\partial}{\partial s}\left(3\mu I_1 \frac{\partial^2 \alpha}{\partial s \partial t}\right) = F(t)\cos\alpha + G(t)\sin\alpha. \tag{5.79}$$

Notice the equivalence between this and the equation for a two–dimensional inertia–free viscous sheet, namely (3.24). The behaviour of solutions of this equation was discussed in BNT.

5.8 Higher order body forces

In deriving equations (5.66) to (5.74) we assumed that the body forces were small enough that they only entered the equations at order ϵ. We then found that the leading–order equations were satisfied identically by taking the tension in the fibre to be zero and the cross–sectional area time–independent. It was then necessary

to proceed to order ϵ^2 in order to find equations for the bending and twisting moments analogous to those governing slender elastic rods.

We now consider the case where the body forces are larger, so that they enter the equations at leading order. Though the typical figures quoted in the Introduction reveal that this scaling is less appropriate to problems in glass fibre drawing than that employed thus far, it is interesting for comparison with the theory of chapter 7 on the pressure–driven flow of curved viscous sheets.

We scale the body forces so that the following are all assumed to be order one:

$$\tilde{f}_s = \frac{\rho L^2 f_s}{MU}, \quad \tilde{f}_1 = \frac{\rho L^2 f_1}{MU}, \quad \tilde{f}_2 = \frac{\rho L^2 f_2}{MU}.$$

The analysis of section 5.4 follows without change until the axial force balance (5.41) which gains a term due to the axial body force:

$$\frac{\partial}{\partial s}\left(3\mu^{(0)}A^{(0)}\frac{\partial}{\partial s}(u_s^{(0)} - v_s^{(0)})\right) + A_0\tilde{f}_s = 0. \tag{5.80}$$

Similarly, body force terms enter the transverse stress balances, resulting in

$$3\mu^{(0)}\kappa^{(0)}\frac{\partial}{\partial s}(u_s^{(0)} - v_s^{(0)})\cos\phi^{(0)} + \tilde{f}_1 = 0, \tag{5.81}$$

$$3\mu^{(0)}\kappa^{(0)}\frac{\partial}{\partial s}(u_s^{(0)} - v_s^{(0)})\sin\phi^{(0)} + \tilde{f}_2 = 0. \tag{5.82}$$

Assuming the body forces are known, (5.80), (5.81) and (5.82), along with the mass–conservation equation (5.40) give four equations for the unknowns $\tilde{u}_s = (u_s^{(0)} - v_s^{(0)})$, $A^{(0)}$, $\kappa^{(0)}$ and $\phi^{(0)}$. Hence, with this scaling it is not necessary to consider the bending moments at all in order to find the geometry of the centre–line of the fibre; they will, however, come into the equation for the twist of the fibre about its axis.

As an example, suppose the body forces are due solely to gravity and hence put

$$f_s = \boldsymbol{g}.\boldsymbol{t}, \quad f_1 = \boldsymbol{g}.\boldsymbol{n}_1, \quad f_2 = \boldsymbol{g}.\boldsymbol{n}_2,$$

where $\boldsymbol{g}$ is the constant dimensionless acceleration due to gravity. These give the following relationships between the body force components:

$$\frac{\partial f_s}{\partial s} = \kappa f_1\cos\phi + \kappa f_2\sin\phi, \quad \frac{\partial f_1}{\partial s} = -\kappa f_s\cos\phi, \quad \frac{\partial f_2}{\partial s} = -\kappa f_s\sin\phi. \tag{5.83}$$

These, along with (5.80) to (5.82) imply that, so long as the leading–order curvature of the fibre is nonzero, the leading–order torsion must be zero. Hence the fibre must move in a plane and without loss of generality we may take $\phi^{(0)} = 0$. If the angle between the centre–line of the fibre and the direction of gravity is α, then

$$f_s = g\cos\alpha, \quad f_1 = -g\sin\alpha, \quad f_2 = 0 \ ,$$

and

$$\kappa = \frac{\partial\alpha}{\partial s},$$

so that (5.80) and (5.81) give (dropping superscripts)

$$\frac{\partial T}{\partial s} + gA\cos\alpha = 0, \quad T\frac{\partial\alpha}{\partial s} - gA\sin\alpha = 0, \tag{5.84}$$

where T is the tension in the fibre,

$$T = 3\mu A\frac{\partial}{\partial s}(u_s - v_s).$$

If the cross–sectional area A were assumed to be constant, (5.84) would give the familiar catenary shape for a heavy string hanging under gravity. Here, however, A may not be assumed constant; its evolution is given by the mass–conservation equation (5.40).

5.9 Conclusions

We have found leading–order equations governing the dynamics of a viscous fibre whose curvature is not small. We have considered two possible scalings for the body force acting on the fibre. In the first case (the one of more relevance to glass fibre drawing) we have found equations which generalise those of BNT (who neglected body forces completely). These equations are closely analogous to the equilibrium equations for a slender elastic rod. However, if the body force acting on the fibre is relatively large, we have seen that the theory of BNT must be replaced by a model in which there is a leading–order balance between the body force acting on the fibre and the tension in the fibre.

5.9.1 Relation with nearly straight fibres

Throughout this chapter we have considered fibres whose dimensionless curvature is order one. In the last chapter we confined our attention to fibres which are nearly straight, that is their dimensionless curvature is order ϵ. We would like to be able to match solutions from one regime to the other, for example to model fibres which are initially nearly straight and then buckle under compression, or to model fibres which are initially curved and then straighten under tension.

There is clearly a close analogy between the theories of viscous fibres and of two–dimensional viscous sheets. Consider, for example, the similarity between (3.26) and (4.37), the way that the theory of section 5.6 reduces to that of section 3.1.3 if the fibre is constrained to move in a plane, and that inertia–free theory predicts that the centre–line is straight in either case. Hence it is reasonable to expect the transition between low– and high–curvature scenarios for a viscous fibre via a short timescale to be very similar to that discussed in chapter 3 for a two–dimensional sheet. We shall not attempt to perform any short timescale analysis of viscous fibres, but assert that the main features noted in chapter 3, in particular the dominant length– and timescales, will also apply to viscous fibres.

However, in this chapter we have also encountered a slightly different example in which a short timescale plays a role. In section 5.8 we saw that if body forces acting on a fibre are large enough, instead of forming a straight line, as predicted by Dewynne, Ockendon & Wilmott (1992), it will adopt some other shape, given by the solution of (5.80), (5.81) and (5.82) (for example, a catenary for the case of a uniform fibre hanging under gravity). Hence a fibre which starts with an arbitrary initial shape must evolve over a short timescale, only tending towards the shape given by (5.80), (5.81) and (5.82) instead of straightening. We shall see that analogous behaviour occurs for a viscous sheet moving under an applied pressure drop in chapter 7.

Chapter 6

The dynamics of nearly planar viscous sheets

In this chapter we describe how the theory of two–dimensional viscous sheets developed in chapter 2 may be generalised to describe sheets which vary in two directions. Since the derivations are similar to those used in chapter 2 we shall omit most of the details. Throughout this chapter we restrict our attention to sheets which are nearly flat, so that they may effectively be described using a fixed Cartesian coordinate system. In order to describe sheets which have non–negligible curvature it is necessary to employ a curvilinear coordinate system which moves as the sheet moves; this forms the subject of the next chapter.

In section 6.1 we give the equations governing the Stokes flow of a slender viscous sheet, which are generalisations of the equations of section 2.1. In section 6.2 we discuss how further effects relevant to the "float glass" process described in the Introduction may be incorporated in the model. A simplified one–dimensional model for the float glass process is derived in section 6.3.

In section 6.4 we consider the problem of transverse motion of a viscous sheet, which is of relevance to the windscreen sagging problem described in the Introduction.

6.1 The viscous sheet equations

To start with we shall consider the flow of an inertia–free viscous sheet of constant viscosity. We shall denote the centre–surface of the sheet by $z = H(x, y, t)$ and the thickness of the sheet by $h(x, y, t)$. If L is a typical length in the x- and y-directions, then our asymptotic analysis is based on the assumptions that H/L and h/L are both everywhere much smaller than 1. We shall omit the derivation of the leading–order equations which is analogous to that given in section 2.1 for a purely two–dimensional sheet.

In section 2.1 we found that the leading–order flow was extensional, that is the axial velocity was uniform across the sheet. For the fully three–dimensional sheet, this generalises to the fact that both tangential velocity components are independent of z to leading order: (neglecting subscripts)

$$u = u(x, y, t), \quad v = v(x, y, t) \ . \tag{6.1}$$

Our generalisation of the conservation of mass equation (2.15) is

$$h_t + (uh)_x + (vh)_y = 0. \tag{6.2}$$

Instead of the single axial force balance (2.18) we obtain two tangential stress balances, namely

$$\left.\begin{array}{rcl} [2h(2u_x + v_y)]_x + [h(u_y + v_x)]_y &=& 0 \\ [h(u_y + v_x)]_x + [2h(u_x + 2v_y)]_y &=& 0 \end{array}\right\} \tag{6.3}$$

while the centre–surface of the sheet satisfies the decoupled equation (a generalisation of (2.22)),

$$(2u_x + v_y)H_{xx} + (u_y + v_x)H_{xy} + (u_x + 2v_y)H_{yy} = 0. \tag{6.4}$$

Equation (6.2) is a hyperbolic equation for h whose characteristics are streamlines. Hence suitable boundary and initial conditions are for h to be given at $t = 0$, and along one edge of the fluid sheet (the end where the fluid flows *in*). The system (6.3) for u and v has two pairs of repeated imaginary characteristics (similar to

the biharmonic equation). Hence it is necessary to give two boundary conditions for u and v on the whole of the boundary of the fluid sheet.

As a result of (6.3) we may employ an Airy stress function $\mathfrak{A}(x, y, t)$ satisfying

$$2h(2u_x + v_y) = \mathfrak{A}_{yy}, \quad h(u_y + v_x) = -\mathfrak{A}_{xy}, \quad 2h(u_x + 2v_y) = \mathfrak{A}_{xx}. \tag{6.5}$$

The equation satisfied by $\mathfrak{A}$ may be found by eliminating u and v between these; it is rather complicated so we shall not bother. However, it is easily seen to be of the form

$$h^{-1}\nabla^4\mathfrak{A} = \text{terms involving lower derivatives of } \mathfrak{A},$$

so we may expect it to be similar in character to the biharmonic equation. The evolution of the sheet thickness is related to $\mathfrak{A}$ by

$$\frac{Dh}{Dt} = -\frac{1}{6}\nabla^2\mathfrak{A}, \tag{6.6}$$

so that in particular, if $\mathfrak{A}$ is harmonic then there is no stretching of the sheet.

In terms of $\mathfrak{A}$, the equation for the centre–surface (6.4) takes the form

$$\mathfrak{A}_{yy}H_{xx} - 2\mathfrak{A}_{xy}H_{xy} + \mathfrak{A}_{xx}H_{yy} = 0. \tag{6.7}$$

For a purely two–dimensional sheet, (6.7) implies $H_{xx} = 0$ so the centre–line is straight, as we observed in chapter 2. However, in this more general case, a wide variety of behaviours of H is possible. Indeed, the type of this equation depends on the Hessian of $\mathfrak{A}$, that is $\mathfrak{A}_{xx}\mathfrak{A}_{yy} - \mathfrak{A}_{xy}^2$. If this is positive the equation is elliptic, if it is zero the equation is parabolic and if it is negative the equation is hyperbolic. The kind of boundary conditions which must be imposed on H are therefore dependent on the stresses which are induced in the fluid sheet; each of these three types is possible. In particular, it is clear that in the case mentioned above in which $\mathfrak{A}$ is harmonic, (6.7) is definitely hyperbolic.

Note that

$$\mathfrak{A}_{yy}H_{xx} - 2\mathfrak{A}_{xy}H_{xy} + \mathfrak{A}_{xx}H_{yy} = (\mathfrak{A}_{yy}H)_{xx} - 2(\mathfrak{A}_{xy}H)_{xy} + (\mathfrak{A}_{xx}H)_{yy},$$

so the operator in (6.7) is self–adjoint, and hence H must satisfy the integral constraint

$$\oint_S (\mathfrak{A}_{xx}H_y - \mathfrak{A}_{xy}H_x)\,dx + (\mathfrak{A}_{yy}H_x - \mathfrak{A}_{xy}H_y)\,dy = 0 \tag{6.8}$$

for any closed curve S in the x-y plane.

As a simple example of the dependence of the type of (6.7) on the stresses in the sheet, consider the case in which a sheet of uniform thickness is subjected to a uniform dilatation plus a linear shear in the x-direction. This corresponds to the following trivial solution of (6.2) and (6.3)

$$u = d(t)x + 2s(t)y, \quad v = d(t)y, \quad h = h_0 \exp\left(-2\int_0^t d(\tau)\, d\tau\right). \tag{6.9}$$

The equation for H is then

$$3d(H_{xx} + H_{yy}) + 2sH_{xy} = 0. \tag{6.10}$$

The dependence of the character of this equation upon the relative sizes of d and s is clear. For example, if there is no shear ($s = 0$) then H is harmonic, if there is no dilatation ($d = 0$) then the general solution for H is $H = f_1(x) + f_2(y)$, while in the special case $S = 3d$ (when the equation is parabolic) the general solution for H is $H = (x + y)f_1(x - y) + f_2(x - y)$.

In more general situations, when the stresses are functions of x and y as well as t, equation (6.7) may change type from elliptic to hyperbolic along some line in the x-y plane; we may expect a weak singularity in H along such a "sonic" line.

6.2 A model for the float glass process

We shall now describe how the effects of surface tension, varying viscosity, gravity and a hydrostatic support may be incorporated in the equations of the previous section to give a model for the float glass process described in the Introduction. As the temperature of the glass varies dramatically during the process, the material properties of the glass, particularly its viscosity, likewise have a large variation.

The relevant dimensionless parameters are the capillary number, Stokes number and Reynolds number,

$$Ca = \frac{MU}{\gamma}\ ,\ St = \frac{\rho L^2 g}{MU}\ ,\ Re = \frac{\rho U L}{M}\ ,$$

where, as before, U and L are typical pulling speed and lengthscale, g is the acceleration due to gravity, and ρ and M are the density and typical viscosity of the glass. The relative importance of surface tension, gravity and inertia respectively, compared with viscous stresses, is determined by the order of magnitude of these parameters compared with the slenderness parameter ϵ which we will suppose is around 10^{-3}.

The Reynolds number varies typically from around 10^{-2} at the inlet of the bath to around 10^{-8} at the outlet. This means that to leading order inertia effects may be neglected entirely. The Stokes number varies from around 10^{2} at the inlet to around 10^{-2} at the outlet, so that gravity effects should be included when modelling the flow near the inlet, but may be negligible further downstream. The capillary number varies from around 10^{3} at the inlet to around 10^{10} at the outlet so that surface tension effects may be neglected throughout the body of the flow. However, near the inlet surface tension effects will be important in boundary layers at the edges of the floating glass ribbon.

In this section we shall derive the equations of motion and boundary conditions which are appropriate near the inlet of the bath where the flow is fully two–dimensional and gravity and surface tension effects must be taken into account. In the following section we shall describe a simpler, quasi–one–dimensional model which may be applied further downstream where the geometry is slowly varying and surface tension and gravity are less important.

6.2.1 The float glass equations

We shall now extend the the viscous sheet equations to include the effects of gravity acting downwards on the sheet counteracted by the pressure in the tin. We shall suppose the dimensionless parameters

$$\tilde{g} = \frac{\epsilon \rho L^2 g}{MU}, \quad \alpha = \frac{\rho}{\rho_{tin}} \tag{6.11}$$

are both $O(1)$ constants. The flow in the tin is at high Reynolds number and is likely to be turbulent. We shall make the assumption that the dominant force

exerted on the glass by the tin is that due to hydrostatic pressure; that is, we shall neglect both viscous drag due to the tin and the tin's inertia. As a result of these assumptions, the only changes to the derivations used in the previous section are the addition of a body force in the negative z–direction and a normal pressure on the lower surface $z = H - h/2$ proportional to the depth, $p_{tin} = -\rho_{tin} g(H - h/2)$.

With the scalings implied by (6.11) we find that there is a leading–order balance between the weight of the glass and the buoyancy of the tin. Hence (dropping subscripts) the leading–order centre–surface of the glass ribbon is given in terms of the glass thickness by

$$H = (\tfrac{1}{2} - \alpha)h. \tag{6.12}$$

The mass conservation equation is as before

$$h_t + (uh)_x + (vh)_y = 0, \tag{6.13}$$

and the in–plane stress balances receive terms due to gravity:

$$\begin{aligned} [2h(2u_x + v_y)]_x + [h(u_y + v_x)]_y &= \tilde{g}(1-\alpha)hh_x, \\ [h(u_y + v_x)]_x + [2h(u_x + 2v_y)]_y &= \tilde{g}(1-\alpha)hh_y. \end{aligned} \tag{6.14}$$

The terms on the right–hand side of (6.14) are a combination of the horizontal components of the pressure force due to the tin, and the contributions to the in–plane stresses σ_{xx} and σ_{yy} of hydrostatic pressure in the glass.

6.2.2 Edge conditions

Suppose the edge of the glass ribbon is given by $y = b(x,t)$ (see figure 1.4). As noted in section 6.1, at a fixed boundary we would expect to apply two conditions on u and v; at this free boundary we anticipate having to apply three conditions on u, v and b. The first is the kinematic condition

$$v = b_t + ub_x. \tag{6.15}$$

The stress tensor in the plane is given by

$$\bar{\sigma} = \begin{pmatrix} 2\mu(2u_x + v_y) + \tilde{g}[z + (\alpha - 1)h] & \mu(u_y + v_x) \\ \mu(u_y + v_x) & 2\mu(u_x + 2v_y) + \tilde{g}[z + (\alpha - 1)h] \end{pmatrix}. \tag{6.16}$$

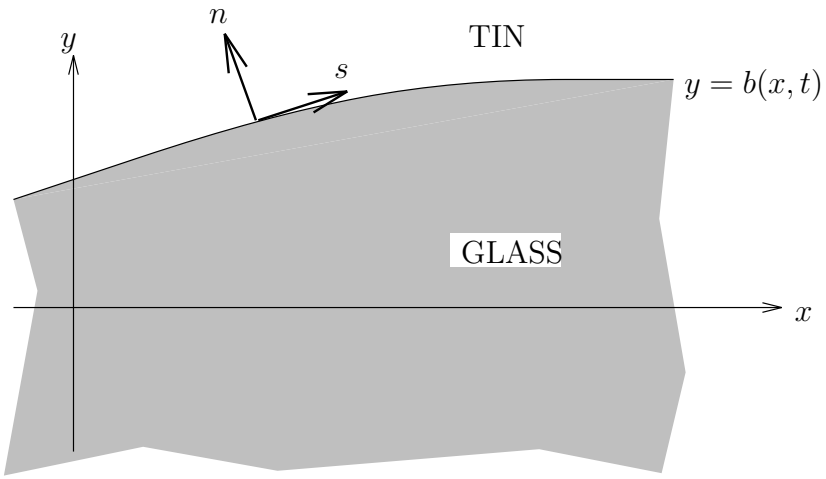

Figure 6.1: Plan view of the edge of a glass ribbon

We shall denote by s and n the tangent and normal to the edge $y = b(x,t)$ in the x-y plane: see figure 6.1. As previously, we shall neglect viscous drag due to the tin and hence set the tangential stress to zero at the ribbon edge:

$$\bar{\sigma}_{ns} = 0 \quad \text{on } y = b(x,t),$$

whence,

$$2b_x(u_x - v_y) = (1 - b_x^2)(u_y + v_x) \quad \text{on } y = b(x,t). \tag{6.17}$$

However, there will be a normal stress on the edge due to surface tension. A heuristic derivation of the appropriate condition is given below.

We perform a normal force balance on a small region of fluid between the edge $y = b(x,t)$ and a nearby line $y = c(x,t)$ which is far enough from the edge that our scaling assumptions that the gradients h_x and h_y be small are valid at $y = c$. The normal component of force on this region is provided by internal stress on $y = c(x,t)$, surface tensions on the glass–air (T_{ga}), glass–tin (T_{gt}) and tin–air (T_{ta}) interfaces and the hydrostatic pressure on the bottom surface $z = H - h/2$. As before we neglect the inertia of the glass. The normal forces are depicted schematically in figure 6.2.

In dimensional variables the normal force balance is written

$$T_{ta} - \left[\frac{T_{gt}}{\sqrt{1 + (H_n - \frac{1}{2}h_n)^2}} + \frac{T_{ga}}{\sqrt{1 + (H_n + \frac{1}{2}h_n)^2}} \right]_{y=c(x,t)} =$$

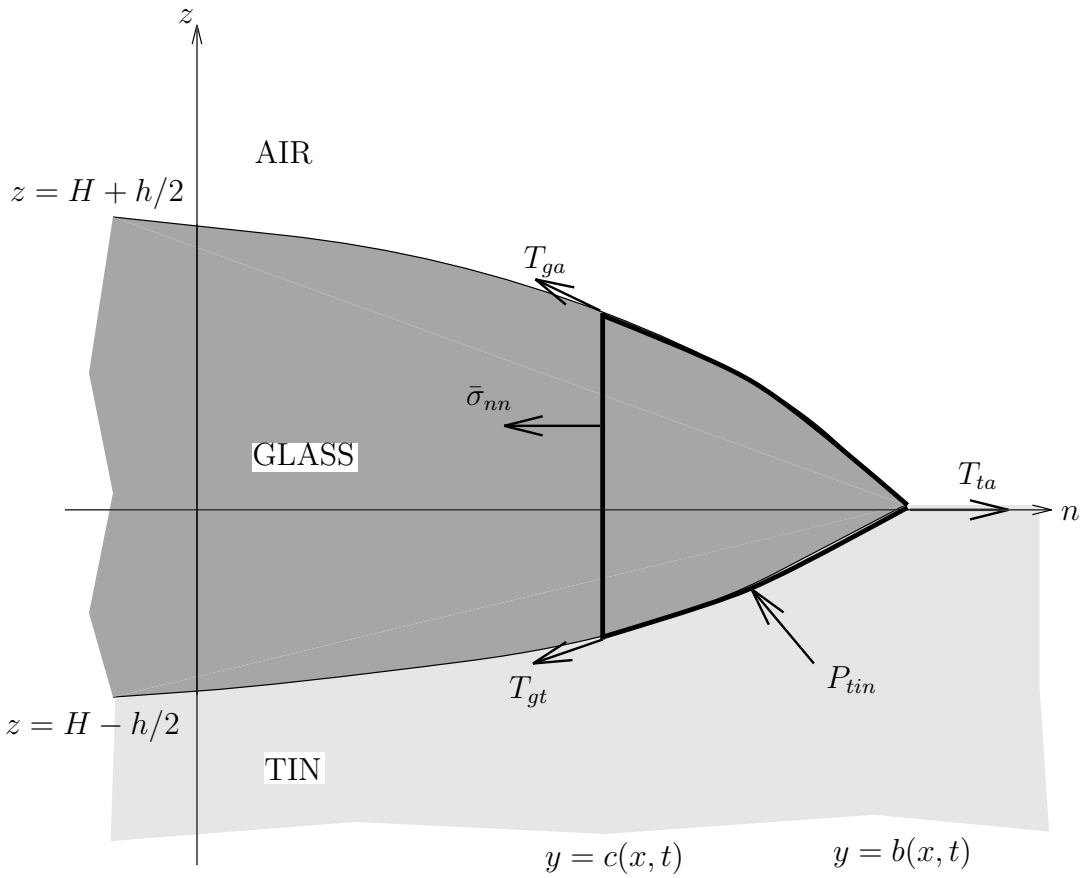

Figure 6.2: Normal forces at the edge of a glass ribbon

$$\int_{H(x,c,t)-\frac{1}{2}h(x,c,t)}^{H(x,c,t)+\frac{1}{2}h(x,c,t)} \bar{\sigma}_{nn} dz - \rho_{tin} g \int_c^b (H - \tfrac{1}{2}h)(H_x - \tfrac{1}{2}h_x)\, dx.$$

We now nondimensionalise, substitute for $\bar{\sigma}_{nn}$, perform the integrations and obtain the leading–order edge condition

$$\frac{2\mu}{1+b_x^2}\left(b_x^2(2u_x+v_y)+(u_x+2v_y)-b_x(u_y+v_x)\right) = \frac{(1-\alpha)}{2}\tilde{g}h - \frac{T}{h}, \tag{6.18}$$

where the net dimensionless surface tension at the edge is given by

$$T = \frac{T_{ga} + T_{gt} - T_{ta}}{\epsilon M U}. \tag{6.19}$$

For simplicity we may assume the glass ribbon is symmetric about the x-axis, and hence we also have the conditions on $y = 0$,

$$v = u_y = 0. \tag{6.20}$$

We would also expect to be given b, h, u and v at the inlet, say $x = 0$, and u and v at the outlet, say $x = 1$, as well as b and h at $t = 0$. Then a typical solution procedure would be:

- suppose that at some instant of time $h(x, y)$ and $b(x)$ are known functions;
- using the edge conditions (6.17) and (6.18), along with the given u and v at the two ends of the ribbon $x = 0$ and $x = 1$, solve the elliptic problem (6.14) for u and v;
- using the given h and b at the inlet $x = 0$, update h using (6.13) and b using (6.15).

Numerical solutions of these equations and boundary conditions have been considered for example by Bryant (1992) and Motoichi & Hiroshi (1991). These solutions reveal among other things that, except for a small region near the inlet where the glass spreads rapidly in all directions due to gravity, the flow is nearly unidirectional, the thickness of the glass is practically uniform across the ribbon (except in the boundary layers at the edges), and the geometry of the glass ribbon varies gradually in the direction of flow. This means that for much of the flow a simpler one–dimensional model may be employed. We shall now derive such a model.

6.3 One–dimensional approximation

We choose the x-axis to point in the direction of flow. The basis of the following analysis is that the length–scale in the y-direction is much smaller than that in the x-direction. Thus we rescale the float glass equations and edge conditions as follows:

$$y = \delta Y, \quad v = \delta V, \quad b = \delta B, \tag{6.21}$$

where $\delta \ll 1$. The method, analogous to that used in deriving the float glass equations, is to seek solutions which are asymptotic expansions in powers of δ^2. It is necessary to assume (as must certainly be a good approximation in practice) that the thickness of the glass is uniform across the ribbon, that is that h is independent of Y (except in the boundary layer close to the ribbon edge)[1]. If this assumption is made, the following leading–order extensional equations result for the ribbon thickness $h(x,t)$, breadth $b(x,t)$ and axial velocity $u(x,t)$.

The axial velocity and cross–sectional area satisfy the Trouton model (c.f. chapter 2) with force terms due to surface tension and gravity:

$$(Bh)_t + (uBh)_x = 0, \quad (3\mu Bhu_x)_x = -\frac{T}{2}B_x + \frac{\tilde{g}(1-\alpha)}{4}(Bh^2)_x, \tag{6.22}$$

while the evolution of the shape of the cross–section is given by

$$\frac{\partial}{\partial t}\left(\frac{h}{B}\right) + u\frac{\partial}{\partial x}\left(\frac{h}{B}\right) = \frac{2T - \tilde{g}(1-\alpha)h^2}{4\mu B}. \tag{6.23}$$

Appropriate initial and boundary conditions for this system are given B and h at $t = 0$ and at $x = 0$, and given u at the two ends of the sheet, $x = 0$ and $x = 1$. In the case $T = \tilde{g} = 0$ the system reduces to the Trouton model for a fibre, along with the fact that each cross–section preserves its aspect ratio as it convects along. This agrees with the theory of chapter 4 for nonaxisymmetric viscous fibres in which each cross–section was found to preserve its shape. Notice that the Trouton ratio is 3 in this system, though for a purely two–dimensional sheet we showed in chapter 2 that the Trouton ratio is 4. We shall discuss this change from 3 to 4 further in chapter 8.

[1] In fact it is only necessary to assume that h is independent of Y at $t = 0$ and at $x = 0$. It may then be shown to hold everywhere.

These equations may be simplified by transforming to Lagrangian variables as in chapter 2. However, for processes such as this where glass is fed in and out of the sheet, the conditions at the ends of the sheet are not well–suited to a Lagrangian description, which is better suited to describing such inherently unsteady batch processes as optical fibre tapering. The present problem is more akin to fibre draw–down, and hence it is more useful and practical to look for steady state solutions and, if desired, linearise about them, as in Matovich & Pearson (1969) and Pearson & Matovich (1969), for example.

6.3.1 Steady state solution

A steady–state solution of (6.22) and (6.23) must satisfy the physically obvious mass–conservation relation

$$uBh = \text{const.} = 1, \tag{6.24}$$

where without loss of generality we suppose that the scalings have been chosen in such a way that $u(0) = B(0) = h(0) = 1$. Then we find that u may be written in terms of B:

$$u(x) = B(x)e^{F\phi(x)/2}, \tag{6.25}$$

where

$$\phi(x) = \int_0^x \frac{d\xi}{\mu(\xi)}, \tag{6.26}$$

and F is an arbitrary constant (equal to the tension in the glass ribbon). Hence the problem may be reduced to the solution of a single first–order o.d.e. for $B(x)$, namely,

$$6B^2B' + F\phi'B^3 + T\phi'B^4 = \frac{\tilde{g}(1-\alpha)}{2}\phi' e^{-F\phi}. \tag{6.27}$$

The constant F is found by specifying the relative speed with which the glass is drawn off $u(1)$. In general this must be performed via some "shooting" algorithm: given an F, solve (6.27) with the initial value $B(0) = 1$, check for agreement between the resulting $u(1)$ and the specified $u(1)$, alter F accordingly and try again. Hence, given the drawing–off speed $u(1)$ the corresponding tension F, and hence the resulting breadth and thickness of the glass sheet, can be found. Alternatively, given a desired geometry of glass sheet, the required tension F can be found, and hence the appropriate drawing–off speed can be determined.

6.3.2 Neglecting gravity

As noted earlier, in the regions of the flow for which our one–dimensional approximation is valid, the parameters $\tilde{g}$ and T are both likely to be small. In particular, if $\tilde{g}$ is neglected then the one–dimensional problem may be solved explicitly to give

$$B(x) = \frac{Fe^{-F\phi(x)/6}}{F + T(1 - e^{-F\phi(x)/6})}, \tag{6.28}$$

$$u(x) = \frac{Fe^{F\phi(x)/3}}{F + T(1 - e^{-F\phi(x)/6})}, \tag{6.29}$$

$$h(x) = \frac{\left(F + T(1 - e^{-F\phi(x)/6})\right)^2}{F^2 e^{F\phi(x)/2}}. \tag{6.30}$$

If T is also neglected, these reduce to the one–dimensional "stiff–ribbon" equations given by Narayanaswamy (1977). If no tension is applied to the sheet ($F \to 0$) then the sheet narrows and thickens under surface tension, giving

$$h = \left(1 + \frac{T\phi}{6}\right)^2, \quad B = \left(1 + \frac{T\phi}{6}\right)^{-1}.$$

However, so long as F is greater than zero, it is easily shown that h and B are both strictly decreasing functions of F for any fixed x, while u increases monotonically with F. Hence there is a single–valued functional relationship between $u(1)$ and F; for small F they are related asymptotically by

$$F \sim \frac{2(1 + \frac{T\phi(1)}{6})^2}{(4 + \frac{5T\phi(1)}{6})\phi(1)} \left(u(1) - \frac{1}{(1 + \frac{T\phi(1)}{6})}\right)$$

as $u(1) \to (1 + \frac{T\phi(1)}{6})^{-1}$ while

$$F \sim \frac{3}{\phi(1)} \log\left(u(1)\right) \quad \text{as } u(1) \to \infty.$$

6.4 Transverse motion of a viscous sheet

In the models we have presented thus far, we have considered viscous sheets which are both slender and almost planar. However, we have also made one further assumption, namely that the fluid velocity is principally in the plane of the sheet.

We shall now consider sheets whose velocity is principally transverse. An example of such a sheet is a windscreen in the first stages of the sagging process described in the introduction. The limitation of the theory to follow is that we can only expect it to be valid for a limited period of time while the sheet remains nearly planar; when this ceases to be the case it will be necessary to resort to the more complicated theory of the following chapter.

As before, we suppose that if a typical length–scale in the x- and y-directions is L, then the thickness of the sheet and the displacement of the centre–surface, given by $z = H(x, y, t)$ are both typically of order ϵL, where $\epsilon \ll 1$. Here, however, we suppose a typical velocity in the z-direction is V, and that the velocities in the x- and y-directions are an order of magnitude smaller, that is of order ϵV.

6.4.1 The Stokes equations and boundary conditions

We suppose the sheet is driven by gravity acting in the negative z-direction. A simple force balance gives an order of magnitude for the transverse velocity

$$V \sim \frac{\rho g L^2}{\epsilon^2 \mu},$$

so we measure gravitational effects using the dimensionless parameter

$$g^* = \frac{\rho g L^2}{\epsilon^2 \mu V}.$$

After nondimensionalisation as implied by the scalings described above, the Stokes equations take the form

$$\epsilon^2 u_x + \epsilon^2 v_y + w_z = 0, \tag{6.31}$$

$$\epsilon^2 p_x = \epsilon^2 u_{xx} + \epsilon^2 u_{yy} + u_{zz}, \tag{6.32}$$

$$\epsilon^2 p_y = \epsilon^2 v_{xx} + \epsilon^2 v_{yy} + v_{zz}, \tag{6.33}$$

$$\epsilon^2 p_z = -\epsilon^4 g^* + \epsilon^2 w_{xx} + \epsilon^2 w_{yy} + w_{zz}. \tag{6.34}$$

On the two free surfaces of the sheet, $z = H \pm h/2$, we have the kinematic condition

$$w = H_t \pm \tfrac{1}{2} h_t + \epsilon^2 u(H_x \pm \tfrac{1}{2} h_x) + \epsilon^2 v(H_y \pm \tfrac{1}{2} h_y), \tag{6.35}$$

and, neglecting surface tension for the moment, the dynamic conditions,

$$\epsilon^2(H_x \pm \tfrac{1}{2}h_x)(-p + 2u_x) + \epsilon^2(H_y \pm \tfrac{1}{2}h_y)(u_y + v_x) = u_z + w_x, \tag{6.36}$$

$$\epsilon^2(H_x \pm \tfrac{1}{2}h_x)(u_y + v_x) + \epsilon^2(H_y \pm \tfrac{1}{2}h_y)(-p + 2v_y) = v_z + w_y, \tag{6.37}$$

$$\epsilon^2(H_x \pm \tfrac{1}{2}h_x)(u_z + w_x) + \epsilon^2(H_y \pm \tfrac{1}{2}h_y)(v_z + w_y) = -\epsilon^2 p + 2w_z. \tag{6.38}$$

Notice that these are simply the three–dimensional version of equations (3.3) to (3.8), the governing equations for the short–timescale motion of an inertia–free viscous sheet; the short timescale analysis of section 3.1 is equivalent to looking for a scenario in which the motion of the sheet is principally transverse. Hence our leading–order equations are three–dimensional generalisations of equations (3.10), (3.11), (3.12) and (3.13), namely

$$h_t = 0, \tag{6.39}$$

$$u = \bar{u}(x, y, t) + H_{xt}(H - z), \quad v = \bar{v}(x, y, t) + H_{yt}(H - z), \tag{6.40}$$

$$\left.\begin{array}{rcl} \dfrac{\partial \bar{\sigma}_{xx}}{\partial x} + \dfrac{\partial \bar{\sigma}_{xy}}{\partial y} & = & 0 \\ \dfrac{\partial \bar{\sigma}_{xy}}{\partial x} + \dfrac{\partial \bar{\sigma}_{yy}}{\partial y} & = & 0 \end{array}\right\} \tag{6.41}$$

where the in–plane stresses are given by

$$\left.\begin{array}{rcl} \bar{\sigma}_{xx} & = & 2h[2(\bar{u}_x + H_x H_{xt}) + (\bar{v}_y + H_y H_{yt})] \\ \bar{\sigma}_{xy} & = & h[(\bar{u}_y + H_y H_{xt}) + (\bar{v}_x + H_x H_{yt})] \\ \bar{\sigma}_{yy} & = & 2h[(\bar{u}_x + H_x H_{xt}) + 2(\bar{v}_y + H_y H_{yt})] \end{array}\right\}, \tag{6.42}$$

and the equation for the centre–surface of the sheet,

$$\bar{\sigma}_{xx}H_{xx} + 2\bar{\sigma}_{xy}H_{xy} + \bar{\sigma}_{yy}H_{yy} = \frac{1}{6}[h^3(2H_{xxt} + H_{yyt})]_{xx} + \frac{1}{3}[h^3 H_{xyt}]_{xy} + \frac{1}{6}[h^3(H_{xxt} + 2H_{yyt})]_{yy} + g^* h. \tag{6.43}$$

For a purely two–dimensional sheet, where gravity and all y variations are neglected, these equations clearly reduce to the short timescale equations of section 3.1.

6.4.2 Uniform thickness

Consider the example, relevant to the "windscreen sagging" problem, in which the sheet has uniform thickness initially. Then because of (6.39) we may set $h = 1$ for all time. As a result of (6.41) we may employ an Airy stress function $\mathfrak{A}$ satisfying

$$\bar{\sigma}_{xx} = \mathfrak{A}_{yy}, \quad \bar{\sigma}_{xy} = -\mathfrak{A}_{xy}, \quad \bar{\sigma}_{yy} = \mathfrak{A}_{xx}. \tag{6.44}$$

For this simple case of uniform thickness, u and v may eliminated from (6.42) to give the following equation for $\mathfrak{A}$:

$$\nabla^4 \mathfrak{A} + 3\frac{\partial}{\partial t}(H_{xx}H_{yy} - H_{xy}^2) = 0, \tag{6.45}$$

and equation (6.43) for H reduces to

$$\mathfrak{A}_{yy}H_{xx} - 2\mathfrak{A}_{xy}H_{xy} + \mathfrak{A}_{xx}H_{yy} = \frac{1}{3}\nabla^4 H_t + g^*. \tag{6.46}$$

This nonlinear system for $\mathfrak{A}$ and H is similar to the so–called von Kármán equations for a thin elastic plate (see, for example, Love (1927), article 335E). Indeed, the von Kármán equations may be obtained from (6.45) and (6.46) by deleting the time derivatives.

The system (6.45) and (6.46) has one real and eight imaginary characteristics; suitable boundary and initial conditions are given H at $t = 0$ along with two conditions each on H and $\mathfrak{A}$ on the boundary of the sheet (see the footnote on page 66). This can be seen from the following proposed solution procedure:

- suppose at some instant of time H is known;
- solve (6.45) and (6.46) as a boundary value problem for $\mathfrak{A}$ and H_t;
- using the calculated H_t, update H.

The problem for $\mathfrak{A}$ and H_t may be written in a symmetric form as follows. Set $w = H_t$ and the self–adjoint operator

$$\mathfrak{D}^2 = H_{yy}\frac{\partial^2}{\partial x^2} - 2H_{xy}\frac{\partial^2}{\partial x \partial y} + H_{xx}\frac{\partial^2}{\partial y^2}.$$

In terms of these, (6.45) and (6.46) take the form

$$\begin{aligned} \nabla^4 \mathfrak{A} + 3\mathfrak{D}^2 w &= 0, \\ \nabla^4 w - 3\mathfrak{D}^2 \mathfrak{A} &= -3g^*. \end{aligned} \tag{6.47}$$

As a simple example of the behaviour we may expect of H, we return to the combination of a uniform dilatation and a linear shear introduced in section 6.1. This corresponds to $\bar{\sigma}_{xx} = \bar{\sigma}_{yy} = 6d$, $\bar{\sigma}_{xy} = 2s$, where d and s are functions only of t. For simplicity we neglect gravity. Clearly (6.41) is satisfied identically, and the centre–surface satisfies

$$6d(H_{xx} + H_{yy}) + 4sH_{xy} = \frac{1}{3}\nabla^4 H_t. \tag{6.48}$$

Consider the response of a typical Fourier component,

$$H = e^{\lambda t} \cos\left[k(y\cos\alpha - x\sin\alpha)\right].$$

Substitution into (6.48) gives

$$\lambda = \frac{6(s\sin(2\alpha) - 3d)}{k^2}. \tag{6.49}$$

Hence all such modes decay if $s < 3d$ (which corresponds to the steady state equation being elliptic), while some modes will grow exponentially if $s > 3d$ (so that the steady state equation is hyperbolic). In the latter case, the fastest growing modes lie on $\alpha = \pi/4$ and are of long wavelength. This has been discussed by Benjamin & Mullin (1988) in the context of buckling instabilities induced by shearing a thin layer of viscous fluid. They chose to extend the theory by adopting a scaling similar to that employed in the study of Stokes surface waves, in contrast with our scaling which is analogous to that employed in shallow water theory; see the discussion in section 2.3.

6.5 Surface tension and inertia

We have neglected surface tension and inertia effects throughout this chapter, except when deriving edge conditions for the float glass model. We now describe briefly how this can be rectified.

Surface tension effects may be incorporated with relative ease; as in section 2.5.1 they contribute to the tension in the sheet, so that (6.4) becomes

$$(\bar{\sigma}_{xx} + \gamma^*)H_{xx} + 2\bar{\sigma}_{xy}H_{xy} + (\bar{\sigma}_{yy} + \gamma^*)H_{yy} = 0, \tag{6.50}$$

with an analogous change to the left–hand side of (6.43).

When inertia effects are included, it is necessary, as in section 3.3, to allow for the possibility of short timescale and lengthscale behaviour; the paradigm centre–surface equation corresponding to (3.35) is

$$\bar{\sigma}_{xx}H_{xx} + 2\bar{\sigma}_{xy}H_{xy} + \bar{\sigma}_{yy}H_{yy} = \frac{\epsilon^2}{3}\nabla^4 H_t + ReH_{tt}. \tag{6.51}$$

As in section 3.3, the dominant length– and timescales may be determined by examining the linear growth rate of a typical Fourier component, treating $\bar{\sigma}_{xx}$, $\bar{\sigma}_{xy}$ and $\bar{\sigma}_{yy}$ as constants. However, depending on the relative magnitudes of these stresses, a wealth of different behaviours is possible, in which different length– and timescales dominate in different directions. We shall not persue this further here.

6.6 Conclusions

We have derived models for sheets whose curvature is small enough that they may effectively be described using a fixed Cartesian coordinate system. In particular, we have derived a fully two–dimensional model for the float–glass process which we have simplified to a one–dimensional model for the case of slowly varying geometry. We have also considered transverse motion of nearly planar viscous sheet, and have shown that such a motion may be modelled by equations similar to the von Kármán equations of linear elasticity.

In the next chapter we shall employ a moving curvilinear coordinate system to model a viscous sheet with non–negligible curvature.

Chapter 7

The dynamics of curved viscous sheets

We now consider the dynamics of a more general slender sheet of viscous fluid where the curvature of the sheet is not small. We employ curvilinear coordinates fixed in the "centre–surface" of the sheet, and choose them in such a way that the coordinate system so defined is orthogonal. The basic geometrical considerations are discussed in section 7.1. The Stokes equations and kinematic and stress–free boundary conditions are written down in our coordinate system in section 7.2 and nondimensionalised in section 7.3. In section 7.4 we derive the leading–order equations in a perturbation scheme based on the slenderness parameter of the sheet. With the bottle–blowing problem in mind, we add the effect of an imposed pressure drop across the sheet in section 7.5, while writing the equations derived in the previous section in a concise manner which emphasises their analogy with the shell equations of linear elasticity.

In sections 7.6 and 7.7 we apply these equations to two relatively simple geometries: an axisymmetric sheet and a two–dimensional sheet respectively. In each case we find that a constant pressure–drop across the sheet leads to finite–time blow–up.

We discuss the extension of the model to include the effects of surface tension and inertia in sections 7.8 and 7.9. We draw conclusions from the chapter in section 7.10.

7.1 Geometrical preamble

7.1.1 Setting up the coordinate system

We suppose that the centre–surface of the sheet is given by

$$\boldsymbol{r} = \boldsymbol{r}_c(x_1, x_2, t),$$

where x_1 and x_2 are spatial parameters and t is time. The unit normal to this surface is given by

$$\boldsymbol{n} = \left|\frac{\partial \boldsymbol{r}_c}{\partial x_1} \wedge \frac{\partial \boldsymbol{r}_c}{\partial x_2}\right|^{-1} \left(\frac{\partial \boldsymbol{r}_c}{\partial x_1} \wedge \frac{\partial \boldsymbol{r}_c}{\partial x_2}\right). \tag{7.1}$$

If the thickness of the fluid sheet is $h(x_1, x_2, t)$, then the two free surfaces are given by

$$\boldsymbol{r} = \boldsymbol{r}_c \pm \tfrac{1}{2} h \boldsymbol{n}.$$

We choose to parametrise the sheet in such a way that lines of constant x_1 and x_2 are lines of curvature of the centre–surface $\boldsymbol{r} = \boldsymbol{r}_c$ (see for example Kreyszig (1959)). This means that

$$\frac{\partial \boldsymbol{r}_c}{\partial x_1}.\frac{\partial \boldsymbol{r}_c}{\partial x_2} = 0 \quad \text{and} \quad \frac{\partial^2 \boldsymbol{r}_c}{\partial x_1 \partial x_2}.\boldsymbol{n} = 0,$$

so that the first and second fundamental forms of the surface are both diagonal. We put

$$a_1 = \left|\frac{\partial \boldsymbol{r}_c}{\partial x_1}\right|, \quad a_2 = \left|\frac{\partial \boldsymbol{r}_c}{\partial x_2}\right| \tag{7.2}$$

and then we may define an orthonormal basis $\{\boldsymbol{e}_1, \boldsymbol{e}_2, \boldsymbol{n}\}$, where

$$\boldsymbol{e}_1 = \frac{1}{a_1}\frac{\partial \boldsymbol{r}_c}{\partial x_1} \text{ and } \boldsymbol{e}_2 = \frac{1}{a_2}\frac{\partial \boldsymbol{r}_c}{\partial x_2}. \tag{7.3}$$

The derivatives of these basis vectors are given by

$$\frac{\partial \boldsymbol{e}_1}{\partial x_1} = -\frac{1}{a_2}\frac{\partial a_1}{\partial x_2}\boldsymbol{e}_2 + \kappa_1 a_1 \boldsymbol{n}, \quad \frac{\partial \boldsymbol{e}_1}{\partial x_2} = \frac{1}{a_1}\frac{\partial a_2}{\partial x_1}\boldsymbol{e}_2, \tag{7.4}$$

$$\frac{\partial \boldsymbol{e}_2}{\partial x_2} = -\frac{1}{a_1}\frac{\partial a_2}{\partial x_1}\boldsymbol{e}_1 + \kappa_2 a_2 \boldsymbol{n}, \quad \frac{\partial \boldsymbol{e}_2}{\partial x_1} = \frac{1}{a_2}\frac{\partial a_1}{\partial x_2}\boldsymbol{e}_1, \tag{7.5}$$

$$\frac{\partial \boldsymbol{n}}{\partial x_1} = -\kappa_1 a_1 \boldsymbol{e}_1 \text{ and } \frac{\partial \boldsymbol{n}}{\partial x_2} = -\kappa_2 a_2 \boldsymbol{e}_2, \tag{7.6}$$

where κ_1 and κ_2 are the principal curvatures of the centre–surface. Elimination between these equations leads to three identities linking a_1, a_2, κ_1 and κ_2, namely

$$a_1\frac{\partial\kappa_1}{\partial x_2} = (\kappa_2 - \kappa_1)\frac{\partial a_1}{\partial x_2}, \tag{7.7}$$

$$a_2\frac{\partial\kappa_2}{\partial x_1} = (\kappa_1 - \kappa_2)\frac{\partial a_2}{\partial x_1}, \tag{7.8}$$

and

$$\frac{\partial}{\partial x_1}\left(\frac{1}{a_1}\frac{\partial a_2}{\partial x_1}\right) + \frac{\partial}{\partial x_2}\left(\frac{1}{a_2}\frac{\partial a_1}{\partial x_2}\right) + a_1a_2\kappa_1\kappa_2 = 0. \tag{7.9}$$

We shall be using the coordinates (x_1, x_2, n) to describe a general point of the fluid sheet whose position is given by

$$\boldsymbol{r} = \boldsymbol{r}_c + n\boldsymbol{n}. \tag{7.10}$$

The metric for this coordinate system is then given by

$$g_{ij} = \frac{\partial\boldsymbol{r}}{\partial x_i}.\frac{\partial\boldsymbol{r}}{\partial x_j} = \begin{pmatrix} a_1^2(1-\kappa_1 n)^2 & 0 & 0 \\ 0 & a_2^2(1-\kappa_2 n)^2 & 0 \\ 0 & 0 & 1 \end{pmatrix}, \tag{7.11}$$

and hence, because of our choice that x_1 and x_2 parametrise lines of curvature of the centre–surface $\boldsymbol{r} = \boldsymbol{r}_c$, this coordinate system is orthogonal, with scaling factors given by

$$\begin{array}{rcl} l_1 &=& a_1(1-\kappa_1 n), \\ l_2 &=& a_2(1-\kappa_2 n), \\ l_3 &=& 1. \end{array} \tag{7.12}$$

7.1.2 Velocity of the centre–surface

Now we recall that the centre–surface $\boldsymbol{r} = \boldsymbol{r}_c$ is time–dependent and resolve its velocity onto the x_1-, x_2- and n-directions:

$$\frac{\partial\boldsymbol{r}_c}{\partial t} = v_1\boldsymbol{e}_1 + v_2\boldsymbol{e}_2 + v_3\boldsymbol{n}. \tag{7.13}$$

Then differentiation reveals that

$$\frac{\partial^2\boldsymbol{r}_c}{\partial x_1\partial t} = \left(\frac{\partial v_1}{\partial x_1} + \frac{v_2}{a_2}\frac{\partial a_1}{\partial x_2} - a_1\kappa_1 v_3\right)\boldsymbol{e}_1 + \left(\frac{\partial v_2}{\partial x_1} - \frac{v_1}{a_2}\frac{\partial a_1}{\partial x_2}\right)\boldsymbol{e}_2 + \left(a_1\kappa_1 v_1 + \frac{\partial v_3}{\partial x_1}\right)\boldsymbol{n}, \tag{7.14}$$

$$\frac{\partial^2 \boldsymbol{r}_c}{\partial x_2 \partial t} = \left(\frac{\partial v_1}{\partial x_2} - \frac{v_2}{a_1}\frac{\partial a_2}{\partial x_1} \right) \boldsymbol{e}_1 + \left(\frac{\partial v_2}{\partial x_2} + \frac{v_1}{a_1}\frac{\partial a_2}{\partial x_1} - a_2\kappa_2 v_3 \right) \boldsymbol{e}_2 + \left(a_2\kappa_2 v_2 + \frac{\partial v_3}{\partial x_2} \right) \boldsymbol{n} \tag{7.15}$$

and

$$\frac{\partial \boldsymbol{n}}{\partial t} = -\left(\kappa_1 v_1 + \frac{1}{a_1}\frac{\partial v_3}{\partial x_1} \right) \boldsymbol{e}_1 - \left(\kappa_2 v_2 + \frac{1}{a_2}\frac{\partial v_3}{\partial x_2} \right) \boldsymbol{e}_2. \tag{7.16}$$

Now we note the three identities

$$\frac{\partial^2 \boldsymbol{r}_c}{\partial x_1 \partial t}.\frac{\partial \boldsymbol{r}_c}{\partial x_2} + \frac{\partial^2 \boldsymbol{r}_c}{\partial x_2 \partial t}.\frac{\partial \boldsymbol{r}_c}{\partial x_1} = 0, \quad \frac{\partial^2 \boldsymbol{r}_c}{\partial x_1 \partial t}.\frac{\partial \boldsymbol{r}_c}{\partial x_1} = a_1\frac{\partial a_1}{\partial t}, \quad \frac{\partial^2 \boldsymbol{r}_c}{\partial x_2 \partial t}.\frac{\partial \boldsymbol{r}_c}{\partial x_2} = a_2\frac{\partial a_2}{\partial t}$$

to give three equations for v_1, v_2 and v_3, namely

$$v_1\frac{\partial a_1}{\partial x_2} + v_2\frac{\partial a_2}{\partial x_1} = a_1\frac{\partial v_1}{\partial x_2} + a_2\frac{\partial v_2}{\partial x_1}, \tag{7.17}$$

$$a_2\frac{\partial a_1}{\partial t} = a_2\frac{\partial v_1}{\partial x_1} + v_2\frac{\partial a_1}{\partial x_2} - a_1 a_2 \kappa_1 v_3, \tag{7.18}$$

and

$$a_1\frac{\partial a_2}{\partial t} = a_1\frac{\partial v_2}{\partial x_2} + v_1\frac{\partial a_2}{\partial x_1} - a_1 a_2 \kappa_2 v_3. \tag{7.19}$$

7.2 The Stokes equations and boundary conditions

As a result of our choice of an orthogonal coordinate system, the Stokes equations may be written down relatively easily (we postpone the consideration of inertia effects until section 7.9). We denote by (u_1, u_2, u_3) the fluid velocities in the $\boldsymbol{e}_1-$, $\boldsymbol{e}_2-$ and $\boldsymbol{n}-$directions. The incompressibility condition may be written

$$\frac{\partial}{\partial x_1}(l_2 u_1) + \frac{\partial}{\partial x_2}(l_1 u_2) + \frac{\partial}{\partial n}(l_1 l_2 u_3) = 0, \tag{7.20}$$

and force balances in the $\boldsymbol{e}_1$, $\boldsymbol{e}_2$ and $\boldsymbol{n}$ directions give

$$\frac{\partial}{\partial x_1}(l_2\sigma_{11}) + \frac{\partial}{\partial x_2}(l_1\sigma_{12}) + \frac{\partial l_1}{\partial x_2}\sigma_{12} + \frac{\partial}{\partial n}(l_1 l_2 \sigma_{13}) + l_2\frac{\partial l_1}{\partial n}\sigma_{13} - \frac{\partial l_2}{\partial x_1}\sigma_{22} + \rho l_1 l_2 f_1 = 0, \tag{7.21}$$

$$\frac{\partial}{\partial x_1}(l_2\sigma_{12}) + \frac{\partial l_2}{\partial x_1}\sigma_{12} + \frac{\partial}{\partial x_2}(l_1\sigma_{22}) + \frac{\partial}{\partial n}(l_1 l_2 \sigma_{23}) + l_1\frac{\partial l_2}{\partial n}\sigma_{23} - \frac{\partial l_1}{\partial x_2}\sigma_{11} + \rho l_1 l_2 f_2 = 0, \tag{7.22}$$

$$\frac{\partial}{\partial x_1}(l_2\sigma_{13}) + \frac{\partial}{\partial x_2}(l_1\sigma_{23}) + \frac{\partial}{\partial n}(l_1 l_2 \sigma_{33}) - l_2\frac{\partial l_1}{\partial n}\sigma_{11} - l_1\frac{\partial l_2}{\partial n}\sigma_{22} + \rho l_1 l_2 f_3 = 0, \tag{7.23}$$

where f_i are the components of the body force acting on the sheet. The physical components of stress are given by

$$\sigma_{11} = -p + \frac{2\mu}{l_1}\left(\frac{\partial u_1}{\partial x_1} + \frac{u_2}{l_2}\frac{\partial l_1}{\partial x_2} + u_3\frac{\partial l_1}{\partial n}\right), \tag{7.24}$$

$$\sigma_{22} = -p + \frac{2\mu}{l_2}\left(\frac{\partial u_2}{\partial x_2} + \frac{u_1}{l_1}\frac{\partial l_2}{\partial x_1} + u_3\frac{\partial l_2}{\partial n}\right), \tag{7.25}$$

$$\sigma_{33} = -p + 2\mu\frac{\partial u_3}{\partial n}, \tag{7.26}$$

$$\sigma_{12} = \frac{\mu}{l_1 l_2}\left(l_1\frac{\partial u_1}{\partial x_2} - \frac{\partial l_1}{\partial x_2}u_1 + l_2\frac{\partial u_2}{\partial x_1} - \frac{\partial l_2}{\partial x_1}u_2\right) \tag{7.27}$$

$$\sigma_{13} = \frac{\mu}{l_1}\left(l_1\frac{\partial u_1}{\partial n} - \frac{\partial l_1}{\partial n}u_1 + \frac{\partial u_3}{\partial x_1}\right), \tag{7.28}$$

$$\sigma_{23} = \frac{\mu}{l_2}\left(l_2\frac{\partial u_2}{\partial n} - \frac{\partial l_2}{\partial n}u_2 + \frac{\partial u_3}{\partial x_2}\right). \tag{7.29}$$

On the free boundaries given by $n = \pm\frac{1}{2}h$ we neglect surface tension and impose zero stress conditions,

$$\sigma_{13} = \pm\frac{1}{2l_1}\frac{\partial h}{\partial x_1}\sigma_{11} \pm \frac{1}{2l_2}\frac{\partial h}{\partial x_2}\sigma_{12}, \tag{7.30}$$

$$\sigma_{23} = \pm\frac{1}{2l_1}\frac{\partial h}{\partial x_1}\sigma_{12} \pm \frac{1}{2l_2}\frac{\partial h}{\partial x_2}\sigma_{22}, \tag{7.31}$$

$$\sigma_{33} = \pm\frac{1}{2l_1}\frac{\partial h}{\partial x_1}\sigma_{13} \pm \frac{1}{2l_2}\frac{\partial h}{\partial x_2}\sigma_{23}, \tag{7.32}$$

and the kinematic condition, which, using the convective derivative

$$\frac{D}{Dt} = \frac{\partial}{\partial t} + \left(\boldsymbol{u} - \frac{\partial \boldsymbol{r}_c}{\partial t} - n\frac{\partial \boldsymbol{n}}{\partial t}\right).\nabla, \tag{7.33}$$

may be written in the form

$$\begin{aligned} u_3 - v_3 = \pm\frac{1}{2}\frac{\partial h}{\partial t} \quad &\pm \quad \frac{1}{2l_1}\frac{\partial h}{\partial x_1}\left[u_1 - v_1 \pm \frac{h}{2}\left(\kappa_1 v_1 + \frac{1}{a_1}\frac{\partial v_3}{\partial x_1}\right)\right] \\ &\pm \quad \frac{1}{2l_2}\frac{\partial h}{\partial x_2}\left[u_2 - v_2 \pm \frac{h}{2}\left(\kappa_2 v_2 + \frac{1}{a_2}\frac{\partial v_3}{\partial x_2}\right)\right]. \end{aligned} \tag{7.34}$$

7.3 Nondimensionalisation and scaling

Now we use the slenderness of the sheet in our nondimensionalisation of the equations. We suppose L is a typical lengthscale for the sheet, while ϵL is a typical thickness and $\epsilon \ll 1$. We suppose a typical velocity scale is U, and that the curvature of the sheet is of order $1/L$. We allow for varying viscosity, but suppose that it is typically of order M. Without loss of generality we may assume that the parameters x_1 and x_2 have the dimensions of length. Hence the scalings we employ are

$$\begin{aligned} &x_1 = Lx_1', \quad x_2 = Lx_2', && n = \epsilon L n', \\ &u_1 = Uu_1', \quad u_2 = Uu_2', && u_3 = Uu_3', \\ &\boldsymbol{r}_c = L\boldsymbol{r}_c', \quad \kappa_1 = L^{-1}\kappa_1', && \kappa_2 = L^{-1}\kappa_2', \\ &h = \epsilon L h', \quad p = MUL^{-1}p', && t = LU^{-1}t', \\ &\mu = M\mu'. \end{aligned} \tag{7.35}$$

These scalings are used to nondimensionalise the Stokes equations and boundary conditions. Then solutions are sought in the form of asymptotic expansions in powers of the slenderness parameter ϵ, typically (dropping primes)

$$u_1 \sim u_1^{(0)} + \epsilon u_1^{(1)} + \epsilon^2 u_1^{(2)} + \ldots.$$

7.4 Leading–order equations

The leading–order Stokes equations and stress–free boundary conditions reveal that $u_1^{(0)}$, $u_2^{(0)}$ and $u_3^{(0)}$ are all independent of n. Then the kinematic condition (7.34) gives

$$u_3^{(0)} = v_3^{(0)}. \tag{7.36}$$

Hence the leading–order stress components are given by

$$\sigma_{11} \sim -p^{(0)} + \frac{2\mu^{(0)}}{a_1^{(0)}} \left(\frac{\partial u_1^{(0)}}{\partial x_1} + \frac{u_2^{(0)}}{a_2^{(0)}} \frac{\partial a_1^{(0)}}{\partial x_2} - a_1^{(0)} \kappa_1^{(0)} v_3^{(0)} \right) + O(\epsilon), \tag{7.37}$$

$$\sigma_{22} \sim -p^{(0)} + \frac{2\mu^{(0)}}{a_2^{(0)}} \left(\frac{\partial u_2^{(0)}}{\partial x_2} + \frac{u_1^{(0)}}{a_1^{(0)}} \frac{\partial a_2^{(0)}}{\partial x_1} - a_2^{(0)} \kappa_2^{(0)} v_3^{(0)} \right) + O(\epsilon), \tag{7.38}$$

$$\sigma_{33} \sim -p^{(0)} + 2\mu^{(0)} \frac{\partial u_3^{(1)}}{\partial n} + O(\epsilon), \tag{7.39}$$

$$\sigma_{12} \sim \frac{\mu^{(0)}}{a_1^{(0)} a_2^{(0)}} \left(a_1^{(0)} \frac{\partial u_1^{(0)}}{\partial x_2} - u_1^{(0)} \frac{\partial a_1^{(0)}}{\partial x_2} + a_2^{(0)} \frac{\partial u_2^{(0)}}{\partial x_1} - u_2^{(0)} \frac{\partial a_2^{(0)}}{\partial x_1} \right) + O(\epsilon), \tag{7.40}$$

$$\sigma_{13} \sim \mu^{(0)} \left(\frac{\partial u_1^{(1)}}{\partial n} + \kappa_1^{(0)} u_1^{(0)} + \frac{1}{a_1^{(0)}} \frac{\partial v_3^{(0)}}{\partial x_1} \right) + O(\epsilon), \tag{7.41}$$

$$\sigma_{23} \sim \mu^{(0)} \left(\frac{\partial u_2^{(1)}}{\partial n} + \kappa_2^{(0)} u_2^{(0)} + \frac{1}{a_2^{(0)}} \frac{\partial v_3^{(0)}}{\partial x_2} \right) + O(\epsilon). \tag{7.42}$$

The equation of terms of order ϵ in the continuity equation (7.20) gives

$$\frac{\partial u_3^{(1)}}{\partial n} = (\kappa_1^{(0)} + \kappa_2^{(0)}) v_3^{(0)} - \frac{1}{a_1^{(0)} a_2^{(0)}} \left(\frac{\partial}{\partial x_1} (a_2^{(0)} u_1^{(0)}) + \frac{\partial}{\partial x_2} (a_1^{(0)} u_2^{(0)}) \right), \tag{7.43}$$

with the $O(\epsilon)$ kinematic condition on $n = \pm \frac{1}{2} h^{(0)}$,

$$\begin{aligned} u_3^{(1)} - \boldsymbol{n}^{(1)} . \frac{\partial \boldsymbol{r}_c^{(0)}}{\partial t} - \boldsymbol{n}^{(0)} . \frac{\partial \boldsymbol{r}_c^{(1)}}{\partial t} \quad &= \quad \pm \frac{1}{2} \frac{\partial h^{(0)}}{\partial t} \pm \frac{1}{2a_1^{(0)}} \frac{\partial h^{(0)}}{\partial x_1} (u_1^{(0)} - v_1^{(0)}) \\ &\quad \pm \frac{1}{2a_2^{(0)}} \frac{\partial h^{(0)}}{\partial x_2} (u_2^{(0)} - v_2^{(0)}). \end{aligned} \tag{7.44}$$

These give an expression for $u_3^{(1)}$,

$$\begin{aligned} u_3^{(1)} &= \boldsymbol{n}^{(1)} . \frac{\partial \boldsymbol{r}_c^{(0)}}{\partial t} + \boldsymbol{n}^{(0)} . \frac{\partial \boldsymbol{r}_c^{(1)}}{\partial t} \\ &+ \frac{n}{a_1^{(0)} a_2^{(0)}} \left(a_1^{(0)} a_2^{(0)} (\kappa_1^{(0)} + \kappa_2^{(0)}) u_3^{(0)} - \frac{\partial}{\partial x_1} (a_2^{(0)} u_1^{(0)}) - \frac{\partial}{\partial x_2} (a_1^{(0)} u_2^{(0)}) \right), \end{aligned} \tag{7.45}$$

and an equation linking the leading–order unknowns which may be arranged, using the identities (7.18) and (7.19) to give an equation representing conservation of mass:

$$\frac{\partial}{\partial t} (a_1^{(0)} a_2^{(0)} h^{(0)}) + \frac{\partial}{\partial x_1} \left(a_2^{(0)} h^{(0)} (u_1^{(0)} - v_1^{(0)}) \right) + \frac{\partial}{\partial x_2} \left(a_1^{(0)} h^{(0)} (u_2^{(0)} - v_2^{(0)}) \right) = 0. \tag{7.46}$$

Now (7.23) with boundary condition (7.32) gives the leading–order pressure

$$p^{(0)} = \frac{2\mu^{(0)}}{h_1^{(0)} h_2^{(0)}} \left(h_1^{(0)} h_2^{(0)} (\kappa_1^{(0)} + \kappa_2^{(0)}) v_3^{(0)} - \frac{\partial}{\partial x_1} (a_2^{(0)} u_1^{(0)}) - \frac{\partial}{\partial x_2} (a_1^{(0)} u_2^{(0)}) \right), \tag{7.47}$$

and (7.21), (7.22) with boundary conditions (7.30), (7.31) give the first–order velocities

$$u_1^{(1)} = F_1(x_1, x_2, t) - n \left(\kappa_1^{(0)} u_1^{(0)} + \frac{1}{a_1^{(0)}} \frac{\partial v_3^{(0)}}{\partial x_1} \right), \tag{7.48}$$

$$u_2^{(1)} = F_2(x_1, x_2, t) - n\left(\kappa_2^{(0)} u_2^{(0)} + \frac{1}{a_2^{(0)}}\frac{\partial v_3^{(0)}}{\partial x_2}\right), \tag{7.49}$$

for some arbitrary functions F_1 and F_2. Now it is necessary to proceed yet further in the expansions. From (7.23),

$$\frac{\partial \sigma_{33}^{(1)}}{\partial n} + \kappa_1^{(0)}\sigma_{11}^{(0)} + \kappa_2^{(0)}\sigma_{22}^{(0)} + f_3 = 0, \tag{7.50}$$

where f_3 is the dimensionless normal body force, with boundary condition (7.32),

$$\sigma_{33}^{(1)} = 0 \text{ on } n = \pm\tfrac{1}{2}h^{(0)}\ , \tag{7.51}$$

and, using the identities (7.18) and (7.19), we obtain the transverse stress balance

$$\begin{aligned}
& (2\kappa_1^{(0)} + \kappa_2^{(0)})\left(a_2^{(0)}\frac{\partial a_1^{(0)}}{\partial t} + (u_2^{(0)} - v_2^{(0)})\frac{\partial a_1^{(0)}}{\partial x_2} + a_2^{(0)}\frac{\partial}{\partial x_1}(u_1^{(0)} - v_1^{(0)})\right) \\
+ \quad & (\kappa_1^{(0)} + 2\kappa_2^{(0)})\left(a_1^{(0)}\frac{\partial a_2^{(0)}}{\partial t} + (u_1^{(0)} - v_1^{(0)})\frac{\partial a_2^{(0)}}{\partial x_1} + a_1^{(0)}\frac{\partial}{\partial x_2}(u_2^{(0)} - v_2^{(0)})\right) \\
+ \quad & \frac{a_1^{(0)}a_2^{(0)}f_3}{2\mu^{(0)}} = 0.
\end{aligned} \tag{7.52}$$

Similarly, (7.21) and (7.22) give expressions for the n-derivatives of $\sigma_{13}^{(1)}$ and $\sigma_{12}^{(1)}$ which may be integrated between the two free surfaces, applying boundary conditions from (7.30) and (7.31) to give stress balances in the x_1- and x_2-directions:

$$\begin{aligned}
& \frac{\partial}{\partial x_1}\left\{\frac{2\mu^{(0)}h^{(0)}}{a_1^{(0)}}\left[2\left(a_2^{(0)}\frac{\partial a_1^{(0)}}{\partial t} + (u_2^{(0)} - v_2^{(0)})\frac{\partial a_1^{(0)}}{\partial x_2} + a_2^{(0)}\frac{\partial}{\partial x_1}(u_1^{(0)} - v_1^{(0)})\right)\right.\right. \\
& \qquad \left.\left. + \left(a_1^{(0)}\frac{\partial a_2^{(0)}}{\partial t} + (u_1^{(0)} - v_1^{(0)})\frac{\partial a_2^{(0)}}{\partial x_1} + a_1^{(0)}\frac{\partial}{\partial x_2}(u_2^{(0)} - v_2^{(0)})\right)\right]\right\} \\
& + \frac{1}{a_1^{(0)}}\frac{\partial}{\partial x_2}\left\{\frac{\mu^{(0)}a_1^{(0)}h^{(0)}}{a_2^{(0)}}\left[a_1^{(0)}\frac{\partial}{\partial x_2}(u_1^{(0)} - v_1^{(0)}) + a_2^{(0)}\frac{\partial}{\partial x_1}(u_2^{(0)} - v_2^{(0)})\right]\right\} + a_1^{(0)}a_2^{(0)}h^{(0)}f_1 \\
& = \frac{2\mu^{(0)}h^{(0)}}{a_1^{(0)}a_2^{(0)}}\frac{\partial a_2^{(0)}}{\partial x_1}\left[\left(a_2^{(0)}\frac{\partial a_1^{(0)}}{\partial t} + (u_2^{(0)} - v_2^{(0)})\frac{\partial a_1^{(0)}}{\partial x_2} + a_2^{(0)}\frac{\partial}{\partial x_1}(u_1^{(0)} - v_1^{(0)})\right)\right. \\
& \qquad \left. + 2\left(a_1^{(0)}\frac{\partial a_2^{(0)}}{\partial t} + (u_1^{(0)} - v_1^{(0)})\frac{\partial a_2^{(0)}}{\partial x_1} + a_1^{(0)}\frac{\partial}{\partial x_2}(u_2^{(0)} - v_2^{(0)})\right)\right],
\end{aligned} \tag{7.53}$$

and

$$\frac{\partial}{\partial x_2}\left\{\frac{2\mu^{(0)}h^{(0)}}{a_2^{(0)}}\left[\left(a_2^{(0)}\frac{\partial a_1^{(0)}}{\partial t} + (u_2^{(0)} - v_2^{(0)})\frac{\partial a_1^{(0)}}{\partial x_2} + a_2^{(0)}\frac{\partial}{\partial x_1}(u_1^{(0)} - v_1^{(0)})\right)\right.\right.$$

$$+2\left(a_1^{(0)}\frac{\partial a_2^{(0)}}{\partial t}+(u_1^{(0)}-v_1^{(0)})\frac{\partial a_2^{(0)}}{\partial x_1}+a_1^{(0)}\frac{\partial}{\partial x_2}(u_2^{(0)}-v_2^{(0)})\right)\Bigg]\Bigg\}$$

$$+\frac{1}{a_2^{(0)}}\frac{\partial}{\partial x_1}\left\{\frac{\mu^{(0)}a_2^{(0)}h^{(0)}}{a_1^{(0)}}\left[a_1^{(0)}\frac{\partial}{\partial x_2}(u_1^{(0)}-v_1^{(0)})+a_2^{(0)}\frac{\partial}{\partial x_1}(u_2^{(0)}-v_2^{(0)})\right]\right\}+a_1^{(0)}a_2^{(0)}h^{(0)}f_2$$

$$=\frac{2\mu^{(0)}h^{(0)}}{a_1^{(0)}a_2^{(0)}}\frac{\partial a_1^{(0)}}{\partial x_2}\left[2\left(a_2^{(0)}\frac{\partial a_1^{(0)}}{\partial t}+(u_2^{(0)}-v_2^{(0)})\frac{\partial a_1^{(0)}}{\partial x_2}+a_2^{(0)}\frac{\partial}{\partial x_1}(u_1^{(0)}-v_1^{(0)})\right)\right.$$

$$\left.+\left(a_1^{(0)}\frac{\partial a_2^{(0)}}{\partial t}+(u_1^{(0)}-v_1^{(0)})\frac{\partial a_2^{(0)}}{\partial x_1}+a_1^{(0)}\frac{\partial}{\partial x_2}(u_2^{(0)}-v_2^{(0)})\right)\right]. \qquad (7.54)$$

7.5 The "viscous shell" equations

With, for example, applications in bottle–blowing in mind, we would like to incorporate the effect of a pressure drop across the sheet into the model. A simple force balance reveals that a pressure drop $\mathcal{P}$ across the sheet will induce velocities of order $\mathcal{P}L/(\epsilon\mu)$, so we nondimensionalise the applied pressures on the two free surfaces with $\epsilon MU/L$. The effect on our equations is to replace the boundary condition (7.51) by

$$\sigma_{33}^{(1)}=-P_{\pm}\text{ on }n=\pm\tfrac{1}{2}h^{(0)}\ , \qquad (7.55)$$

where $P_{\pm}$ are the dimensionless pressures applied to the two surfaces. The net result is easily seen to be to replace f_3 with $f_3+\mathcal{P}/h^{(0)}$ in the leading–order equations, where $\mathcal{P}$ is now the dimensionless drop in pressure from $n=-\frac{1}{2}h$ to $n=+\frac{1}{2}h$.

We now rewrite the leading–order equations of the previous section in a more familiar form which emphasises their analogy with the shell equations of linear elasticity. We shall drop superscripts throughout and use the velocities of the fluid relative to the velocity of the centre–surface:

$$\tilde{u}_1=u_1-v_1\text{ and }\tilde{u}_2=u_2-v_2. \qquad (7.56)$$

The tensions in the sheet are given by

$$\bar{\sigma}_{11}=\frac{2\mu h}{a_1a_2}\left[2\left(a_2\frac{\partial a_1}{\partial t}+\tilde{u}_2\frac{\partial a_1}{\partial x_2}+a_2\frac{\partial\tilde{u}_1}{\partial x_1}\right)+\left(a_1\frac{\partial a_2}{\partial t}+\tilde{u}_1\frac{\partial a_2}{\partial x_1}+a_1\frac{\partial\tilde{u}_2}{\partial x_2}\right)\right], \qquad (7.57)$$

$$\bar{\sigma}_{22} = \frac{2\mu h}{a_1 a_2}\left[\left(a_2\frac{\partial a_1}{\partial t} + \tilde{u}_2\frac{\partial a_1}{\partial x_2} + a_2\frac{\partial \tilde{u}_1}{\partial x_1}\right) + 2\left(a_1\frac{\partial a_2}{\partial t} + \tilde{u}_1\frac{\partial a_2}{\partial x_1} + a_1\frac{\partial \tilde{u}_2}{\partial x_2}\right)\right], \quad (7.58)$$

$$\bar{\sigma}_{12} = \frac{\mu h}{a_1 a_2}\left[a_1\frac{\partial \tilde{u}_1}{\partial x_2} + a_2\frac{\partial \tilde{u}_2}{\partial x_1}\right]. \quad (7.59)$$

In terms of these, the equations of the previous section become

$$\frac{\partial}{\partial t}(a_1 a_2 h) + \frac{\partial}{\partial x_1}(\tilde{u}_1 a_2 h) + \frac{\partial}{\partial x_2}(\tilde{u}_2 a_1 h) = 0, \quad (7.60)$$

representing conservation of mass,

$$\frac{\partial}{\partial x_1}(a_2\bar{\sigma}_{11}) + \frac{\partial}{\partial x_2}(a_1\bar{\sigma}_{12}) + \frac{\partial a_1}{\partial x_2}\bar{\sigma}_{12} - \frac{\partial a_2}{\partial x_1}\bar{\sigma}_{22} + a_1 a_2 h f_1 = 0, \quad (7.61)$$

and

$$\frac{\partial}{\partial x_1}(a_2\bar{\sigma}_{12}) + \frac{\partial}{\partial x_2}(a_1\bar{\sigma}_{22}) + \frac{\partial a_2}{\partial x_1}\bar{\sigma}_{12} - \frac{\partial a_1}{\partial x_2}\bar{\sigma}_{11} + a_1 a_2 h f_2 = 0, \quad (7.62)$$

representing force balances in the x_1- and x_2- directions, and a normal force balance,

$$\kappa_1\bar{\sigma}_{11} + \kappa_2\bar{\sigma}_{22} + f_3 h + \mathcal{P} = 0. \quad (7.63)$$

Equations (7.7 – 7.9), (7.60 – 7.63) form a closed system for the unknowns h, $\tilde{u}_1$, $\tilde{u}_2$, a_1, a_2, κ_1 and κ_2. Equations (7.61 – 7.63) are identical to the equations of linear shell theory. However, in our formulation the geometry is not prescribed; it must be found from coupled evolution equations. This is made clearer by reference to the following possible solution procedure:

- suppose the geometry of the sheet is known at some instant of time, that is h, a_1, a_2, κ_1 and κ_2 are all known functions of x_1 and x_2;
- solve (7.61 – 7.63) for $\bar{\sigma}_{11}$, $\bar{\sigma}_{12}$ and $\bar{\sigma}_{22}$ by usual shell theory methods;
- update the geometry using the evolution equations (7.57 – 7.60). This last step will require use of the remaining identities.

In general, the solution of these equations is hampered by the dependence of the geometry on time. One aspect of this is that the form of the coordinate system is not known in advance. However, we shall now describe two simple situations in

which some symmetries of the geometry are preserved as the sheet evolves, and hence some analytical progress may be made.

The first situation is that of an axisymmetric surface, which is discussed in section 7.6. The second case concerns a purely two–dimensional sheet, where there is no dependence on x_2; this case is discussed in section 7.7.

7.6 The axisymmetric "bottle"

The viscous shell equations may be simplified considerably if the sheet under consideration is axisymmetric. There are two main reasons for this: firstly, we may expect the axisymmetry to be preserved as the sheet evolves, and secondly, the lines of curvature of an axisymmetric surface are known to be the meridians and parallels.

We parametrise the centre–surface by polar angle θ ($= x_2/L$) and arc–length s in the r-z plane ($= x_1$):

$$\boldsymbol{r}_c = \begin{pmatrix} R(s,t)\cos\theta \\ R(s,t)\sin\theta \\ z(s,t) \end{pmatrix}, \text{ where } ds^2 = dR^2 + dz^2. \tag{7.64}$$

The scaling factors and principal curvatures are then given by

$$a_s = 1, \quad a_\theta = R, \tag{7.65}$$

$$\kappa_s = -\left[1 - \left(\frac{\partial R}{\partial s}\right)^2\right]^{-\frac{1}{2}} \frac{\partial^2 R}{\partial s^2}, \quad \kappa_\theta = \frac{1}{R}\left[1 - \left(\frac{\partial R}{\partial s}\right)^2\right]^{\frac{1}{2}}. \tag{7.66}$$

We suppose all variables are independent of θ and that the body force acting on the sheet is gravity, denoted by the dimensionless parameter St, in the negative z-direction. Denoting by u_s and u_θ the fluid velocity components in the s- and θ-directions relative to the moving centre–sheet, the equations of motion may be written in the form

$$\frac{\partial}{\partial t}(Rh) + \frac{\partial}{\partial s}(u_s R h) = 0, \tag{7.67}$$

$$\kappa_s \bar{\sigma}_{ss} + \kappa_\theta \bar{\sigma}_{\theta\theta} = \left(St\, h \frac{\partial R}{\partial s} + \mathcal{P}\right), \tag{7.68}$$

and

$$\frac{\partial}{\partial s}(R^2\kappa_\theta\bar{\sigma}_{ss}) = St\,Rh + \mathcal{P}R\frac{\partial R}{\partial s}, \tag{7.69}$$

where the averaged extensional and hoop stresses are given by

$$\bar{\sigma}_{ss} = \frac{2\mu h}{R}\left[2R\frac{\partial u_s}{\partial s} + \left(\frac{\partial R}{\partial t} + u_s\frac{\partial R}{\partial s}\right)\right], \tag{7.70}$$

$$\bar{\sigma}_{\theta\theta} = \frac{2\mu h}{R}\left[R\frac{\partial u_s}{\partial s} + 2\left(\frac{\partial R}{\partial t} + u_s\frac{\partial R}{\partial s}\right)\right]. \tag{7.71}$$

The rotational velocity u_θ satisfies a decoupled equation

$$\frac{\partial}{\partial s}\left(\mu R^2 h\frac{\partial u_\theta}{\partial s}\right) = 0. \tag{7.72}$$

We shall not discuss the solution of these equations, which will require some numerical work. Instead we concentrate on two simple examples which can be solved explicitly.

7.6.1 The two–dimensional circular bottle

Neglecting gravity and all s-variations leads to the following pair of o.d.e.'s for the radius and thickness of a two–dimensional, radially symmetric, slender sheet.

$$\frac{d}{dt}(Rh) = 0, \quad \frac{dR}{dt} = \frac{\mathcal{P}R^2}{4\mu h}. \tag{7.73}$$

These are readily solved to give (for constant $\mathcal{P}$ and μ)

$$R = R_0\left(1 - \frac{\mathcal{P}R_0 t}{2\mu h_0}\right)^{-\frac{1}{2}}, \quad h = h_0\left(1 - \frac{\mathcal{P}R_0 t}{2\mu h_0}\right)^{\frac{1}{2}}, \tag{7.74}$$

so that the radius becomes infinite, and the thickness zero, in a finite time $t^* = 2\mu h/(\mathcal{P}R_0)$.

Note that this problem can be solved *exactly*, without using the slenderness of the sheet, by simply solving the Stokes equations in cylindrical polar coordinates. The result is the system

$$\frac{d}{dt}(Rh) = 0, \quad \frac{dR}{dt} = \frac{\mathcal{P}}{4\mu h}\left(R^2 - \frac{h^2}{4}\right), \tag{7.75}$$

whose solution is

$$R^2 = \frac{R_0 h_0}{2}\coth\left(\frac{\mathcal{P}}{4\mu}(t^* - t)\right), \quad h^2 = 2R_0 h_0 \tanh\left(\frac{\mathcal{P}}{4\mu}(t^* - t)\right), \tag{7.76}$$

where the blow–up time is now given by

$$t^* = \frac{4\mu}{\mathcal{P}}\tanh^{-1}\left(\frac{h_0}{2R_0}\right). \tag{7.77}$$

The simple solution found above is clearly the leading–order term of this exact solution as $h_0/R_0 \to 0$.

We have the mathematically interesting result that the radius of a circular fluid sheet will become infinite in finite time under a constant pressure drop. Of course, maintaining this pressure drop as the volume inside the sheet becomes large is not physically realisable. More realistically we may prescribe the mass of gas inside the sheet as a function of time, and suppose the gas satisfies a gas law to give the pressure; indeed it is easy to show that this will result in the radius remaining finite.

We shall discuss more general two–dimensional configurations in section 7.7.

7.6.2 The spherical bottle

Another simple example of an axisymmetric surface for which an explicit solution of the viscous shell equations can be found is a sphere. Assuming radial symmetry, the radius and thickness now satisfy

$$\frac{d}{dt}(R^2 h) = 0, \quad \frac{dR}{dt} = \frac{\mathcal{P}R^2}{12\mu h}, \tag{7.78}$$

and hence are given by

$$R = R_0\left(1 - \frac{\mathcal{P}R_0 t}{4\mu h_0}\right)^{-\frac{1}{3}}, \quad h = h_0\left(1 - \frac{\mathcal{P}R_0 t}{4\mu h_0}\right)^{\frac{2}{3}}. \tag{7.79}$$

The blow–up time is $4\mu h_0/(\mathcal{P}R_0)$. In this case, the exact solution of the radially symmetric Stokes equations is given implicitly by

$$(R + \tfrac{1}{2}h)^3 - (R - \tfrac{1}{2}h)^3 = (R_0 + \tfrac{1}{2}h_0)^3 - (R_0 - \tfrac{1}{2}h_0)^3 = V, \text{ say,}$$

and

$$(R+\tfrac{1}{2}h)^3 = \frac{V}{e^{3\mathcal{P}(\tau^*-\tau)/4\mu}-1},$$

where the blow–up time, $\tau^* = 8\mu\tanh^{-1}(h_0/2R_0)/\mathcal{P}$.

7.7 The dynamics of a two–dimensional curved sheet

In the case where the sheet is flat in the x_2-direction, we may simplify the viscous shell equations by setting

$$a_1 = a_2 = 1, \kappa_2 = \tilde{u}_2 = v_2 = \frac{\partial}{\partial x_2} = f_2 = 0.$$

The choice $a_1 = 1$ means that x_1 may be identified with arc length s, and the equations of section 7.5 become

$$\frac{\partial h}{\partial t} + \frac{\partial}{\partial s}(\tilde{u}_1 h) = 0, \tag{7.80}$$

$$4\mu\kappa\frac{\partial \tilde{u}_1}{\partial s} = \frac{\mathcal{P}}{h} - f_3, \tag{7.81}$$

$$\frac{\partial}{\partial s}\left(4\mu h\frac{\partial \tilde{u}_1}{\partial s}\right) + hf_1 = 0. \tag{7.82}$$

Note that if there are no forces acting on the sheet, that is $f_1 = f_3 = \mathcal{P} = 0$, we obtain the model derived in section 2.1 for a nearly flat viscous sheet. This gives either $\kappa = 0$ (so that the sheet is straight) plus the Trouton model for h and $\tilde{u}_1$, or if κ is nonzero then $\tilde{u}_1 = 0$, $h_t = 0$ and it is necessary to proceed further with the expansions to find an expression for κ (c.f. chapter 3). This latter case has been considered by Buckmaster, Nachman & Ting (1975), and is analogous to the curved viscous fibre constrained to move in a plane described in chapter 5. However, when body forces are included it is unnecessary to proceed any further with the expansions, as we noted in section 5.8.

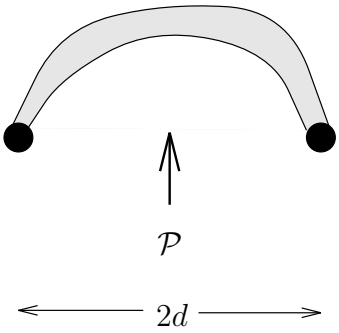

Figure 7.1: Configuration for a two–dimensional bottle

7.7.1 The two–dimensional "bottle"

With the bottle–blowing problem in mind, we neglect the body forces f_1 and f_3, and suppose the sheet is fixed at its two ends and blown out under an applied pressure drop; see figure 7.1.

The two–dimensional equations above lead to

$$\frac{\partial \kappa}{\partial s} = 0, \tag{7.83}$$

that is, the curvature of the sheet is uniform along its length, which means that the sheet must form a circular arc. Then h and $\tilde{u}_1$ satisfy the Trouton model:

$$\frac{\partial h}{\partial t} + \frac{\partial}{\partial s}(\tilde{u}_1 h) = 0, \quad 4\mu h \frac{\partial \tilde{u}_1}{\partial s} = T(t), \tag{7.84}$$

where T, the tension in the sheet, is given in terms of the radius R of the arc formed by the sheet by

$$T(t) = \mathcal{P}R. \tag{7.85}$$

The viscosity μ will typically be an empirical function of the temperature, which must be found from a coupled heat transfer equation. For simplicity we shall now only pursue the isothermal case, though we note that the case in which μ is convected faithfully with the flow is also covered by the analysis to follow by rescaling h with μ.

The techniques used to solve the Trouton model in section 2.4 may be employed here, though the boundary conditions are different. In 2.4 we supposed that the

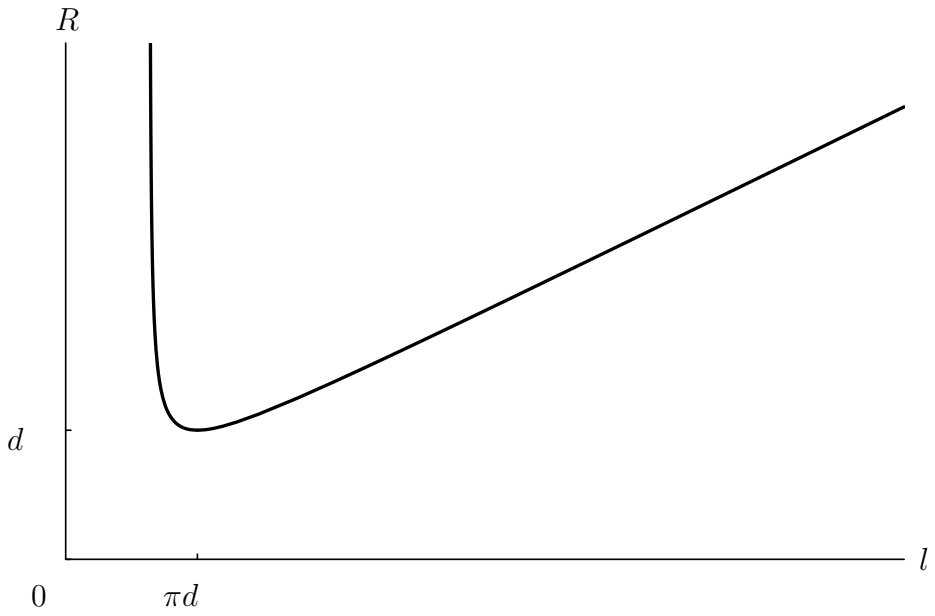

Figure 7.2: The sheet radius as a function of its length

length l of the sheet was a given function of time; here, the tension is given as a function of R, which is in turn a function of l. Indeed, it is easily seen that R and l are related by

$$l = \begin{cases} 2R\sin^{-1}\left(\frac{d}{R}\right) & \text{for } 2d \le l \le \pi d \ , \\ 2R\left[\pi - \sin^{-1}\left(\frac{d}{R}\right)\right] & \text{for } \pi d \le l < \infty \ . \end{cases} \tag{7.86}$$

A plot of R against l is shown in figure 7.2. Notice the minimum $R = d$ at $l = \pi d$, which occurs when the sheet is semicircular. The asymptotic behaviour of $R(l)$ when the sheet is nearly straight is given by

$$R \sim d\left[\left(\frac{d}{3(l-2d)}\right)^{\frac{1}{2}} + \frac{27}{40}\left(\frac{l-2d}{3d}\right)^{\frac{1}{2}} + O\left(\frac{l-2d}{d}\right)^{\frac{3}{2}}\right], \tag{7.87}$$

for small $l - 2d$; near its minimum when the sheet is semicircular, R is given asymptotically by

$$R \sim d\left[1 + \frac{1}{8}\left(\frac{\pi d - l}{d}\right)^2 + \frac{\pi}{32}\left(\frac{\pi d - l}{d}\right)^3 + O\left(\frac{\pi d - l}{d}\right)^4\right], \tag{7.88}$$

when l is close to πd; and as the sheet length becomes large,

$$R \sim l\left[\frac{1}{2\pi} + \frac{1}{\pi}\left(\frac{d}{l}\right) + \frac{2\pi}{3}\left(\frac{d}{l}\right)^3 + O\left(\frac{d}{l}\right)^4\right], \tag{7.89}$$

as $l/R \to \infty$ and the sheet approaches a full circle.

We now transform the problem into the Lagrangian variables defined in section 2.4. We assume that the sheet is straight initially, and scale the problem in such a way that $d = \frac{1}{2}$, so that the length of the fibre in Lagrangian variables is 1. This leads to

$$h(\xi, \tau) = h_0(\xi) - f(\tau), \tag{7.90}$$

where

$$\dot{f}(\tau) = \frac{\mathcal{P}R}{4\mu}\ ,\ f(0) = 0, \tag{7.91}$$

R is related to l by (7.86) and l to f by

$$l(\tau) = 1 + f(\tau)\int_0^1 \frac{d\xi}{h_0(\xi) - f(\tau)}. \tag{7.92}$$

Hence we have an integro–differential equation for f which is complicated by the awkward implicit form (7.86). However, some interesting results about the asymptotic behaviour of f, and hence R, h and l, may be obtained using the approximations (7.87) to (7.89).

7.7.2 Asymptotic behaviour of a two–dimensional bottle

First, let us consider the initial behaviour of the sheet when it is nearly straight. For small f, R is given asymptotically by (7.87) where

$$l \sim 1 + I_1 f + O(f^2)\ ;\ I_1 = \int_0^1 \frac{d\xi}{h_0(\xi)}. \tag{7.93}$$

Then the leading–order o.d.e. for f (7.91) may be solved to give

$$f \sim \frac{1}{8}\left(\frac{3\mathcal{P}^2}{\mu^2 I_1}\right)^{\frac{1}{3}} \tau^{\frac{2}{3}} + O(\tau^{\frac{4}{3}}), \tag{7.94}$$

and hence,

$$l \sim 1 + \frac{1}{8}\left(\frac{3I_1^2\mathcal{P}^2}{\mu^2}\right)^{\frac{1}{3}} \tau^{\frac{2}{3}} + O(\tau^{\frac{4}{3}}), \tag{7.95}$$

as $\tau \to 0$.

When the sheet is near a semicircular configuration, f will be close to some f_m, where

$$\int_0^1 \frac{h_0(\xi)d\xi}{h_0(\xi) - f_m} = \frac{\pi}{2}, \tag{7.96}$$

and the leading–order behaviour is found to be

$$f \sim f_m + \frac{\mathcal{P}(\tau - \tau_m)}{8\mu} + O(\tau - \tau_m)^3, \tag{7.97}$$

$$l \sim \frac{\pi}{2} + \frac{\mathcal{P}(\tau - \tau_m)}{8\mu} \int_0^1 \frac{h_0(\xi)d\xi}{(h_0(\xi) - f_m)^2} + O(\tau - \tau_m)^2, \tag{7.98}$$

where τ_m is the time taken for the sheet to reach a semicircular shape, given by

$$\tau_m = \frac{4\mu}{\mathcal{P}} \int_0^{f_m} \frac{df}{R(l(f))}. \tag{7.99}$$

Of particular interest is the behaviour of the sheet when it is close to break–up, that is when f is close to the minimum value of h_0, say $h_0(b)$. The asymptotic form of l as a function of the minimum thickness $h_m = h(b, \tau)$ was found in section 2.4 to be

$$l \sim \pi h_0(b) \left(\frac{2}{h_0''(b) h_m} \right)^{\frac{1}{2}} \text{ as } h_m \to 0, \tag{7.100}$$

assuming $h_0''(b)$ exists and is nonzero. Hence

$$R \sim h_0(b)(2h_0''(b)h_m)^{-\frac{1}{2}}, \tag{7.101}$$

and the leading–order solution of (7.91) reveals that the minimum thickness goes to zero like

$$h_m \sim \frac{1}{4} \left(\frac{9\mathcal{P}^2 h_0(b)^2}{2\mu^2 h_0''(b)} \right)^{\frac{1}{3}} (\tau^* - \tau)^{\frac{2}{3}}, \tag{7.102}$$

while the radius goes to infinity like

$$R \sim \left(\frac{4\mu h_0(b)^2}{3\mathcal{P} h_0''(b)} \right)^{\frac{1}{3}} (\tau^* - \tau)^{-\frac{1}{3}}, \tag{7.103}$$

where the blow–up time is given by

$$\tau^* = \frac{4\mu}{\mathcal{P}} \int_0^{h_0(b)} \frac{df}{R(l(f))}. \tag{7.104}$$

This time must be finite since $R \geq \frac{1}{2}$.

As noted in section 7.6 this finite–time blow–up is not physically realisable, but the contrast between the case of uniform initial thickness ($R \sim (\tau^* - \tau)^{-\frac{1}{2}}$ as shown in section 7.6) and the case where the initial thickness is nonuniform presented here is interesting nevertheless.

7.8 Surface tension effects

If we are to include surface tension in the model, we must, as in section 2.5, make some assumptions about the relative size of the surface tension coefficient. For an extremely slender film, for example a lamella in a foam, we may expect the geometry to be dominated by surface effects; this type of scaling has been considered for such an application by Ida & Miksis (1994). For problems in the glass industry (like bottle–blowing), however, we expect surface tension effects to be less important than viscous stresses in the glass, and a different type of scaling is appropriate. In order to model this type of process, we scale the dimensionless surface tension coefficient as follows;

$$\gamma^* = \frac{1}{\epsilon\, Ca} = O(1).$$

The approximate values given in the Introduction suggest that this parameter is certainly no greater than order one for a typical bottle–blowing process. After this scaling, the viscous shell equations are unchanged except for the normal force balance (7.63) which becomes

$$\kappa_1(\bar{\sigma}_{11} + \gamma^*) + \kappa_2(\bar{\sigma}_{22} + \gamma^*) + f_3 h + \mathcal{P} = 0. \tag{7.105}$$

As an example of the stabilising effect of surface tension, we now consider the evolution of a two–dimensional viscous sheet with surface tension.

7.8.1 A two–dimensional bottle with surface tension

In section 7.7 we noted that an inertia–free, slender two–dimensional viscous sheet will always form a circular arc under an applied pressure drop. This property

is preserved when surface tension effects are included, and the only effect on the Trouton model of section 7.7 is to change the tension equation (7.91) to

$$\dot{f} = \frac{\mathcal{P}R - \gamma^*}{4\mu}, \quad f(0) = 0. \tag{7.106}$$

As a result of this, if $\gamma^* > \mathcal{P}d$ then there is a stable steady state at which $\dot{f} = 0$.

7.9 Inertia effects

In a typical bottle–blowing process, the viscosity may vary dramatically. The approximate figures given in the Introduction suggest that the Reynolds number is typically much less than one so that inertia effects can usually be ignored; however, in extreme cases, they may become important. We also note that many authors (for example Burley & Graham (1991), Graham, Burley & Carling (1992)) who have written finite element codes for bottle–blowing processes have chosen to solve the (parabolic) Navier–Stokes equations rather than the (elliptic) quasi–steady Stokes equations, and incorporating inertia effects into our model may prove useful when comparing it with numerical results.

In order to include inertia effects in the viscous shell equations, it is necessary to calculate the acceleration vector of the fluid. This may be done using the convective derivative calculated in section 7.1 and noting that, for a vector field $\boldsymbol{V}$,

$$\frac{D\boldsymbol{V}}{Dt} = \frac{\partial \boldsymbol{V}}{\partial t} + \frac{\partial \boldsymbol{V}}{\partial x_i}\frac{Dx_i}{Dt},$$

where the sum is from $i = 1$ to 3. Then, employing the leading–order equations of section 7.4, the leading–order components of the acceleration vector are given by (dropping superscripts)

$$\begin{aligned} \boldsymbol{n}.\frac{D\boldsymbol{u}}{Dt} \sim & \quad \frac{\partial v_3}{\partial t} + \frac{\tilde{u}_1}{a_1}\frac{\partial v_3}{\partial x_1} + \frac{\tilde{u}_2}{a_2}\frac{\partial v_3}{\partial x_2} + \kappa_1 u_1^2 + \kappa_2 u_2^2 \\ & + \quad \frac{u_1}{a_1}\frac{\partial v_3}{\partial x_1} + \frac{u_2}{a_2}\frac{\partial v_3}{\partial x_2} + O(\epsilon), \end{aligned} \tag{7.107}$$

$$\begin{aligned} \boldsymbol{e}_1.\frac{D\boldsymbol{u}}{Dt} \sim & \quad \frac{\partial u_1}{\partial t} + \frac{\tilde{u}_1}{a_1}\frac{\partial u_1}{\partial x_1} + \frac{\tilde{u}_2}{a_2}\frac{\partial u_1}{\partial x_2} - v_3\left(\kappa_1 u_1 + \frac{1}{a_1}\frac{\partial v_3}{\partial x_1}\right) \\ & + \quad \frac{u_2}{a_2}\left(\frac{\partial v_1}{\partial x_2} + \frac{\tilde{u}_1}{a_1}\frac{\partial a_1}{\partial x_2} - \frac{u_2}{a_1}\frac{\partial a_2}{\partial x_1}\right) + O(\epsilon), \end{aligned} \tag{7.108}$$

$$\begin{aligned} \boldsymbol{e}_2.\frac{D\boldsymbol{u}}{Dt} \sim & \quad \frac{\partial u_2}{\partial t} + \frac{\tilde{u}_1}{a_1}\frac{\partial u_2}{\partial x_1} + \frac{\tilde{u}_2}{a_2}\frac{\partial u_2}{\partial x_2} - v_3\left(\kappa_2 u_2 + \frac{1}{a_2}\frac{\partial v_3}{\partial x_2}\right) \\ & + \quad \frac{u_1}{a_1}\left(\frac{\partial v_2}{\partial x_1} + \frac{\tilde{u}_2}{a_2}\frac{\partial a_2}{\partial x_1} - \frac{u_1}{a_2}\frac{\partial a_1}{\partial x_2}\right) + O(\epsilon). \end{aligned} \tag{7.109}$$

The viscous shell equations of section 7.5 are modified to take account of inertia by simply replacing f_3 by $f_3 - Re\,\boldsymbol{n}.D\boldsymbol{u}/Dt$ and f_i by $f_i - Re\,\boldsymbol{e}_i.D\boldsymbol{u}/Dt$ for $i = 1, 2$. For example, the equations for a two–dimensional bottle used in section 7.7 become

$$\frac{\partial h}{\partial t} + \frac{\partial}{\partial s}(\tilde{u}_1 h) = 0, \tag{7.110}$$

$$4\mu\kappa h\frac{\partial \tilde{u}_1}{\partial s} = \mathcal{P} + Re\,h\left(\frac{\partial v_3}{\partial t} + (2u_1 - v_1)\frac{\partial v_3}{\partial s} + \kappa u_1^2\right), \tag{7.111}$$

$$\frac{\partial}{\partial s}\left(4\mu h\frac{\partial \tilde{u}_1}{\partial s}\right) = Re\,h\left(\frac{\partial u_1}{\partial t} + \tilde{u}_1\frac{\partial u_1}{\partial s} - \kappa u_1 v_3 - v_3\frac{\partial v_3}{\partial s}\right), \tag{7.112}$$

where, using the identities found in section 7.1,

$$\frac{\partial v_1}{\partial s} = \kappa v_3 \quad \text{and} \quad \frac{\partial \kappa}{\partial t} = \frac{\partial}{\partial s}\left(\frac{\partial v_3}{\partial s} + \kappa v_1\right). \tag{7.113}$$

The inclusion of inertia makes the equations much harder to solve. In particular, the property found in section 7.7 that the sheet will always form a circular arc is lost here, and in general we must solve a coupled problem for the curvature.

However, if we *assume* that the sheet is circular, then the problem can be reduced to an o.d.e. for its radius

$$Re\,\ddot{R} + \frac{4\mu\dot{R}}{R^2} - \mathcal{P}R + \gamma^* = 0, \tag{7.114}$$

where the thickness $h = 1/R$, and for good measure we have included surface tension, with dimensionless coefficient γ^*. A phase plane for this o.d.e. is plotted in figure 7.3. Notice the saddle at $R = \gamma^*/\mathcal{P}$. Any path which starts to the right of the incoming separatrix of this saddle will go to infinity exponentially in time; anything to the left will go to zero like $1/t$.

If the mass of gas inside the sheet is prescribed and the pressure is assumed to satisfy some gas law, then the saddle becomes a stable node or spiral, depending on the parameter sizes. We shall not pursue this further here.

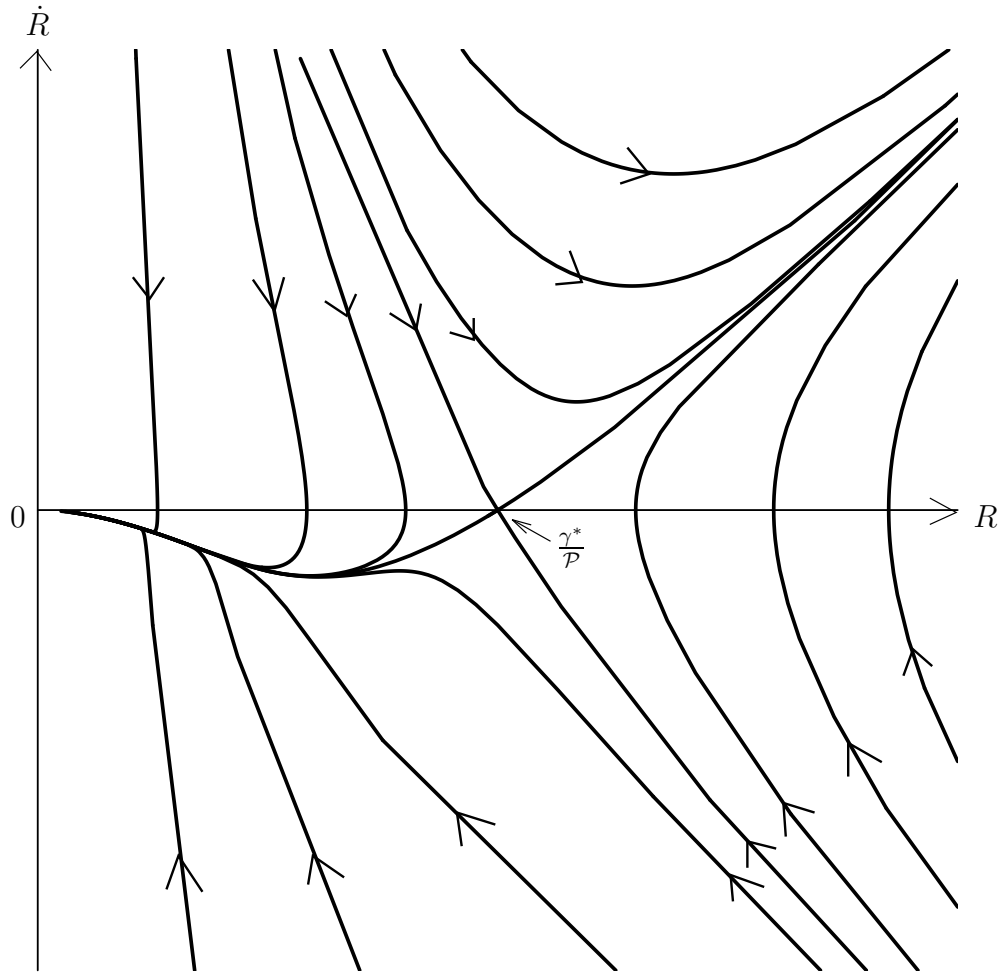

Figure 7.3: Phase plane for a circular sheet with inertia

7.10 Conclusions

In this chapter we have derived the leading–order equations governing the dynamics of a viscous sheet of arbitrary geometry. The resulting equations have a strong analogy with the shell equations of linear elasticity. However, their solution is in general much harder than the corresponding elasticity problems as the geometry changes with time, and indeed is unknown in advance. In cases where the form of the geometry is preserved some analytical progress can be made – we have presented the examples of a strictly two–dimensional sheet and an axisymmetric sheet.

Of particular interest for the bottle–blowing problem is the evolution of a viscous sheet under an applied pressure drop. The simple analytical examples described above suggest that such a sheet is likely to undergo finite–time blow–up if the pressure drop is held constant. The form taken by this blow–up is strongly dependent upon nonuniformities in the sheet thickness.

We have shown how surface tension effects are incorporated into the model fairly easily, and that they have a stabilising effect on the sheet. Inertia effects may also be included, though they make the equations considerably more complicated and necessitate numerical work even in simple geometries.

We noted in chapter 2 that the leading–order solution for Stokes flow of a slender two–dimensional viscous sheet with low curvature reveals that the centre–line of the sheet is straight. We inferred that in order to study the evolution of an initially curved sheet as it straightens it is necessary to consider a short timescale, and did so in chapter 3. Over this timescale, we found that the sheet does indeed straighten under tension, and does so *without stretching*; the stretching of the sheet, governed by the Trouton model, only commences once the sheet has fully straightened.

A similar situation occured in this chapter in section 7.7 where we found that a two–dimensional sheet subjected to a pressure drop is forced to form a circular arc. Again, a sheet of arbitrary initial shape must evolve towards this circular configuration over some short timescale; the appropriate timescale may be determined by

analogy with the theory of chapter 3. Again, we may expect this short timescale evolution to take place without any stretching of the sheet.

We may now ask whether the sheets of more general geometry discussed in this chapter may exhibit some short–timescale behaviour. We should first note the following important difference between a two–dimensional sheet or fibre and a fully three–dimensional sheet: a two–dimensional sheet or fibre may be bent into any desired shape of the same length without any stretching, while given an arbitrary surface, there is a limited class of surfaces into which it can be deformed without stretching — the surfaces to which it is *isometric*. For example, a planar sheet can only be deformed without stretching into a surface which is *developable*.

We therefore conjecture that over a short timescale, a sheet of arbitrary initial shape will evolve to another surface to which it is isometric. The shape of this surface is determined by the forces acting on the sheet: contrast, for example, a two–dimensional sheet placed under tension by pulling its ends apart which will straighten, with a two–dimensional sheet acting under a pressure drop which will form a circular arc.

Our second conjecture is that a sheet moving under an applied pressure drop will evolve over a short timescale to the surface, isometric to its original shape, which maximises the volume enclosed inside the sheet. This is clearly a generalisation of the property discussed above for a purely two–dimensional sheet: a circular arc is the shape which maximises the area enclosed inside a line without changing its length. Once it has adopted this shape, it starts to stretch and the equations of this chapter apply.

It is helpful at this point, though clearly not strictly applicable to our theory, to consider a balloon. As shown in figure 7.4(A), before inflation it starts in some arbitrary crumpled state. When air is blown into the balloon it instantaneously adopts a shape similar to that shown in figure 7.4(B), before inflating over a much longer timescale, as shown in figure 7.4(C). Let us pose the question: given the initial shape shown in figure 7.4(A), can one predict the shape (7.4(B)) which it will instantaneously adopt when blown into ? We assert that the answer is:

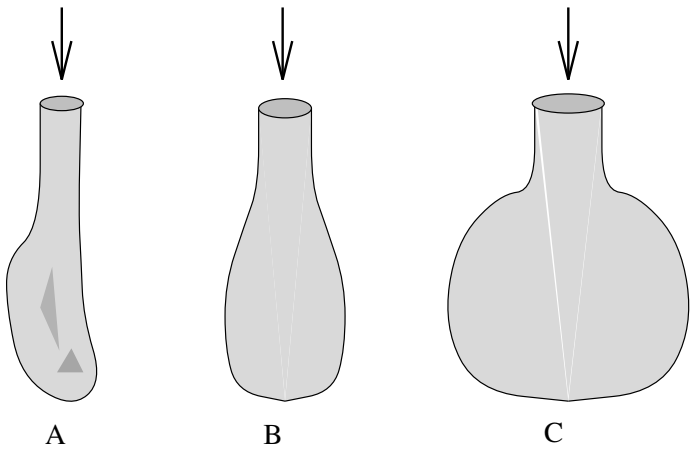

Figure 7.4: An inflating balloon

7.4(B) is the shape, obtainable from 7.4(A) via bending without stretching, which maximises the volume of air inside the balloon.

Now we have to imagine performing a similar experiment with a sheet of viscous fluid replacing the balloon (though, in the author's personal experience, performing such an experiment in practice presents many difficulties). The similarity between the theories of linear elasticity and Stokes flow suggests that we may expect qualitatively similar behaviour.

Chapter 8

The Trouton ratio: 3 or 4 ?

In chapter 2 we showed how a slender two–dimensional viscous sheet and a slender axisymmetric viscous fibre may both be described using the Trouton model, with one important difference: the tension in a two–dimensional sheet is related to its rate of extension by $T = 4\mu h u_x$ while that in an axisymmetric fibre is $3\mu A u_x$. This difference is quantified by the so–called Trouton ratio, which is 4 for a two–dimensional sheet and 3 for an axisymmetric fibre. The physical implication is that a two–dimensional sheet is correspondingly "harder to stretch" than an axisymmetric fibre.

In more general situations it is not immediately clear whether 4 or 3 is the appropriate ratio. Consider for example the viscous sheet equations derived in chapter 6. If all y-variations are neglected in these equations, the ratio 4 for a two–dimensional sheet is recovered. However, in the quasi one–dimensional float glass model of section 6.2 we found that the model reduced to a Trouton model with ratio 3. It is tempting, therefore, to pose the question:

> "Suppose we start with an axisymmetric fibre and we gradually flatten it out so that it becomes more and more like a two–dimensional sheet. Then at what stage does its Trouton ratio change from 3 to 4 ?"

In this chapter we shall attempt to answer this and other related questions. We begin by presenting two simple examples, related to work from previous chapters,

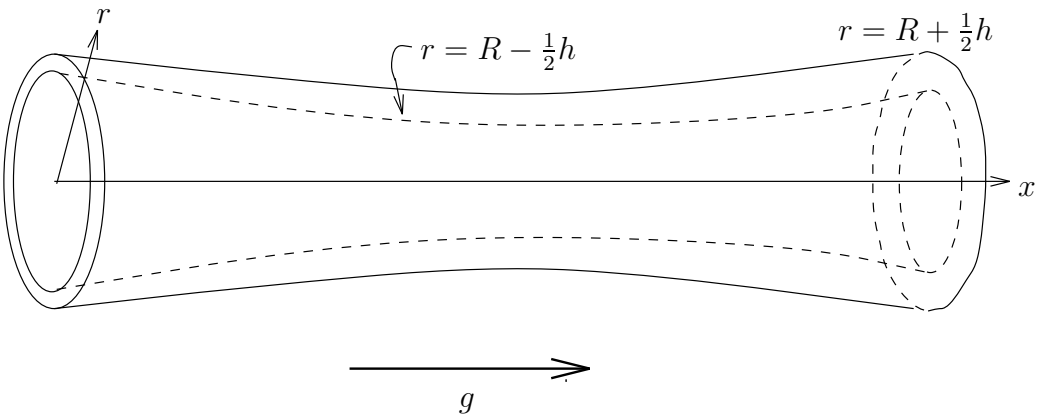

Figure 8.1: Definition sketch for a hollow axisymmetric fibre

in which the change from 3 to 4 can be seen explicitly. These are: in section 8.1, a hollow axisymmetric fibre which is blown from the inside and in section 8.2, a flat sheet with a variable tension applied at its edges. In section 8.3 we then explain the implications of these examples for the question posed above.

8.1 A hollow axisymmetric fibre

Consider a hollow axisymmetric fibre as shown in figure 8.1. We denote by $R(x,t)$ the average of the inner and outer radii, and by $h(x,t)$ the difference between them. We shall suppose that a pressure $\mathcal{P}(x,t)$ is imposed on the inside of the fibre while the outside is stress–free. To emphasise the Trouton ratio we shall also impose a body force g in the x-direction, but we shall neglect all other effects such as surface tension and inertia.

Hence the governing equations are the axisymmetric Stokes equations given in section 2.2. On the two free surfaces $r = R \pm \frac{1}{2}h$ we impose the usual kinematic and stress conditions, in this case incorporating a normal stress $\mathcal{P}$ on the inner surface. We nondimensionalise the equations as in section 2.2, that is, assuming that both R/L and h/L are of order ϵ, where L is a typical lengthscale in the x-direction and $\epsilon \ll 1$, and using a timescale L/U where U is a typical drawing speed. We shall omit the asymptotic analysis which is simple. The resulting leading–order equations are (dropping subscripts), a Trouton model for the cross–sectional area

$(= 2\pi Rh)$ and extensional velocity $u(x,t)$:

$$(Rh)_t + (uRh)_x = 0, \tag{8.1}$$

$$(3Rhu_x)_x + St\,Rh = -\frac{1}{2}\left(R - \frac{h}{2}\right)^2 \mathcal{P}_x, \tag{8.2}$$

with a third equation governing the radius R,

$$(R^2)_t + (uR^2)_x = \frac{R}{2h}\left(R^2 - \frac{h^2}{4}\right)\mathcal{P}. \tag{8.3}$$

Clearly if the pressure is independent of x then this model exhibits a Trouton ratio of 3, as expected for an axisymmetric fibre. However, by the admittedly rather artificial device of allowing the pressure to vary along the length of the fibre, we have added a term to the momentum equation (8.2) which means that the ratio need not be 3. For example, suppose the pressure is controlled in such a way that the outer radius of the fibre is preserved following the flow, *i.e.* that $R_t + \frac{1}{2}h_t + u(R_x + \frac{1}{2}h_x) = 0$. From (8.3), the required pressure is

$$\mathcal{P} = \frac{2Rhu_x}{(R - \frac{1}{2}h)^2},$$

and hence the momentum balance (8.2) becomes

$$(4Rhu_x)_x + St\,Rh = \mathcal{P}(R - \tfrac{1}{2}h)(R_x - \tfrac{1}{2}h_x).$$

The right–hand side of this equation represents the axial component of the force due to the pressure drop. By preventing the fibre from "necking" we have caused its Trouton ratio to change from 3 to 4. The physical implication is that blowing the inside of the fibre in this very special way makes it harder to stretch. In general, (8.2) can be written in the form

$$\frac{\partial}{\partial x}\left(3Rhu_x + \frac{\mathcal{P}}{2}\left(R - \frac{h}{2}\right)\right) + StRh = \mathcal{P}\left(R - \frac{h}{2}\right)\left(R_x - \frac{h_x}{2}\right), \tag{8.4}$$

which makes clear the contribution to the tension in the fibre due to the pressure drop. Indeed, from (8.3), this tension can be related to the relative rate of expansion of the outer radius,

$$d = \frac{1}{(R + \frac{1}{2}h)}\frac{D}{Dt}(R + \tfrac{1}{2}h),$$

by

$$\frac{\mathcal{P}}{2}(R+\tfrac{1}{2}h)^2 = Rh(2d+u_x),$$

so that (8.4) takes the form

$$[2Rh(2u_x+d)]_x + StRh = \mathcal{P}(R-\tfrac{1}{2}h)(R_x-\tfrac{1}{2}h_x). \tag{8.5}$$

Now the crucial part that the necking of the fibre plays in determining the Trouton ratio is clear. In the case where the fibre is prevented from necking, $d = 0$ and the ratio is 4; if no pressure drop is applied, then the cross–section shrinks as the fibre is stretched, $d = -u_x/2$ and the Trouton ratio is 3. In theory, by applying different pressures to the fibre, the ratio may be given any value desired.

8.2 A flat sheet with variable tension at its edge

We shall now consider the stretching of a flat viscous sheet, as shown in figure 8.2. Our model is taken from the float glass model in section 6.3; here we shall suppose the sheet is being drawn vertically, so that gravity acts in the x-direction, and that a normal tension T *which is a function of* x *and* t is applied at the edge of the sheet $y = b(x,t)$. We suppose that the geometry of the sheet varies slowly with x so that a one–dimensional approximation similar to that employed in section 6.3 is valid. The leading–order equations analogous to those of section 6.3 are then found to be the following. The cross–sectional area and extensional velocity satisfy a Trouton model with force terms due to gravity and the tension applied at the edge,

$$(bh)_t + (ubh)_x = 0, \tag{8.6}$$

$$(3bhu_x)_x + Stbh = \frac{1}{2}(T_x b - Tb_x), \tag{8.7}$$

while the evolution of the aspect ratio of the sheet cross–section is governed by

$$\frac{D}{Dt}\left(\frac{h}{b}\right) = \frac{T}{2b}. \tag{8.8}$$

As noted in section 6.3, if T is set to zero we retrieve a fibre–drawing model analogous to the theory of chapter 4, with the usual Trouton ratio of 3. However,

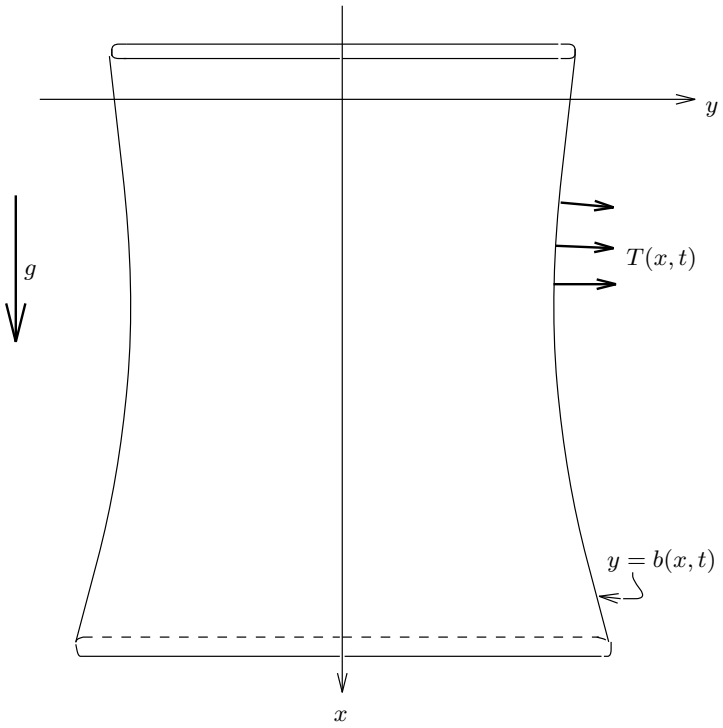

Figure 8.2: Definition sketch for a slender sheet

as in the previous section, by allowing the tension to depend on x and t, we are able to change the Trouton ratio at will. Equation (8.6) can be written in the form

$$(3bhu_x - \tfrac{1}{2}Tb)_x + Stbh = -Tb_x, \tag{8.9}$$

where the right–hand side represents the x-component of the edge tension force. Again the relative rate of expansion of the breadth of the sheet is given by

$$d = \frac{1}{b}\frac{Db}{Dt},$$

and the extra term in the tension in the sheet due to edge tension effects is found to be

$$-\tfrac{1}{2}Tb = bh(u_x + d),$$

so that the momentum balance (8.9) can be related to d, giving

$$[bh(4u_x + d)]_x + Stbh = -Tb_x. \tag{8.10}$$

As in the previous section, we see that if the tension is applied in such a way that d is zero, then the Trouton ratio becomes 4. If no edge tension is applied, then the sheet tapers as it is stretched, d is $-u_x$ and the ratio becomes 3.

8.3 The Trouton ratio

The examples presented above motivate the following explanation of the change in the Trouton ratio from 3 to 4. When a viscous sheet or fibre is stretched in one direction, it must of necessity shrink in some perpendicular direction or directions. A two–dimensional sheet only has one direction in which it is allowed to shrink, while a fibre can shrink in two directions and hence is easier to stretch. However, a fibre can be made harder to stretch, and hence more like a two–dimensional sheet by impeding its tapering, for example by applying a tension along its edges.

A simple explanation for the actual numbers 3 and 4 may be made by considering a general slender viscous sheet as in section 6.1. The tensions in such a sheet are given by

$$\bar{\sigma}_{xx} = 2h(2u_x + v_y), \quad \bar{\sigma}_{yy} = 2h(u_x + 2v_y),$$

so that

$$\bar{\sigma}_{xx} = 4hu_x + 2hv_y = 3hu_x + \tfrac{1}{2}\bar{\sigma}_{yy}. \tag{8.11}$$

The Trouton ratio becomes an issue when a one–dimensional approximation of these equations is sought. For a purely two–dimensional sheet, this is achieved by setting v to zero, resulting in a ratio of 4. For a sheet with stress–free edges (like figure 8.2 with $T = 0$), a one–dimensional model involves setting the transverse tension $\bar{\sigma}_{yy}$ to zero, and hence leads to a ratio of 3.

Chapter 9

Conclusions

In this final chapter we first summarise briefly the main results which we have obtained. We then suggest some related work which could be carried out in the future, and finally give a short discussion of the broader implications of this work.

9.1 Summary of results

In this thesis we have derived models for slender viscous fibres and sheets. Our method throughout has been to reduce the Navier–Stokes equations and free–surface boundary conditions via systematic perturbation techniques. The result in many cases is a system of leading–order *extensional* equations, in which the unknowns are uniform across the cross–section of the fibre or thickness of the sheet. Hence the fully three–dimensional Navier–Stokes equations can be reduced to a simplified one– or two–dimensional system.

We have chosen for simplicity to commence by considering purely viscous flow before introducing the effects of surface tension, gravity and inertia. Each of the models we have presented is aimed at a particular industrial process taken from the glass industry and we have used this to guide us as to typical sizes of the relevant dimensionless parameters.

In chapter 2 we gave simple derivations of the Trouton model for a purely two–dimensional viscous sheet and for an axisymmetric viscous fibre. We showed how

this model may be solved by means of Lagrangian variables and how it can be generalised to incorporate such effects as surface tension, gravity, inertia and twisting. In particular, we found that

- a purely viscous fibre cannot be broken by stretching unless its radius has an initial cusp;
- when surface tension effects are included, a cusp may be formed in the fibre during stretching, and hence it may break even if it is smooth initially;
- for a purely viscous two–dimensional sheet, the leading–order equations predict that the centre–line of the sheet is straight;
- when inertia effects are included, an evolution equation for the centre–line is obtained which changes type from hyperbolic to elliptic depending on whether the sheet is under tension or compression.

We noted that the prediction that the centre–line of a two–dimensional viscous sheet is straight implies that the problem for the centre–line is a singular perturbation in time. This motivated us in chapter 3 to consider the response of of a two–dimensional sheet over a short timescale: an analysis which was previously performed by Buckmaster, Nachman & Ting (1975). We went on to show that the short timescale behaviour is dramatically altered if inertia effects are included, resulting in the introduction of a new dominant lengthscale which depends on the size of the Reynolds number.

In chapter 4 we derived extensional models for nonaxisymmetric viscous fibres, including the effects of inertia, gravity and surface tension. We considered two possible scalings for the surface tension coefficient. If it is relatively small we found that surface tension effects have no net effect of the evolution of the fibre, though they certainly have a pointwise effect on its boundary. In this case we derived, by methods similar to those employed by Dewynne, Ockendon & Wilmott (1992), extensional equations governing the cross–sectional area and axial velocity of the fibre, along with decoupled equations for the evolution of the centre–line of the fibre and the twist of the fibre about its centre–line. For larger values of

the surface tension coefficient we found that the evolution of the shape of the fibre cross–section can be described by means of a conformal map which depends on time and distance along the fibre. This is a generalisation of the work of Richardson (1992).

In chapter 5 we derived a model for a viscous fibre whose dimensionless curvature is order one. The model consists of equations balancing the averaged axial stresses in the fibre with the bending and twisting moments, along with expressions for the bending and twisting moments in terms of the rates of change of the curvature and torsion of the fibre. These equations bear a strong similarity to those governing the equilibrium of a slender linearly elastic rod. We demonstrated that they reduce to the "viscida" equation of Buckmaster, Nachman & Ting (1975) if the fibre is constrained to move in a plane. We went on to find equations governing the motion of such a fibre under a large body force. In this case, the equations comprise simple balances between the body force acting on the fibre and the tension in the fibre, and are similar to the equations governing the shape of a catenary.

In chapter 6 we derived models for the flow of nearly planar viscous sheets. We found that different models result depending on whether the motion of the sheet is assumed to be principally in–plane or transverse. We extended the former case to give a model for the float glass process, which we then simplified to a one–dimensional model for a slowly–varying float glass ribbon. We showed that for realistic parameter regimes, explicit solutions of this model may be found. For transverse motion of a sheet, we derived equations similar to the von Kármán equations of linear elasticity.

In chapter 7 we derived equations governing the motion of a curved viscous sheet. These equations were found to be similar to the shell equations of linear elasticity, though harder to solve in general because of the dependence of the geometry on time. However, we found a number of simple exact solutions which led us to make the following conjectures:

- if a constant pressure drop is applied to a viscous sheet it will undergo finite time blow–up;

- the form taken by this blow–up is dependent on nonuniformities in the thickness of the sheet;
- the sheet may be stabilised by the inclusion of surface tension effects or by applying some gas law instead of a constant pressure drop;
- when the pressure drop is first applied, the sheet will instantaneously adopt a new shape isometric to its initial shape;
- it will do so in such a way as to maximise the volume which it encloses.

In chapter 8 we demonstrated the precise way in which the Trouton ratio of a viscous sheet or fibre measures its ability to taper under tension.

9.2 Future Work

Many of the models we have presented in this thesis comprise systems of coupled nonlinear partial differential equations which do not yield readily to analytical techniques. Hence there is still much work to be done on numerical solution, asymptotic analysis, and simplification via symmetry analysis of these models. This applies for example to the generalised Trouton models of section 2.5, the viscous sheet equations of sections 6.1 and 6.4 and the viscous shell equations of section 7.5.

On the other hand, many of the models we have presented for specific industrial processes are vastly over–simplified; there are many relevant physical effects which we have not yet considered. To construct truly realistic models, we should include, for example, heat transfer effects in all our models, the contact between the glass and the mould in the bottle–blowing problem and edge forces on the float glass ribbon due to the edge rollers and tiles. It would also be important for many related industrial processes to allow for more general rheology than incompressible Newtonian liquid.

We also note the following particular areas which we have covered which require further attention.

- In section 2.5.2 we showed how an axisymmetric fibre may break up under surface tension. However, we noted in section 2.5.3 that whether the same result holds for a two–dimensional sheet remains an open question. The answer to this question may have implications for the bursting of bubbles due to surface tension.

- The procedure presented in section 4.4 for determining the evolution of a nonaxisymmetric fibre with surface tension is extremely cumbersome. Even when the shape of the cross–section is described using a conformal map, the problem for its rotation requires the calculation of a number of rather difficult integrals at each timestep. However, it may be possible to use some crafty complex analysis to simplify the procedure somewhat.

- It would be interesting to look more closely at the equations of section 5.6 for highly curved viscous fibres to see if they can predict the three–dimensional buckling and coiling instabilities which are familiar to anybody who has ever poured honey onto toast. These instabilities are also of much practical importance in fibre draw–down processes.

- For completeness we should consider the effects of inertia and surface tension on the large curvature theory of chapter 5 for comparison with the work in chapters 4 and 7.

- The derivation of the edge conditions for a float glass ribbon in section 6.2.2 is less than convincing. A more thorough analysis would require consideration of a boundary layer near the ribbon edge which must then be matched with the outer flow.

- Some more work should be done on the viscous shell equations to try to verify the conjectures made at the end of chapter 7.

9.3 Discussion

Though nearly straight slender fibres have received much interest in the literature, relatively little work has been done on the theory of curved fluid sheets and fibres.

This is surprising, as the corresponding theory in linear elasticity of shells and rods has been well–established for many years. We have demonstrated that the asymptotic methods traditionally employed in the study of slender jets can be combined with geometrical techniques similar to those used in the study of elastic rods and shells, and hence models can be derived for fluid flows in many different slender geometries. These models are potentially far more interesting than the corresponding theories in linear elasticity because the geometry is not known in advance; the ability of the fluid to flow means that the evolution of the geometry is coupled with stress balances similar to those encountered in linear elasticity. We have also seen that inertia can have a far more dramatic effect than it does in the theory of elastic solids.

As noted in the previous section, at present our theory is far from complete. However, it is our hope that it may form the first step in the development of a comprehensive theory of slender fluid flows which will become as standard as the theories of rods and shells are now.

References

S.E. Bechtel, K.D. Bolinger, J.Z. Cao & M.G. Forest, 1994 Torsional effects in high–order viscoelastic thin–filament models, SIAM J. Appl. Math., (to appear).

S.E. Bechtel, M.G. Forest, D.D. Holm & K.J. Lin, 1988 One-dimensional closure models for three-dimensional incompressible visco-elastic free jets: von Karman flow geometry and elliptical cross-section, J. Fluid Mech., **196**, 241–262.

S.E. Bechtel & K.J. Lin, 1988 On the behaviour of visco-elastic free jets with elliptical cross section, J. Non-Newtonian Fluid Mech., **27**, 87–126.

T.B. Benjamin & T. Mullin, 1988 Buckling instabilities in layers of viscous liquid subjected to shearing, J. Fluid Mech., **195**, 523–540.

H.D. Bryant, 1992 Solution of a viscous free boundary flow problem derived from float–glass stretching, MSc dissertation, University of Oxford.

J.D. Buckmaster & A. Nachman, 1978 The buckling and stretching of viscida II — Effects of Surface Tension,Quart. J. Mech. Appl. Math., **31**, 157-168.

J.D. Buckmaster, A. Nachman & L. Ting, 1975 The buckling and stretching of viscida, J. Fluid Mech., **69**, 1–20.

D.M. Burley & S.J. Graham, 1991 The blowing of thin films into moulds with applications in the glass container industry, The Mathematics of Finite Elements and Applications VII, 279–286.

J.N. Dewynne, J.R. Ockendon & P. Wilmott, 1989 On a mathematical model for fiber tapering, SIAM J. Appl. Math., **49**, 983–990.

J.N. Dewynne, J.R. Ockendon & P. Wilmott, 1992 A systematic derivation of the

leading-order equations for extensional flows in slender geometries, J. Fluid Mech., **244**, 323–338.

J.N. Dewynne, P.D. Howell & P. Wilmott, 1994 Slender viscous fibres with inertia and gravity. Quart. J. Mech. Appl. Math.,(to appear).

C.K. Edge, 1992 Float–glass forming: production considerations, Ceramic Bulletin, **6**, 936–942.

J. Eggers, 1993 Universal pinching of 3D axisymmetric free–surface flow, Phys. Rev. Lett., **71**, 3458–3460.

F.T. Geyling, 1976 Basic fluid dynamic considerations in the drawing of optical fibers, Bell Sys. Tech. J., **55**, 1011–1056.

F.T. Geyling & G.M. Homsy, 1980 Extensional instabilities of the glass fiber drawing process, Glass Tech., **21**, 95-102.

S.J. Graham, 1987 Mathematical modelling of glass flow in container manufacture, PhD thesis, University of Sheffield.

S.J. Graham, D.M. Burley & J.C. Carling, 1992 Fluid flow in thin films using finite elements, Math. Engng Ind., **3**, 229–246.

R.W. Hopper, 1990 Plane Stokes flow driven by capillarity on a free surface, J. Fluid Mech., **213**, 349–375.

M.P. Ida & M.J. Miksis, 1994 Dynamics of a lamella in a capillary tube, SIAM J. Appl. Math., (to appear).

E. Kreyszig, 1959 Differential geometry, University of Toronto Press (reprinted Dover, 1991).

A.E.H. Love, 1927 A treatise on the mathematical theory of elasticity, Cambridge University Press.

M.A. Matovich & J.R.A. Pearson, 1969 Spinning a molten threadline, Ind. Engng. Chem. Fund., **8**, 512–519.

J.D. Morgan, 1994 Codimension–two free boundary problems, doctoral thesis, Uni-

versity of Oxford.

I. Motoichi & M. Hiroshi, 1991 Numerical simulation of float glass forming process, Reports Res. Lab. Asahi Glass Co. Ltd., **41**, 9–12.

O.S. Narayanaswamy, 1977 A one–dimensional model of stretching float glass, J. Ame. Ceram. Soc., **60**, 1–5.

J.R.A. Pearson & M.A. Matovich, 1969 Spinning a molten threadline, Indust. Engng. Chem. Fund., **8**, 605–609.

H. Rawson, 1974 Physics of glass manufacturing processes, Physics Technol., **2**, 91–114.

S. Richardson, 1992 Two–dimensional slow viscous flows with time–dependent free boundaries driven by surface tension, Euro. Jnl Appl. Math., **3**, 193–207.

W.W. Schultz & S.H. Davis, 1982 One-dimensional liquid fibers, Journal of Rheology, **26**, 331–345.

F.T. Shah & J.R.A. Pearson, 1972 On the stability of non-isothermal fibre spinning, Indust. Engng. Chem. Fund., **11**, 145–149.

G.I. Taylor, 1968 Instability of jets, threads and sheets of viscous fluid, Proc. Int. Cong. Appl. Mech. Springer-Verlag.

F.T. Trouton, 1906 On the coefficient of viscous traction and its relation to that of viscosity, Proc. Roy. Soc., **77A**, 426–440.

P. Wilmott, 1989 The stretching of a thin viscous inclusion and the drawing of glass sheets, Phys. Fluids A, **1**, 1098–1103.